

Functional Characterization of NLRC3

Dissertation

zur Erlangung des Doktorgrades der
Mathematisch-Naturwissenschaftlichen Fakultät der
Christian-Albrechts-Universität zu Kiel

vorgelegt von

Lars Bremer

Kiel, 2014

Erster Gutachter: **Prof. Dr. Philip Rosenstiel**

Zweiter Gutachter: **Prof. Dr. Thomas Roeder**

Tag der mündlichen Prüfung: 15. Mai 2014

Zum Druck genehmigt:

gez. Prof. Dr. Wolfgang J. Duschl, Dekan

Contents

1 Abstract/Zusammenfassung	1
1.1 Abstract	1
1.2 Zusammenfassung	2
2 Introduction	3
2.1 The immune system	3
2.1.1 Inflammation	4
2.1.2 Pattern recognition receptors	4
2.1.3 NOD-like receptors	5
2.1.4 Evolution of NLRs	7
2.2 NOD-like receptor CARD domain containing 3 (NLRC3)	8
2.2.1 Gene organisation	8
2.2.2 Domain architecture	9
2.2.3 Protein expression	10
2.2.4 Function of NLRC3	11
2.3 Mitochondria	11
2.3.1 Inner mitochondrial membrane protein (IMMT)/Mitofilin	12
2.4 Cytokines and chemokines	13
2.5 NF κ B	16
2.6 Inflammatory bowel diseases	17
2.6.1 Dextran sulfate sodium induced colitis as mouse model for IBD	17
2.7 Aim of this work	18
3 Material and Methods	19
3.1 Materials and reagents	19
3.1.1 Plasmids and bacteria	19
3.1.2 Cell lines and media	19
3.1.3 Oligonucleotides	21
3.1.4 Antibodies and dyes	21
3.1.5 Buffer	22

3.2	Methods of molecular biology	23
3.2.1	Polymerase chain reaction	23
3.2.2	Gateway cloning	26
3.2.3	Isolation of plasmids	27
3.2.4	Purification from gel	27
3.2.5	RNA isolation and cDNA synthesis	28
3.2.6	Analysis of proteins	28
3.2.7	Coverslip staining	30
3.3	Methods of cell biology	31
3.3.1	Cell culture	31
3.3.2	Transfection	32
3.3.3	Stimulation	33
3.3.4	Cell fractionation	33
3.3.5	Isolation of mitochondria	33
3.3.6	Dual luciferase assay	34
3.3.7	Enzyme-linked immunosorbent assay	34
3.3.8	MTS assay	35
3.4	Generation of <i>Nlrc3</i> ^{-/-} mice	35
3.4.1	Handling of mice	36
3.4.2	Bone marrow derived macrophages	37
3.4.3	Mixed splenocytes	37
3.4.4	Acute dextran sodium sulfate induced colitis	37
3.4.5	Histology	39
3.4.6	Blood analysis	40
3.5	Statistical analysis	40
4	Results	41
4.1	NLRC3 is differentially expressed in various tissues	41
4.1.1	<i>Nlrc3</i> is expressed in cDNA of immune related tissues	41
4.1.2	High transcript level of <i>NLRC3</i> and <i>Nlrc3</i> are found in immune related tissues, but not in the intestinal tract	41
4.1.3	NLRC3/ <i>Nlrc3</i> in human and murine cell lines	42
4.1.4	Cell fractions demonstrate the cytosolic localization of NLRC3	43

4.2	Analysis of functional interaction and colocalization between NLRC3 and Mitofilin	43
4.2.1	Co-immunoprecipitation of NLRC3 and IMMT	44
4.2.2	Cell staining reveals spatial position of NLRC3	44
4.2.3	NLRC3 was detected in a mitochondrial lysates via MS/MS	48
4.2.4	<i>In silico</i> prediction of probability of NLRC3 being imported into mitochondria	49
4.2.5	NLRC3 influences the ERSE mediated unfolded protein response	50
4.3	NLRC3 and its impact on NFκB activation	51
4.4	Stimulation and downstream signaling	52
4.4.1	NLRC3 in response to TNFα stimulation	52
4.4.2	TRAF6 and NLRC3	53
4.4.3	Human peripheral blood mononuclear cells show distinct transcript patterns after stimulation	54
4.5	Nlrc3 ^{-/-} mice do not exhibit a spontaneous phenotype	54
4.5.1	Basal phenotyping	54
4.5.2	Murine blood analysis	57
4.6	Response of Nlrc3 ^{-/-} BMDM to lipopolysaccharide stimuli	58
4.6.1	Murine splenocytes as <i>in vitro</i> model for immune cells	62
4.7	Implication of NLRC3 in autoimmune and chronic inflammatory diseases	63
4.7.1	Wegener's granulomatosis/granulomatosis with polyangiitis	63
4.7.2	Crohn's disease	64
4.8	Impact of acute dextran sodium sulfate induced colitis on WT and KO mice	64
4.8.1	DSS-induced colitis heavily affects the colon	65
4.8.2	DAI and MEICS score	66
4.8.3	Nlrc3 ^{+/+} mice are less affected of tissue damage and infiltration by immune cells	68
4.8.4	Serum and transcript level of interleukins	69
4.8.5	NFκB is upregulated in DSS treated mice	72
4.8.6	Mitochondrial stress markers are not affected in colonic tissue after DSS treatment	72
4.8.7	TRAF6 is diminished in DSS treated mice	74
5	Discussion	75

5.1	NLRC3/Nlrc3 is localized in immune relevant tissues	75
5.2	NLRC3 in mitochondria associated immune functions	76
5.2.1	Mitochondria in innate immunity	76
5.2.1.1	Supramolecular mitochondrial structures	78
5.2.1.2	Mitochondrial unfolded protein response (mtUPR)	79
5.3	NLRC3 is involved in central immune signaling pathways	80
5.3.1	NLRC3 is involved in the NFκB signaling pathway	80
5.3.2	NLRC3 mediated NFκB signaling pathway is modulated by TRAF6	81
5.4	Interleukins	83
5.4.1	Pro-inflammatory cytokines are elevated in <i>Nlrc3</i> ^{-/-} BMDMs	83
5.4.2	Anti-inflammatory cytokine IL-10 is upregulated in <i>Nlrc3</i> ^{-/-} BMDMs	84
5.4.3	Translation of murine results to human systems	84
5.5	Splenocytes exhibit surprising behavior upon stimulation	85
5.6	DSS colitis	85
5.6.1	<i>Nlrc3</i> ^{-/-} mice display a stronger onset of disease	85
5.6.2	NFκB increased in DSS treated mice	87
5.6.3	Interleukin levels are altered in DSS treated <i>Nlrc3</i> ^{-/-} mice	87
5.6.4	<i>Nlrc3</i> influences mtUPR marker	88
5.6.5	Final conclusions on DSS experiment	89
5.7	Relevance of NLRC3 in several diseases	89
5.7.1	NLRC3 is downregulated in Wegener's granulomatosis patients	90
5.7.2	Phase II dasatinib study: NLRC3 is downregulated, while NFκB2 is increased	90
5.7.3	NLRC3 is downregulated during aging	90
5.8	Summary	91
5.9	Outlook	92
6	Supplement	94
6.1	Isoforms of NLRC3	94
6.2	Generation of mice	95
6.3	MS/MS	96
6.4	Abbreviations	96

Bibliography	100
Danksagung	131
Curriculum vitae	132
Eidesstattliche Erklärung	133

1 Abstract/Zusammenfassung

1.1 Abstract

The innate immune system relies on several pattern recognition receptors (PRRs) to identify pathogen associated molecular patterns (PAMPs). One of the most prominent non-clonal, germline encoded but yet not fully characterized PRR group are the NOD-like receptors (NLRs). Here I aim to characterize a hitherto rarely described member of the NLRs named NOD-like receptor CARD domain containing 3 (NLRC3). Recent studies indicated, that NLRC3 is a cytosolic receptor which negatively regulates T cell function.

This thesis utilizes several experimental approaches to access the cellular localization of NLRC3, its functional interactions, and role in inflamed tissue. Microscopical studies showed, that NLRC3 is localized in the cytoplasm. Analysis of different organs indicated, that *NLRC3* transcript level are elevated in immune relevant tissues, but not in the intestinal tract. A Y2H screen indicated a potential interaction with the mitochondrial protein IMMT/Mitofilin. Although a direct interaction remained elusive, NLRC3 was detected in close spatial proximity of mitochondria via immunofluorescence and identified in mitochondrial lysates. NLRC3 was found to interfere with NF κ B signaling in a dose dependent manner. Dual luciferase assays were performed revealing connections to TRAF6 and ERSE. NLRC3 seems to negatively regulate the TRAF6 mediated NF κ B response. In combination with a potent stressor, such as tunicamycin elevates NLRC3 the ERSE promoter activity. This reaction connects NLRC3 to cellular mechanisms of the unfolded protein response, and subsequently to mitochondrial stress reactions. NLRC3 was found to be downregulated in biopsies of WG patients. During this thesis *Nlrc3*^{+/+} and *Nlrc3*^{-/-} mice were bred and utilized in several experiments. Cytokine level in bone marrow derived macrophages varied between *Nlrc3*^{+/+} and *Nlrc3*^{-/-} in response to LPS stimulation. A DSS induced colitis was conducted and revealed, that NLRC3 seems to be beneficial for survival and disease severity. These experiments significantly enlarged the knowledge about NLRC3, pointing at the protective role of NLRC3 during cellular stress response and inflammation. NLRC3 is an important regulator in immune modulation.

1.2 Zusammenfassung

Das angeborene Immunsystem basiert auf einer Vielzahl von Mustererkennenden Rezeptoren (PRR, von engl. *pattern recognition receptors*) zur Identifikation molekularer pathogen-assoziiierter Muster. Eine der bekanntesten nicht-klonalen, keimbahn-kodierten, jedoch noch unvollständig beschriebene PRR-Gruppe sind die NOD ähnlichen Rezeptoren (NLR, von engl. *NOD-like receptors*). Diese Arbeit hat die Charakterisierung eines bisher kaum beschriebenen Mitglieds der NLRs, dem Protein NLRC3 zum Ziel. Bisherige Studien zeigen, dass NLRC3 ein zytosolischer Rezeptor ist, der einen negativ-regulatorischen Einfluss auf T-Zellen aufweist.

Im Verlauf dieser Arbeit wurden unterschiedliche experimentelle Ansätze verwendet, um die zelluläre Lokalisation von NLRC3, seine funktionellen Interaktionen, sowie die Rolle in entzündetem Gewebe zu charakterisieren. Mikroskopische Studien konnten zeigen, dass NLRC3 im Zytoplasma verortet ist. Die Untersuchung verschiedener Gewebe ergab dabei, dass sich *NLRC3* hauptsächlich in immunrelevanten Geweben, nicht jedoch im Gastrointestinaltrakt nachweisen lässt. Nachdem ein Hefe-2-Hybrid Experiment das mitochondriale Protein IMMT/Mitofilin als potentiellen Interaktionspartner für NLRC3 gezeigt hatte, konnte NLRC3 durch Immunfluoreszenzanalysen in unmittelbarer Nähe von Mitochondrien detektiert werden. Zudem gelang die Identifikation von NLRC3 in Mitochondrienlysaten. Der Einfluss von NLRC3 auf den NF κ B Signalweg ist dosisabhängig und konnte mittels Luziferase-Test auch im Zusammenhang mit TRAF6 und ERSE gezeigt werden. NLRC3 scheint die TRAF6 vermittelte NF κ B Antwort negativ zu regulieren. In Kombination mit Tunicamycin führte NLRC3 zu einer erhöhten ERSE Promotoraktivität. Diese Ergebnisse bringen NLRC3 in Zusammenhang mit den zellulären Mechanismen der Antwort auf Proteinfehlfaltung und damit schließlich zu mitochondrialen Stressreaktionen. Zudem konnte gezeigt werden, dass NLRC3 in WG Patienten herab reguliert ist. Für diese Arbeit wurden zusätzlich *Nlrc3*^{+/+} und *Nlrc3*^{-/-} Mäuse gezüchtet und in verschiedenen Experimenten untersucht. Die Zytokinpiegel in Makrophagen des murinen Knochenmarks unterschieden sich zwischen den beiden Genotypen nach Stimulation mit LPS. In einer DSS induzierten Kolitis konnte gezeigt werden, dass sich NLRC3 in Bezug auf Überlebensrate und Schwere der Krankheit positiv auswirkte.

Die vorliegenden Experimente erweitern deutlich das bisherige Wissen über NLRC3. Die protektive Wirkung von NLRC3 während Zellstress und Entzündung stellt einen bisher unbekanntem Aspekt des Wirkspektrums dar. NLRC3 ist dabei ein wichtiger Regulator der Immunmodulation.

2 Introduction

The human body is composed of approximately 10^{13} cells. At the same time the body is colonized by 10^{14} bacteria, representing up to 3 % of the total body mass [1, 2]. A mutualistic co-existence of host and microbes is based on the homeostatic relations between the two. To maintain the homeostasis the host needs effective monitoring systems to recognize imbalanced microbial compositions or bacteria/constituents like endotoxins or flagellin in "off limit" areas like the bloodstream or internal organs. A mutual gut bacterium beneficial to the hosts' gut may cause severe infections upon breaching the intestinal mucosa and reaching the bloodstream.

Within the human body, several barrier types occur. Barriers rely on chemical properties like pH values, on physical resistance as displayed by dermis or mucus, or on biological activities like anti microbial peptides [3, 4, 5, 6].

The mucus layer may be breached actively by pathogenic bacteria or passively due to a weakened mucus layer as observed in ulcerative colitis, where the stratified mucus layer becomes penetrable [7]. Thus the constant monitoring of the microbial load, search for invading pathogens and, if necessary a fast and appropriate response are achieved by the immune system.

2.1 The immune system

The immune system can be subdivided into two interacting parts - the innate and adaptive. The innate immune system is germ-line encoded, highly conserved, and the first to be activated. It relies mostly on a variety of conserved receptors and a set of responding cells, such as leukocytes, dendritic cells, and macrophages. The innate immune response, once triggered, is non-specific and does not provide memory for long lasting immunity.

The adaptive immune system develops during life, is strongly influenced by its environment, and relies on humoral and cellular components. The humoral response is based on specific antibodies and B lymphocytes honed against matching antigens. The cellular response is based on T lymphocytes. Both, the B and the T cells are key to immunological memory [8]. Additionally, the innate immune system elicits an immediate response in mere hours, in contrast to the adaptive immune response which may take days to weeks to fully form.

The immune system has three main functions: first the recognition of a diverse array of pathogens, such as pathogenic bacteria, viruses, fungi, and protists. Second, killing of those pathogens, and

third all the while tolerating the host [9]. Thus the immune system is also multi-layered surveillance and response mechanism to discriminate between pathogenic and mutualistic important bacteria [10].

The experiments and results presented in this thesis focus on the innate immune system.

2.1.1 Inflammation

Inflammation is a non-specific immune response of an organism toward injury [11]. Inflammatory processes may be divided in acute, described by an immediate onset and limited duration, and chronic with delayed onset and a potential life long duration. Clinical cardinal sinuses are since ancient times *rubor et calor cum tumor et dolor (et functio laesa)* [12]. Activating the innate immune system results generally in inflammation, recruitment of phagocytes and the reduction and release of a diverse repertoire of defensive molecules and substances like anti-microbial peptides and reactive oxygen species (ROS) [13, 14]. A malfunction of T lymphocytes or a dysregulation of cytokines and chemokines may lead to an uncontrolled inflammation reaction affecting both the adaptive and innate immune system [15]. Hence, research on molecular inflammatory processes is of importance for the understanding of innate immunity.

2.1.2 Pattern recognition receptors

The innate immune system enables eukaryotes to detect potential pathogenic elicitors along anatomical sites exposed to microbes and other pathogens. It relies on germline-encoded pattern recognition receptors (PRRs) to identify conserved molecular motifs among microbial species, known as pathogen-associated molecular patterns (PAMPs), and danger/damage-associated molecular patterns (DAMPs) [16]. PAMPs are a diverse and dynamic group of molecules, ranging from molecular CpGs to endotoxins, such as lipopolysaccharides (LPS) [17, 18]. DAMPs encompass endogenous molecules released from damaged cells as well as signals, such as pathogen-derived proteins, lipids, alterations of ion levels, crystalline materials, and cytosolic mitochondrial DNA (mtDNA) [19]. The most prominent non-clonal, germline-encoded PRRs are subdivided into five groups executing different functions. Toll-like receptors (TLR), retinoic acid inducible gene (RIG)-like receptors (RLR), absent in melanoma (AIM)-2-like receptors (ALRs), C-type lectins (CTLs), and Nucleotide-binding oligomerization domain and leucine-rich repeat containing (NOD)-like receptors (NLR) [19]. TLRs detect extracellular PAMPs, such as flagellin, LPS or intracellular viral RNA [20, 21, 22, 23]. RLRs are found to act as a receptor for dsRNA [24],

while ALRs detect cytosolic dsDNA [25]. CTLs are capable of binding terminal monosaccharide residues characteristic of bacterial and fungal cell surfaces [26]. NLRs are a diverse group and still not fully characterized. NLRs represent a group of receptors and mediators which are located within the cytosol, thereby acting as intracellular receptors for invading PAMPs and possibly for cytosolic DAMPs. In general, the activation of PRRs trigger the recruitment of adapter molecules or the initiation of signaling cascades leading to the regulation of cytokine and chemokine production [27].

2.1.3 NOD-like receptors

General domain architecture

NOD-like receptor proteins belong to the protein family of signal transduction ATPases with numerous domains (STAND) subclade of the AAA+ ATPase superfamily [28]. They are characterized by a modular organization of three to four different structural elements. At the N-terminus highly-variable domains represent the most unique feature to distinguish the different protein family members. The N-terminus features acidic transactivation domains (AD), baculovirus inhibitor of apoptosis protein repeat (BIR)-like domains, caspase recruitment domains (CARD) or pyrin domains PYD domains [29, 30]. Most NLRs share the centrally located nucleotide-binding domain (NBD) or NACHT (NLR family apoptosis inhibitory protein, Class II transcription activator, Heterokaryon incompatibility-E, and Telomerase-associated protein-1). The C-terminus has a variable number of leucine-rich repeats (LRR). Some of this classifications are still matter of debate as for NLRC3, NLRC5, and NLRX1. The domain structures are given in Fig. 2.1.

General induction and response

NLRs play a crucial role in sensing invading pathogen components and in initiating a molecular defense cascade. A well observed, albeit not generally described mechanism of NLR induction is based upon ligand binding followed by conformational changes and oligomerization. The NLR-mediated response includes the attraction of leukocytes, activation of defensins, initiating a pro-inflammatory response, resulting in caspase-1 processing, forming inflammasomes, modulating immune functions, and playing crucial, albeit not fully understood roles in development [19, 31, 32, 33, 34, 35, 36].

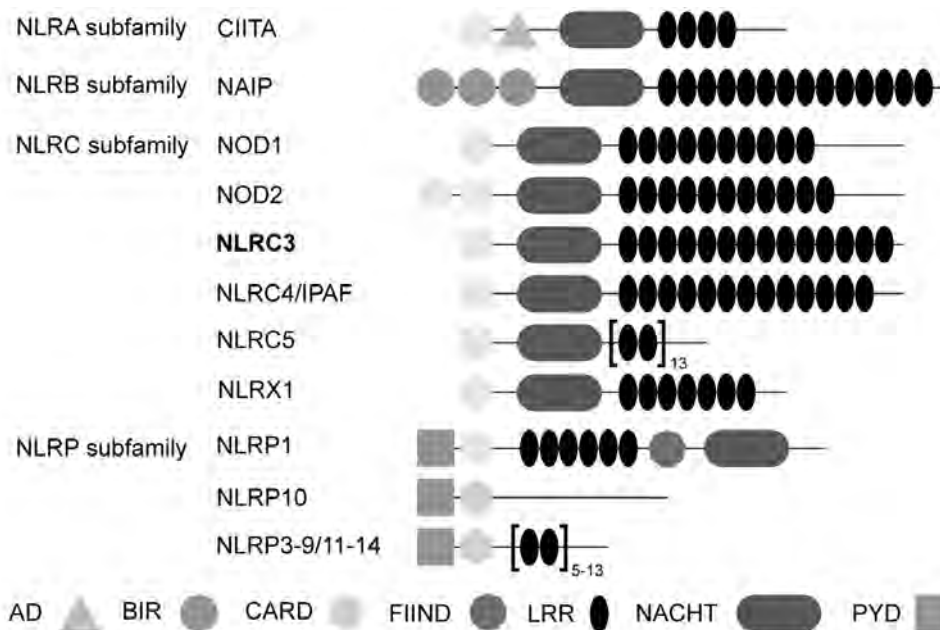


Fig. 2.1: Domain architecture of NLR proteins. The architecture of the human NLR family with regard to their domain organization and resulting subfamily structure. Abbreviations used: AD: acidic activation domain; BIR: baculovirus inhibitor of apoptosis protein repeat; CARD: caspase recruitment domain; CIITA: class II transcription activator; FIIND: function to find; LRR: leucine rich repeats; NACHT/NBD: nucleotide binding domain named for NAIP, CIITA, HET-E, and TP-1 protein families with this domain; NOD: Nucleotide-binding, oligomerization domain and leucine-rich repeat containing protein; NOD3: NLRC3; NLR: NOD-like receptor; PYD: pyrin domain.

General occurrence

NLR have been found in a variety of organisms from different kingdoms including fungi, plants, and animals. Higher plants contain up to 508 different NLRs while the human genome codes for about 23 different NLRs [37, 38, 39]. Molecular evidence suggests that NLRs evolved to a high pathogen specificity [40]. The tripartite structure of NLRs has been found in mammals to a high diversity and was discovered in plants, too. In animals, NLRs show a strong similarity to plant resistance proteins which recognize virulence factors [35, 41]. Since plants lack an adaptive immune system or any yet known specialized immune cells, they solely rely on the innate immune system to detect non-self components and combat against invading pathogens [42]. The recognition of invading pathogens in plants and the detection by R proteins is closely related to rapid cell death [43, 44].

General nomenclature

NLRs have been classified by two different systems. Schroder *et al.* distinguished the NLRs in three phylogenetic subclades (NOD, IPAF, and NLRP) [33], while others focused on a classification by additional domains [30, 45]. Due to a rising amount of members and therefore different

names, the NLR nomenclature has been standardized in 2008. The agreed nomenclature will be used as further reference [30].

2.1.4 Evolution of NLRs

Phylogenetic analysis indicates that NLRC3 is basal to all NACHT-domain containing proteins found in tetrapods [46]. Comparative analysis to the genomic sequences of chicken (*Gallus gallus*) led to the hypothesis that NOD3/NLRC3 is basal to the other groups of NACHT containing proteins and originated together with NOD1 and CIITA as a result of a gene duplication event before the bird-mammal divergence, which occurred approximately 310 million years ago [46, 47].

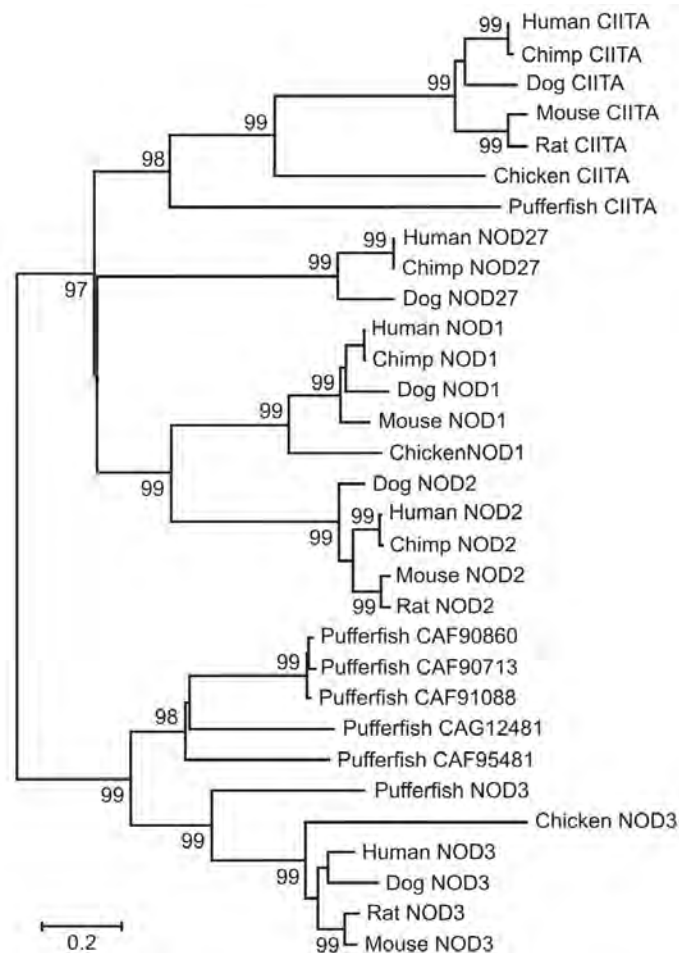


Fig. 2.2: Phylogenetic analysis of NACHT-domain containing proteins among tetrapods. Results derived from Hughes *et al.* [46]. Numbers on the branches are confidence level of standard error test; only values $\geq 95\%$ are shown. Abbreviations used: CAF/CAG: prefix of accession number; CIITA: class II transcription activator; NOD: nucleotide-binding oligomerization domain; NOD3: NLRC3.

Additionally, a more recent phylogenetic analysis on mammalian, zebrafish, and the catfish NLRs

by Shae *et al.* showed, that NLR family X1 (NLRX1), followed by NOD1 and NOD2 were most conserved among those analyzed, but NLRC3 (NOD3) seemed most divergent [48].

2.2 NOD-like receptor CARD domain containing 3 (NLRC3)

NLRC3 is a member of the NLRC family, a subfamily of the NLRs and was formerly known as NOD3 and CATERPILLER 16.2 (CLR16.2). The NLRC3 is conserved in vertebrates, from the zebrafish *Danio rerio* to *Homo sapiens* [49]. NLRC3 has been described as a cytosolic receptor of an unknown substrate, and it was shown to be a negative regulator of T cell function [50]. A recent study claimed that NLRC3 attenuates Toll-like receptor signaling via modification of the signaling adaptor TRAF6 and transcription factor nuclear factor κ -light-chain-enhancer of activated B cells (NF κ B) [51].

NLRC3 orthologues have been identified and studied in channel catfish (*Ictalurus punctatus*). NLRC3 found in kidney, intestine, spleen, and leukocytes in channel catfish lacked the structural and characteristic NACHT domain [48]. However, Rajendran *et al.* in 2011 were able to detect NLRC3 orthologs in other tissues and identified a truncated version with only four LRRs—markedly 11 LRRs less than previously identified variants. The expression levels of the truncated NLRC3 ortholog (named NOD3b) were analyzed in intestine, head kidney, spleen, and liver, and monitored during intracellular, gram-negative bacterial infection. Levels in intestine and head kidney were significantly down regulated, while up regulated in spleen and liver [52]. The receptor HmNLR in medical leech (*Hirudo medicinalis*) shows the highest homology to human NLRC3 and has been connected with neuroimmune functions [53].

2.2.1 Gene organisation

The human *NLRC3* gene is located on chromosome 16p13.3. It has 20 exons with the translation initiation in exon 1, and preceded by a 178 bp 5'UTR.

The murine *Nlrc3* is encoded on chromosome 16 (A1;16), and contains 18 exons with the initial start codon in exon 1 and followed by a 225 bp 5'UTR. The open reading frame is terminated in exon 18, followed by a 2442 bp 3'UTR. According to predictions a CARD domain is encoded by exon 2 [54]. Following those predictions a NACHT domain including two Walker B motifs is encoded by exon 3, the LRRs originate in the exons 5 to 14. The murine knockout variant generated for the experiments of this thesis contains a deletion of exons 2 and 3, which corresponds to a deletion of 2.5 kb of the whole gene and includes 1990 bp coding sequence (Fig. 6.1).

2.2.2 Domain architecture

Members of the NLR family are characteristically organized by modular domains. At the N-terminus is an effector binding domain followed by a central NOD domain, and at the C-terminus is a ligand recognition domain which contains mostly several LRRs. Some members like NOD1 (NLRC1), carry an additional NACHT-associated domain (NAD) [30]. Based on the first, albeit partial predicted sequence of NLRC3 in 2002 [55], this protein contains three characteristic domain motifs. Although there is ongoing discussion about the C-terminal effector domain, the central NACHT domain for protein oligomerization and the LRR are widely accepted (Fig. 2.3).

Effector domain

Currently the architecture of the NLRC3 effector domain at the N-terminus remains uncertain. Ting *et al.* proposed a CARD-NACHT-NAD-LRR structure in 2008, whereas Chen *et al.* and several others published an X-NOD-LRR organization, where X represents a heretofore undefined domain [27, 30, 56, 57]. Analysis of the gene organization in channel catfish *Ictalurus punctatus* showed no effector domain, but an additional LRR compared to the human sequence [48]. Neither the human nor the murine sequence stored in NCBI (www.ncbi.nlm.nih.gov) and uniprot (www.uniprot.org) databases are indicating a CARD domain structure. CARD domains are structurally related to death domains and death effector domains, having a similar size and secondary structure [58]. A structure based multiple sequence alignment of CARD domains indicated, that NLRC3 does possess a CARD domain. The authors also indicated that the findings by Ting *et al.*, the published human cDNA clone of NLRC3, referred to as CLR16.2 included two striking differences: a point mutation Q41H and a N-terminal truncation of 47 amino acids (aa). These differences detected by Albrecht *et al.* may prove to be crucial for the folding and function of the CARD domain [59]. Thus, due to the discordant identity of the N-terminal sequence, the characterization of the NLRC3 effector domain is of importance to understand its function in downstream signaling.



Fig. 2.3: Domain structure of NLRC3. The domain structure of NLRC3 can be subdivided in three major motifs- the N-terminal effector domain, the central NACHT domain capable for oligomerization and the C-terminal LRR responsible for ligand binding. The existence of a CARD or yet to be defined domain at the N-terminus and a NAD domain are still under investigation.

Oligomerization domain

It has been proposed that upon recognition of PAMPs by the LRRs, NLR proteins oligomerize via the NACHT domain leading to the recruitment or activation of downstream target proteins through its effector domain [29, 60]. The centrally-located NACHT domain is encoded by a single exon and has been found to be involved in the oligomerization processes in the presence of ATP [61]. However it is still unclear whether it allows for homo- or hetero-oligomers.

Ligand binding domain

The 14 LRRs at the C-terminus of the NLRC3 protein are assigned for binding of ligands. Each LRR is encoded by one exon. Upon comparison of the similar, horseshoe-shaped structures of the ligand binding domain LRRs, Istomin *et al.* concluded, that the specificity of LRRs seems to depend on surface properties, such as hydrophobicity, charge, and glycosylation sites [62]. The phylogenetic analysis showed that NLRC3 clusters to NLRC1 and NLRC2 and a little more distant to NLRC4 and CIITA. The same study revealed that NLRC3 contains ten consensus N-glycosylation sites, which is a markedly higher amount compared to all other NLRCs, with none to two sites. The hydropathy plot of NLRC3 is similar to NALP3, but no similarities within the whole NLRC protein group were obvious when considering charge distribution.

Studies indicate that NLRs might be negatively regulated by their LRRs [40]. Thus far, no prediction of putative ligands have been made, but it was hypothesized that LRRs may either bind ligands/DAMPs or possibly some intermediate molecules [62, 63]. In fact, LRRs are found in a variety of other proteins and confer different roles, such as ligand binding and general structure.

2.2.3 Protein expression

The human NLRC3 protein is localized in the cytosol and is expressed as four isoforms of different length due to alternative splicing (Fig. 6.1).

Isoform 1 was chosen as canonical sequence with 1065 aa and of 114.7 kDa size according to the uniprot database. For the second isoform with 1111 aa and 119.4 kDa markedly differs from isoform 1 at the initial methionine, which has been replaced by a 47 aa long sequence. Isoform 3 of 761 aa and 83.5 kDa size contains an alternate sequence at aa positions 728 - 761 and is missing aa from 762 - 1065. The 1037 aa long isoform 4 lacks the canonical aa sequence from 869 - 896. The latter two isoforms have not been experimentally confirmed yet. All sequences are stored in the public available uniprot database under the identifier Q7RTR2-X (with X being the numerator

for the isoforms).

In contrast, the murine *Nlrc3* is expressed as five murine isoforms although isoforms 3 to 5 are not experimentally confirmed yet (Fig. 6.1). The sequences are saved under the identifier Q5DU56-X in the uniprot database. Isoform 1 with 1064 aa and 116 kDa size is regarded as the canonical sequence. Isoform 2 with 726 aa and 80.8 kDa size differs at three sequences with respect to isoform 1, where aa sequences 1 - 27 and 643 - 688 are altered and 689 - 1064 are missing. Isoform three is truncated to 397 aa and 41.7 kDa where the aa sequence from 1 - 677 is missing and altered from 668 - 670. Isoform 4 is equally truncated to 312 aa and 32.9 kDa size and aa 679 has been changed from D to E and the isoform lacks the canonical sequence representing aa 980 - 1064. The last known isoform of 239 aa and 25.5 kDa lacks the aa sequence and 876 - 1064, 1 - 636 and has two substitutions 637 - 641 and 841 - 875 respectively. The aa sequence 876 - 1064 is missing compared to the canonical isoform.

The canonical sequence is conserved in human, chimpanzee, dog, cow, mouse, rat, and zebrafish. The homology between mouse and human canonical sequences is 80 %. Representative diagrams of the isoforms are shown in the chapter Supplement (chapter 6).

2.2.4 Function of NLRC3

It has been stated that NLRC3 is a negative regulator of T cell function and a proposed negative regulatory role via the NF κ B pathway [50]. Results from a previously performed Y2H screen indicated an interaction of NLRC3 with the mitochondrial protein IMMT. Additionally, the involvement of several NLRs in pathways finally leading to apoptosis, either in an enhancing or in an inducing way, has been published [64, 65, 66, 67]. Recent studies indicated, that NLRs may exhibit functions beyond the mere recognition of pathogens, such as maintaining tissue homeostasis and apoptosis [34]. With regard to methodical findings Ling *et al.* stated, that the overexpression of NLRC3 results in non-specific post-transcriptional inhibition of luciferase reporter assays [68].

2.3 Mitochondria

Mitochondria are one of the most important cell organelles. They are enclosed by two membrane layers, referred to simply as the outer and inner mitochondrial membranes. The former membrane structure is mainly responsible for selective transport. In contrast, the inner mitochondrial membrane forms a highly dynamic and extended network, forming cisterna structures in either a tubular or cristae way. This membrane is similar to bacterial membrane, which is hypothesized to be from

an endosymbiotic event in which a double-membrane proteobacterium was engulfed by a precursor eukaryote. By this event the eukaryote cell gained the capability of aerobic respiration [69]. The mitochondrial proteome consists of approximately 1513 proteins, of which 13 are encoded by the mtDNA and roughly 1500 by the nuclear DNA [70]. The metabolic functions of mitochondria are diverse and the list of processes involving mitochondria is still growing. One of the central features of the mitochondria is the electron transport chain, which occurs along its inner membrane and generates adenosine triphosphate and NADPH.

In fact, some complexes of the electron transport chain are composed of mtDNA- and nuclear-encoded proteins. Thus, any disturbance of mtDNA or its encoded proteins would lead to mitochondrial stress as the nuclear encoded proteins would still be imported. Lacking a mitochondrial partner the proteins would fail to assemble appropriately, for instance in stoichiometric correct complexes. A strong control and regulatory mechanism, such as the mitochondrial unfolded protein response (mtUPR) evolved to detect specific mis- or unfolded mitochondrial proteins and to react upon those. A similar system is well known for the endoplasmic reticulum, called erUPR, but the perturbations that induce mtUPR do not induce erUPR [71]. Recent studies show, that mitochondria are also involved in cell signaling for cell death and innate immunity by serving as hubs for signaling interactions and regulating intracellular signaling molecules, such as ROS and Ca^{2+} [72]. ROS have been shown to modulate the NF κ B pathway [73]. They are either generated by complex I or III of the electron transport chain or by cellular members of the NOX/DUOX family [74, 75, 76, 77]. Additionally, mitochondria are able to release Ca^{2+} , cytochrome c, and, after lysis, mtDNA, which might be regarded as DAMPs that trigger downstream signaling cascades. The importance of mitochondria and its maintenance is further underlined by the fact that cells possess a system to dispose dysfunctional mitochondria. This lysosome dependent degradation of mitochondria is named mitophagy [78].

2.3.1 Inner mitochondrial membrane protein (IMMT)/Mitofilin

The inner mitochondrial membrane protein also referred to as Mitofilin is a 85 kDa mitochondrial protein. IMMT is anchored in the inner mitochondrial membrane by an N-terminal transmembrane segment, a large hydrophilic part, which contains predicted coiled-coil regions and a conserved C-terminal domain. The protein is exposed to the intermembrane space [79].

Downregulation of IMMT resulted in decreased cell proliferation and increased apoptosis, which indicates mitochondrial dysfunction. Although the mitochondrial fusion and fission was normal,

the inner membrane was disorganized and failed to form cristae. Amorphous cross-linked membrane stacks were observed instead [80]. The C-terminal domain, which is required for the appropriate cristae formation is also an essential linker to high-molecular weight complexes [81]. IMMT is an essential part of the mitochondrial inner membrane organizing system, a large protein complex of crucial importance for membrane architecture [82, 83, 84].

Additionally, IMMT has been shown to be involved in protein transport. The inner mitochondrial membrane consists of two morphologically distinct regions: the inner boundary membrane, which is in close proximity to the outer membrane, and a large tubular invagination of the cristae membranes [85, 86]. Studies have indicated that the inner boundary membrane and cristae domains are distinct subcompartments of the inner membrane, since these exhibit asymmetric protein distribution [87, 88]. Studies using a Yeast-2-hybrid screen indicated that two major components of the protein translocase of the outer membrane (TOM) are potential interaction partners of IMMT - the channel forming TOM40 and the central receptor TOM22 [89, 90, 91]. IMMT seemed to interact with several import and organizing pathways, since a knockout leads to various deficiencies. This indicates that IMMT is a central regulator of the translocation and mitochondrial organization [91]. Beside the translocation through the outer membrane via TOM, first indications appear for a lateral release of proteins by TOM. It has been hypothesized that some sequences promote a lateral release from the TOM complex. A lateral transfer has been shown experimentally, still lacking a full mechanistically understanding [92]. A protein transport by TOM might prove crucial for interactions between cytosolic and mitochondrial proteins, such as IMMT. In summary is IMMT an important protein for mitochondrial structure and protein import.

2.4 Cytokines and chemokines

As it becomes clear, that NLRC3 is involved in immune related signaling, it is necessary to introduce cytokines and chemokines as central members of the downstream immune response. Cytokines are secreted proteins with various functions that determine the nature of an immune response. By binding to their respective receptors of the innate immune system, cytokines can then trigger downstream signal cascades resulting in the activation of transcription factors, such as NF κ B, activator protein 1 (AP-1), and protein53 (p53). These transcription factors themselves enable the production of cytokines. The analysis of the exact function of each cytokine is complicated due to the complex interplay between signaling cascades occurring within a cell, as well as with different states of cellular development and phase of the immune response. First coined in

1979, interleukins (IL) are a diverse group of cytokines mostly perceived by cell surface receptors [93]. In contrast to hormones they act generally in a para- or autocrine manner. Currently, there are 55 known IL and IL-related genes [94]. Further characterization of IL-genes via sequence analysis is hindered by the poor amino acid conservation. A study has shown that seven out of the 25 most divergent genes were cytokines [94, 95]. Cytokines signal mostly via the JAK/STAT pathways, which involve a phosphorylation by a cytosolic tyrosine kinase, followed by dimerization and nuclear translocation. A variety of STAT proteins enable a cytokine-specific reaction [96, 97, 98]. The impact of cytokines on the NF κ B pathway is further described under section 2.5. The cytokines listed in the following are involved in known immune responses, and were analyzed in NLRC3 related experiments:

The **IL-1** cytokine family contains a group of eleven cytokines which share a conserved β -trefoil structure of 12 packed β -sheets [99]. The major function of IL-1 is to activate T lymphocytes by enhancing the production of IL-2 [100]. IL-1 is considered to be a pro-inflammatory interleukin, its absence is marked by a diminished immune response. The work presented here is focused on IL-1 β . IL-1 β is inducible by LPS stimuli via the inflammasome. The induced precursor protein has to be cleaved by caspase-1 to become the active form primarily secreted by stimulated monocytes and macrophages [101, 102].

IL-1 β has already been described in functional context with members of the NLR group (NLRC4, NLRP3) as inflammasome assembly activates pro-caspase-1 which can process IL-1 β and IL-18 [33].

IL-2 is one of the first cytokines identified and characterized [103] featuring a four-helix bundle motif [94]. It has been described as a mediator for T cell homeostasis and differentiation [104]. IL-2 is neither strictly pro- nor anti-inflammatory as it is involved in the production of various cytokines, such as interferon- γ and IL-4 [105]. IL-2 transcription can be abrogated in NOD2- and NLRP3-deficient dendritic cells by stimulation with monosodium urate [106].

IL-6 is a monomeric protein member of a group of long-chain class 1 helical cytokines. It binds to the dimeric receptor IL6R α and associated with another dimeric receptor IL6ST (gp130) in a cooperative manner, forming a special hexameric signaling complex [94]. Recent studies indicate, that IL-6 has a double sided effect on inflammatory pathways. Depending on its targeted receptor

one has to distinguish the *classic* signaling via a membrane bound receptor and the *trans-signaling* via a soluble receptor. Latter seems to promote pro-inflammatory signaling, while the classic way seems to support anti-inflammatory processes [107]. IL-6 is mainly produced by mononuclear phagocytic cells, but is also produced by T and B lymphocytes, and bone marrow cells [108]. IL-6 can be regarded as a key player during the early state of immune response through its involvement in the T cell activation and differentiation [109]. The presence of LPS, an unique feature of gram-negative bacteria, is a known inducer of NLR mediated IL-6 activation [61].

IL-10 was first described as an inhibitor of T helper 1 lymphocyte (TH1) cytokine expression and is one of the best studied anti-inflammatory interleukines [110, 111]. Structurally, IL-10 is characterized by six α -helices in anti-parallel conformation [112]. The anti-inflammatory function of IL-10 has been described for monocytes and dendritic cells in its ability to limit cytokine and chemokine production activated by TLR agonists, such as LPS and bacterial lipoproteins. Upon LPS stimulation of monocytes IL-10 forms a homodimer resulting in a reduction of CD40 ligand and activation of MAPK pathways [113, 114, 115]. IL-10 was able to block NF κ B activation in response to IL-1 β and was shown to reduce I κ B degradation [113, 116]. STAT3 mediated signaling of IL-10 plays a major role in dampening the TNF α induced inflammatory events [117]. Nevertheless, IL-10 may react differently depending on stimulus level and cell type [118].

IL-12 is an interleukin with a bundle of four α -helices, which is encoded by the genes IL-12A (p35) and IL-12B (p40) [119]. Its structure is comparable to IL-6. IL-12 is mostly produced by dendritic cells, but not in B cells [120, 121]. It is important for T cell differentiation, is able to recruit natural killer cells, and plays a major role in the activation of interferon- γ production via STAT pathway [100, 122, 123]. Furthermore it is discussed as anti-tumor agent [124, 125].

Tumor necrosis factor α (TNF α) is a cytokine produced by a variety of cells, including mononuclear cells, natural killer cells, and lymphocytes [126]. TNF α is a homotrimeric transmembrane protein, which is processed by the TNF α -converting enzyme. The soluble form of TNF α is cleaved and mediates its biological activities through binding to types 1 and 2 TNF receptors (TNF-R1 and -R2) [127, 128]. TNF α secretion can be induced by peptidoglycans, lipopolysaccharides, and bacterial DNA CpG motifs that are bound by TLRs [129, 130]. It signals via the TNF receptor, more precisely, by either a TNF-associated factor or a death domain, which is a member of the same

protein superfamily as CARD [131]. The main immune function of TNF α lies in coordinating a concerted cellular immune response of the up to 10^9 different B and T lymphocytes in a single host organism [129]. TNF α is a potent inducer of cell death and generally a pro-inflammatory cytokine. IL-10 induced TNF α expression has been shown to destabilize inflammatory gene transcripts [132].

One group of cytokines are the small chemokines responsible for attracting immune cells to appropriate sites via chemotaxis. Chemokines were first described in 1977 and characterization has revealed over 50 known chemokines with leukocyte chemotactic and cytokine-like activities [133, 134]. In contrast to cytokines and interleukins which utilize cytosolic tyrosine kinases-mediated signaling, chemokines dependent on G proteins [135]. However, the structural homology between the murine and human form is matter of debate [136].

The murine IL-8 is named **CXCL1**, after a specific CXC motif and was formerly known as KC [137]. The dimer is composed of a six-stranded β -sheet and two parallel α -helices [138]. IL-8 is produced in mast cells, macrophages, and endothelial cells [139, 140, 141]. Human IL-8 is inducible by several stimuli, including oxidative stress, LPS, and TNF α [142, 143]. IL-8 was found to be increased in patients with an active ulcerative colitis [144].

2.5 NF κ B

As mentioned above, NLRC3 was proposed to have a negative regulatory function on the NF κ B (nuclear factor κ -light-chain-enhancer of activated B cells) pathway. NF κ B is one of the best studied and nearly ubiquitously expressed transcription factor of mammalian cells. It was first described in 1986 [145]. Mammalian cells possess five NF κ B family members: RelA (p65), RelB, c-Rel, as well as the two transcriptional inactive subunits NF κ B1 (p50) and NF κ B2 (p52) or their respective precursor proteins p100 and p105 [146, 147].

It has been widely accepted that NF κ B is a key regulator in cellular development and response to certain stimuli [148] and that these two processes are considered to be strongly interconnected. The basis of the work presented in this thesis is the involvement of NF κ B in response to stimuli and NLRC3 modulation. A multitude of signaling pathways result in the regulation of NF κ B, implying a complex regulatory system to ensure, that only the aimed effect is gained. Beside a huge variety of stimuli TNF α and ROS have been reviewed to activate NF κ B [149]. Additionally,

NF κ B is a central hub for most interleukins connected to inflammatory responses.

Two general pathways have been identified in NF κ B-mediated signaling. In the canonical pathway NF κ B is bound to its inhibitor I κ B α in the cytoplasm. Upon stimulation the I κ B kinase (IKK) complex consisting of IKK1/IKK α , IKK2/IKK β , and the regulatory subunit IKK γ (NF κ B essential modulator/NEMO) phosphorylates the inhibitory I κ B proteins. The phosphorylation is followed by a course of molecular events involving polyubiquitination of I κ B, its proteosomal degradation, and resulting in an accumulation of active NF κ B. The p50-p65 heterodimer of NF κ B translocates into the nucleus, whereupon it binds to the DNA allowing for transcription to initiate. The non-canonical way is mediated via the phosphorylation of IKK α , which phosphorylates a p100-RelB heterodimer. The phosphorylated precursor protein p100 undergoes ubiquitination followed by proteasomal processing to p52. It then translocates into the nucleus, binds to DNA, and initiates transcription [150, 151]. The NF κ B response to stimuli, such as LPS, is detectable within 30 minutes [145]. The impact of the NF κ B pathway and its constituents have been excessively studied in mice, including all major transgenic overexpressions or knockouts [152, 153] giving a thorough basis for further analysis.

2.6 Inflammatory bowel diseases

Ulcerative colitis and Crohn's disease are subsumed as inflammatory bowel diseases (IBD). IBD as a complex disease is characterized by acute exacerbations followed by remissions. It may display incidence rates of up to 16.8 (cases per 100000 inhabitants per year) depending on the study type and geographical location [154]. The cause of the disease is not fully understood, but several circumstances, such as environmental factors and genetic susceptibility loci seem to play an important role [155, 156]. Nevertheless are the symptoms well reflected by those described for induced murine colitis [157]. Knockout mice develop colitis resembling the human pathologies, such as ulcerative colitis (IL-2^{-/-} [158]) and Crohn's disease (IL-10^{-/-} [159]).

2.6.1 Dextran sulfate sodium induced colitis as mouse model for IBD

Dextran Sulfate Sodium (DSS) is a negatively charged long chain polymer of sulfated glucose. DSS has been described to potently induce colitis, leading to diarrhea, gross rectal bleeding, and weight loss in mice [160]. The molecular mechanisms underlying the DSS-induced colitis are not fully understood yet, but DSS is considered to effect directly the intestinal epithelial cells of the crypts disintegrating the mucosa. It was shown, that only the whole polymer is capable to induce

the colitis [161]. Additionally, disruption of cellular functions and inhibition of ribonucleases have been reported in association with DSS treatment [162, 163]. Laroui *et al.* proposed a negative effect of DSS on cell monolayer resistance, and showed that dextran-loaded nanoparticles were able to induce colitis [161]. DSS-induced colitis is high reproducible and provides a inducible mouse-model without major players of the adaptive immune system [164]. Nevertheless, manipulations of e.g. $\gamma\delta$ T cells are capable of an exacerbation of the disease [165]. In general an oral DSS administration (1 - 10 % solved in drinking water) leads to a disruption of the colonic epithelia, exposing the lamina propria to the gut bacteria [160, 166, 167, 168]. Murine colitis is an useful model for human ulcerative colitis, resembling the penetration of the inner colon mucus layer, which should be impenetrable [7].

2.7 Aim of this work

The aim of this study was the functional characterization of the NOD like receptor NLRC3. Only few studies have investigated the function of NLRC3 yet. To achieve a better understanding of the putative immune receptor NLRC3 following major tasks were assessed:

- Describing the NLRC3 impact on NF κ B signaling via dual luciferase assays and quantifying the interleukin level as the backbone of a functional characterization of NLRC3.
- Analyzing the molecular interaction of NLRC3 and Mitofilin and testing a potential impact of NLRC3 on mitochondrial integrity and apoptosis.
- Establishing and characterization of a *Nlrc3*^{-/-} mouse strain.

The experiments and results presented in this thesis are associated with the innate immune system, and therefore a focus will be set to the respective processes and signaling.

These questions and experimental setups aim at a more detailed understanding of the hitherto largely uncharacterized putative immune receptor NLRC3. Relating experimental data to clinical relevant diseases, enhances the importance of a close analysis of NLRC3. A broader analysis of its abilities and function may help to a better understanding of the complex signaling of the immune system.

3 Material and Methods

3.1 Materials and reagents

3.1.1 Plasmids and bacteria

The following tables are documenting the plasmids and Gateway vectors used for this project. The plasmid backbones, transfer vectors, and negative controls are given in Tab. 3.1 and the vectors cloned via the Gateway system are enlisted in Tab. 3.2. The One shot Top 10 bacteria used for transformation are further specified in Tab. 3.3.

Tab. 3.1: Basic constructs. The basic constructs were used as backbones for newly constructed vectors, as negative controls or for luciferase assay purposes. All constructs were suitable for expression in mammalian cells.

name	description	supplier
pCDNA3.1	vector backbone	Life Technologies
pDONR221	Gateway cloning vector with M13 sequencing site and kanamycin selection marker	Life Technologies
pcDNA-DEST53	Gateway cloning vector with green fluorescent protein gene for N-terminal fusion	Life Technologies
pCEV3.1	flag vector	Life Technologies
pNFκB-Luc	firefly luciferase under control of NFκB promoter	Clontech
pRL-TK	Renilla luciferase under control of thymidin kinase promoter	Promega

Tab. 3.2: Gateway cloned vectors, carrying an Amp^R. The basic constructs were used as backbone for specific vectors.

name	description
pDEST-NLRC3	NLRC3 with N-terminal GFP
pCEV-NLRC3	NLRC3 with 3 N-terminal flag-tags
pCEV-IMMT	IMMT with 3 N-terminal flag-tags
pCEV-NLRC3-CARD	NLRC3 CARD domain with 3 N-terminal flag-tags
pCEV-NLRC3-NACHT	NLRC3 NACHT domain with 3 N-terminal flag-tags
pCEV-NLRC3-LRR	NLRC3 LRR domain with 3 N-terminal flag-tags

3.1.2 Cell lines and media

Following media were used to maintain, cultivate, and transfect primary and secondary cell culture. Media were either used pure (indicated by *medium*^{-/-}) or supplemented with 10 % fetal calf

Tab. 3.3: Bacteria. TOP10 bacteria were used for all transformations. The exact specification is given.

name	description	supplier
Top10	<i>F-mcrA</i> $\Delta(mrr-hsdRMS-mcrBC)$ $\Phi 80lacZ\Delta M15$ $\Delta lacX74$ <i>recA1 araD139</i> $\Delta(araleu)7697$ <i>galU galK rpsL (StrR) endA1</i> <i>nupG</i>	Life Technologies

serum (FCS), glutamine, and 1 % penicillin/streptomycin (pen/strep) (indicated by *medium*^{+/+}). All basic media were bought from PAA Laboratories GmbH (Pasching, Germany). Tab. 3.4 summarizes which medium was used while cultivating the respective cell line. Additionally, OPTI-MEM (Invitrogen/Life Technologies, Darmstadt, Germany) was used for siRNA transfection.

Tab. 3.4: Cell lines. Cell lines used are enlisted with their respective media and reference. Some media were modified to fit specific needs and are indicated as sup(plemented). Basic media are Minimum Essential Medium (MEM), Dulbecco's Modified Eagle Medium (DMEM), Roswell Park Memorial Institute Medium (RPMI), and Mouse Macrophage Medium (MMM). References are given with respect to the accession number (ACC) of the Leibniz Institute DSMZ - German Collection of Microorganisms and Cell Cultures (DSMZ) and literature (lit.). ModeK cells were kindly provided by Prof. Dr. Dirk Haller, Munich. Media were supplemented with FCS, glutamine and pen/strep. The bone marrow derived macrophages (BMDM) medium was additionally enriched with amphotericin and Macrophage colony-stimulating factor.

name	description	medium	DSMZ	lit.
CaCo-2	human colon carcinoma cells	MEM ^{+/+}	ACC-169	[169]
HEK-293	human embryo kidney cells	DMEM ^{+/+}	ACC-305	[170]
HeLa	human cervix carcinoma cells	MEM ^{+/+}	ACC-57	[171]
HT-29	human colon adenocarcinoma cells	DMEM ^{+/+}	ACC-299	[172]
Jurkat	human T cell leukaemia	RPMI ^{+/+}	ACC-282	[173]
THP-1	human acute monocytic leukaemia	RPMI ^{+/+}	ACC-16	[174]
ModeK	murine duodenum cells	sup. DMEM ^{+/+}		[175]
RAW 264.7	murine leukemic monocyte macrophage	sup. DMEM ^{+/+}		[176]
BMDM	murine bone marrow derived macrophages	MMM ^{+/+} + DMEM ^{+/+}		

3.1.3 Oligonucleotides

Oligonucleotides are short, single stranded DNA molecules which were used for end-point PCRs and sequencing approaches. The name used in the documentation, the sequence, expected amplicon size, and melting temperature are given in Tab. 3.5.

Tab. 3.5: Oligonucleotides. The oligonucleotides were used for end-point PCRs and full length sequencing. Amplicon length were non applicable in sequencing approaches. The length may vary due to different inserts or due to the nature of templates (cDNA/gDNA).

Oligo name	sequence (5' → 3')	amplicon size [bp]	T _m [°C]
747 pDONR221-M13fwd	GTAAAACGACGGCCAG	variable	60
746 pDONR221-M13rev	GCCAGGAAACAGCTATGACC	variable	60
Ros1 Nod3_KO_PCR#3_F	GACTTCTCCCTGTGTCTCAGCCAGC	3048	63
Ros1 Nod3_KO_PCR#3_R	GCCCTTCAATGCCAACAGTTCTCC	3048	63
ROS1(Nod3)_KO_PCR#2_F	AGAGCCAGGGAAGCTGAGAGAAGTAGC	2309/2480 4804	63
ROS1(Nod3)_KO_PCR#2_R	CATGACCCCAAGCGTTGCTTACATC	4804	63
m10Nlrc3 f	GAAGAGCTGAGGGGCTGCAGTGA	300	60
m10Nlrc3 r	ATGTTGTCTCCTTCTGCCATGGTGGC	300	60
β-Actin f	GATCGGTGGCTCCATCCTGGC	130	64
β-Actin r	CGCAGCTCAGTAACAGTCCGCC	130	64
mGAPDH f	CCGGGGCTGGCATTGCTCTCA	160/279	64
mGAPDH r	CTTGCTCAGTGTCTTGCTGGGG	160/279	64
608_IMMT_1fwd	CTGCGGGCCTGTCAGTTATC	N/A	55
609_IMMT_2fwd	TACTCAGACAAACTCTTCGA	N/A	55
610_IMMT_3fwd	GATACTCCAGCTTCAGCAAC	N/A	55
611_IMMT_4fwd	GAAGTTGCAGCTCGCCTTGC	N/A	55
612_IMMT_5fwd	TTGAAGGAACGCAGAAAGGC	N/A	55
613_IMMT_6fwd	CTGGTGGTCCAAGCTCGGGA	N/A	55
614_IMMT_7fwd	GAAAAGCGGGCATTGACTC	N/A	55
615_IMMT_8fwd	GAATTACAATTTCTGCTGCT	N/A	55
616_IMMT_9fwd	GCCAACTGTTCTGATAATGA	N/A	55
617_IMMT_10fwd	TGCCCTGAGGATATAAACAC	N/A	55
618_IMMT_11fwd	GCACAGGACTGGCTGAAGGA	N/A	55
619_IMMT_1rev	CCCAGAGCTGCCTGAAGTAG	N/A	55

3.1.4 Antibodies and dyes

For Western blot applications the antibodies were diluted in 5 % skimmed milk powder. All other applications were carried out according to the respective protocol. The antibodies used for Western blot applications are enlisted in Tab. 3.6. Suitable secondary antibodies were purchased from Biomol (Hamburg, Germany) and diluted 1:2000. Cover slip staining were realized utilizing chem-

ical dyes and antibodies. The antibodies listed in Tab. 3.6 were used according Tab. 3.7.

Tab. 3.6: Primary antibodies. Western blots were incubated with unlabeled primary antibodies as listed below. The incubation time varied according to the application between one and 72 hours. Detection was enabled by the application of species specific HRP-coupled secondary antibodies. Abbreviation used: clon: conality; m: mono; p: poly.

name	origin	clon	WB-dilution	target	supplier	catalog
α - β -Actin	mouse	m	1:10000	human/mouse	Sigma-Aldrich	A-5441
α -IMMT	mouse	p	1:500	human	Abcam	ab48139
α -NLRC3	rabbit	p	1:250-1:500	human	Abcam	ab77817
α - β -Tubulin	rabbit	m	1:1000	human	Cell signaling	Kit 4753
α - β -flag	mouse	m	1:1000	human	Stratagene	200472
α -TRAF6	rabbit	m	1:1000	human/mouse	Abcam	ab33915
α -IgG	rabbit	N/A	<i>varied</i>	N/A	Santa-Cruz	sc-2027

To visualize cellular localization several dyes and antibodies were applied according to Tab. 3.7.

Tab. 3.7: Antibodies and dyes. Different dyes and antibodies were applied to the cells. Primary antibodies were detected by secondary antibodies, which were coupled to AlexaFluor fluorochromes purchased from Invitrogen. The respective secondary antibodies are indicated in the experiments. Nuclear staining was performed by DAPI or Syto-45, depending on choice of microscope.

antibody/dye	dilution	incubation time	supplier	catalog
Mitotracker	1:20000	30 min	Life Technologies	M-7512
DAPI	1:100000	10 min	Sigma-Aldrich	D9564
Syto-45	1:100000	10 min	Life Technologies	S11356
α -IMMT	1:500	60 min	Abcam	ab48139
α -NLRC3	1:500	60 min	Abcam	ab77817
α -IgG	equal to α -NLRC3	60 min	Santa-Cruz	sc-2027
α -flag	1:1000	60 min	Stratagene	200472

Several antibodies were tested for histological staining. The successfully tested antibodies are shown in Tab. 3.8. The antibodies against NLRC3 and IMMT failed in histological approaches.

Tab. 3.8: Antibodies for histological staining. Histological staining were conducted according to the Vectastain Elite staining protocol (Vector Laboratories, Burlingame, CA, USA). Primary antibodies not included in the kit are listed below.

name	origin	clon	dilution	target	supplier	catalog
α -TRAF6	rabbit	m	1:50-1:100	human/mouse	Abcam	ab33915
α -NF κ B p65 XP	rabbit	m	1:25-1:50	human/mouse	Cell signaling	8242

3.1.5 Buffer

Buffers were composed according to the list given in Tab. 3.9.

Tab. 3.9: Buffer list. The most important and frequently used buffers and their composition are listed. Buffers were composited ad 1 liter H₂O.

buffer	composition
anode buffer 1	30 mM Tris, 20 % (v/v) CH ₃ OH
anode buffer 2	300 mM Tris, 20 % (v/v) CH ₃ OH
cathode buffer	25 mM Tris, 20 % (v/v) CH ₃ OH, 40 mM NH ₂ (CH ₂) ₅ COOH
cell fractionation 1	10 mM C ₈ H ₁₈ N ₂ O ₄ S, 10 mM KCl, 1.5 mM MgCl ₂ , 10 mM NaF
cell fractionation 2	20 mM C ₈ H ₁₈ N ₂ O ₄ S, 420 mM NaCl, 1.5 mM MgCl ₂ , 0.2 mM C ₁₀ H ₁₆ N ₂ O ₈ , 25 % glycerol, 10 mM NaF
DLB	20 mM Tris/HCl (pH 7.4), 2 % (w/v) SDS
DNA loading dye	50 % (v/v) Glycerol, 0.1 % (w/v) C ₁₉ H ₁₀ Br ₄ O ₅ S, 0.1 % (w/v) C ₂₅ H ₂₇ N ₂ NaO ₆ S ₂
ELISA assay	8 g/l NaCl, 0.2 g/l KCl, 1.13 g/l Na ₂ HPO ₄ , 0.2 g/l KH ₂ PO ₄ , pH 7.4
ELISA stop	1.8 N H ₂ SO ₄
ELISA wash	9 g/l NaCl, 0.1 % (v/v) Tween20
LB Agar	10 g/l tryptone, 5 g/l yeast extract, 5 g/l NaCl, 15 g/l agar agar
LB Medium	10 g/l tryptone, 5 g/l yeast extract, 5 g/l NaCl
loading gel	0.5 M Tris/HCl (pH 6.8), 0.4 % (w/v) SDS
PBS	8 g/l NaCl, 0.2 g/l KCl, 1.56 g/l Na ₂ HPO ₄ , 0.24 g/l KH ₂ PO ₄ , pH 7.4
RIPA	150 mM NaCl, 1 % NP40, 0.5 % C ₂₄ H ₄₀ O ₄ , 0.1 % SDS, 50 mM Tris, pH 8.0
separation gel	1.5 M Tris/HCl (pH 8.8), 0.4 % (w/v) SDS
SOC	2 % (w/v) tryptone, 0.5 % (w/v) yeast extract, 10 mM NaCl, 2.5 mM KCl, 10 mM MgCl ₂ , 10 mM MgSO ₄
Stripping buffer	62.5 mM Tris (pH 6.8), 2 % SDS, HSCH ₂ CH ₂ OH (400 µl per 50 ml)
TAE (25x)	1 M Tris/HCl (pH 8.0), 25 mM EDTA, 500 mM CH ₃ CO ₂ H
TE	10 mM Tris/HCl, 1 mM EDTA
TTBS	20 mM Tris, 137 mM NaCl, 0.1 % (v/v) Tween20

3.2 Methods of molecular biology

3.2.1 Polymerase chain reaction

A polymerase chain reaction (PCR) aims to amplify short sequences of given cDNA or gDNA by the use of specific oligomers, Taq polymerase, dNTPs, and a supplemented buffer.

Oligomers

Oligomers used for PCR based analysis are given in Tab. 3.5. Oligomers were ordered from Microsynth (Balgach, Switzerland). The lyophilized oligomers were resolved in deionized water to 100 µM. The concentration of the working dilution was 10 µM for PCR, 5 µM for plasmid sequencing and 3.3 µM for PCR-product sequencing. Elongation time was estimated as 30 s per 500 bp of expected amplicon. The optimal annealing temperature was evaluated by gradient PCR.

PCR-Systems

Two different Taq-systems were used for end point PCRs. Genotyping of mice was based on the DREAM-Taq system (Thermo Scientific, Bremen, Germany), all other PCRs relied on the GoTaq system (Promega, Mannheim, Germany). The respective mastermix was composed according to manufacturer's guidelines. PCR was performed in 96 well Thermocyclers, T_m is given in Tab. 3.5. An overview of PCR mastermix composition and the cycling procedure is given in Tab. 3.10.

Tab. 3.10: Standard PCR conditions. The composition of a standardized mastermix is given in **A**. The general sequence of a PCR protocol is shown in **B**. The steps indicated in bold were repeated 35 times.

A	mixture		final conc.	B	temp. [°C]	t [s]	cycles
	H ₂ O	12.8 µl			95	240	1
	5x buffer	4 µl	1x		95	30	
	oligos (fwd & rev)	0.5 µl	0.5 µM		T_m	30	35
	dNTPs	0.5 µl	0.2 mM each		72	60 s/kb	
	GoTaq	0.2 µl	1 U		72	240	1
	template (cDNA)	2 µl			10	break	

Amplicons were checked for their size by agarose gel electrophoresis. Agarose gels were poured as 1 % gels in 0.5x TBE buffer (Rotiphorese TBE-Puffer, Carl Roth, Karlsruhe, Germany). Samples were loaded onto the gel and exposed to 400 mA, 130 V for 30 minutes. Size of amplicons was gained by comparing to SmartLadder (Eurogentec, Cologne, Germany).

Real-time quantitative qRT-PCR/TaqMan

The cDNA was adjusted to 2 ng/µl and replenished with water to 5 µl. After adding 4.5 µl Gene-Expression Mastermix and 0.5 µl Gene Expression TaqMan Assay (Life Technologies) the cyclor program according to Tab. 3.11 was applied on a 7900 HT Fast Real-Time PCR System (Applied Biosystems/Life Technologies Corporation, Carlsbad, USA).

All results were normalized to the respective β -Actin housekeeper value. TaqMan assays are indicated either in ΔC_t or in foldchange. Foldchanges relate all data to a reference, while ΔC_t are values more variable between experiments. A summary of experiments, as shown in the IL-screening of bone marrow derived macrophages (Fig. 4.21) has to be done in foldchanges to relate the experiments correctly.

Sanger sequencing

To determine the exact sequence of nucleotides in a plasmid or amplicon the dye-terminator se-

Tab. 3.11: Cyclor program and probe identification for qRT-PCR. The general PCR protocol is given in **A**. The probe identifier and supplier are given in **B**.

A				B		
temp. [°C]	t [s]	cycles		gene	catalog	supplier
50	120			Nlrc3	4331182	Life Technologies
95	600			IL-1 β	01336189	Life Technologies
95	15			IL-2	4331182	Life Technologies
60	60	45		IL-6	99999064	Life Technologies
				IL-10	00439614	Life Technologies
				IL-12	00434174	Life Technologies
				CXCL1	00433859	Life Technologies

quencing technique was applied. The method was based on the sequence method originally described by Sanger *et al.* [177]. In principle a template (amplicon, plasmid) was provided with a specific oligomer, DNA polymerase, supplemented buffer, and fluorescent labeled dideoxynucleotides (ddNTPs) as shown in Tab. 3.12. In the following PCR reaction the ddNTPs were incorporated into the amplicons resulting in a termination of the amplification. As the ddNTPs were labeled with a fluorescent dye specific for a nucleobase and the incorporation occurred randomly it resulted in amplicons of different length. Separating the amplicons by electrophoresis through thin capillaries and detecting their fluorescence by a laser enables the reading of the sequence.

Tab. 3.12: Sanger sequencing. **A** The composition of PCR mixes are given for plasmid or PCR amplicon templates. **B** The PCR program was used for both types of template. BigDye v1.1 was purchased from Life Technologies.

A			B			
	plasmid	PCR amplicon	temp. [°C]	t [s]	cycles	
PCR-H ₂ O	4 μ l	4.8 μ l	96	60	1	
BigDye v1.1	1.5 μ l	0.35 μ l	96	10		
single primer	1 μ l (5 pmol/ μ l)	1 μ l	50	5	25-30	
5x SB buffer	1 μ l	1.85 μ l	60	240		
template	min. 300 ng/2 μ l	2 μ l	10	break	1	

Genotyping

Genotyping was performed by interpreting the results of two different PCRs. Combining the results of both PCRs was a safe system to distinguish between homozygote wildtype (Nlrc3^{+/+}, WT) or knockout (Nlrc3^{-/-}, KO) animals as well as heterozygote mice (Nlrc3^{+/-}) as used during the back crossing events. An overview for the genotyping results is given in Tab. 3.13 and a generic genotyping result is shown in Fig. 3.1.

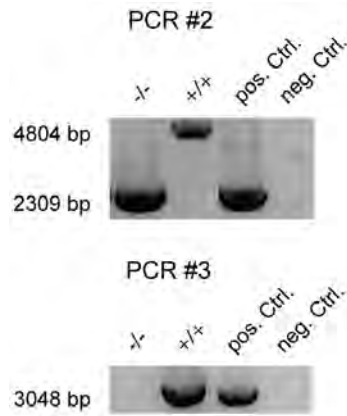


Fig. 3.1: Murine *Nlr3* genotyping. The gDNA was isolated from mouse ear clips or tail biopsies via Qiagen DNeasy kit and PCR was performed using Qiagen Dream-Taq, each according to manufacturer's protocols. Samples were loaded on a 1 % agarose gel and separated at 400 mA, 100 V for 45 minutes. Picture of gel with inverted gray scale.

Tab. 3.13: Amplicon length for murine genotyping PCR. PCR #2 Depending on the genotype bands were expected at 4804 bp (WT), 2309 bp, and 2480 bp (heterozygote) or 2309 bp (KO). **PCR #3** A band at 2048 bp is expected for WT and heterozygote samples, while KO sample do not show a band.

amplicon length [bp]		genotype
PCR #2	PCR #3	
4804	3048	+/+ (WT)
2309+	3048	+/-
2480		
2309	none	-/- (KO)

3.2.2 Gateway cloning

In order to overexpress NLRC3, IMMT, or single domains of NLRC3, in different experimental setups or to visualize its location, several inserts were cloned into a vector system carrying either a green fluorescent protein (GFP) or a flag-tag (Tab. 3.2). The cloning strategy was based upon the Gateway system (Life Technologies). Gateway cloning relied on recombination by λ enzymes.

First the inserts had to be generated. Therefore specific oligomers were generated which were extended by a 25 bp sequence giving an *attB*-recombination site. A PCR reaction was carried out, amplifying the target sequence, and prolonging it with the *attB*-recombination site. The amplicon was analyzed by gel electrophoresis and Sanger sequencing.

The successive cloning was subdivided in two cloning steps. First the amplicon had to be cloned into a donor vector (pDONR221). The components of the BP Clonase II reaction are given in Tab. 3.14 A. The formulation was incubated at 16°C overnight, followed by a Proteinase K treatment (1 μ l, 37°C, 15 minutes) to digest the phage enzymes. The ligated plasmids were transformed into TOP10 *Escherichia coli* (Invitrogen/Life Technologies). For transformation one shot TOP10 cells were thawed on ice. 15 μ l of the *Escherichia coli* suspension were supplemented with 1 μ l Proteinase K treated ligation mix and incubated for 30 minutes on ice. After applying a heat shock (42°C, 30 s) the cells were incubated in 250 μ l SOC-Medium (Life Technologies) at 37°C/300 rpm for at least 1 hour before they were plated on kanamycin supplemented agar plates and incubated overnight at 37°C. Single clones were picked after 24 hours and verified by PCR using vector binding M13 oligomers. Positive clones were transferred to a master plate and stored at 4°C.

Tab. 3.14: Gateway cloning mixtures. The composition of the **A** BP Clonase II and the subsequent **B** LR Clonase is given.

A BP Clonase II reaction		B LR Clonase reaction	
TE buffer	ad 10 μ l	TE buffer	ad 10 μ l
pDONR221	150 ng	pDONR221	200 ng
<i>attB</i> -PCR product	150 ng	pDEST-vector	300 ng
BP Clonase II	2 μ l	BP Clonase II	2 μ l

The second step of the Gateway cloning aimed at a transfer of the vector. The coding sequence of the target gene was transferred from the pDONR221 into a pDEST vector by LR-recombination. Therefore the plasmid DNA of a positive clone of the first reaction was isolated and mixed with the LR Clonase composition (Tab. 3.14 B). In general two pDEST vectors were used for the experiments displayed here, pDEST53 with a N-terminal GFP and pCEV3.1 containing three consecutive N-terminal flag-tags. The reaction was placed on ice for 30 minutes and then transformed in TOP10 *Escherichia coli* cells again.

3.2.3 Isolation of plasmids

Verified clones were transferred into a 15 ml falcon filled with 10 ml LB-Medium supplemented with 10 μ l ampicillin (100 mg/ml) or kanamycin (50 mg/ml) according to their respective resistance cassette. After incubating this pre-culture for 8 hours at 37°C/220 rpm it was dispensed into the main culture (100 ml, antibiotics as mentioned above) and cultured overnight on an orbital shaker. The next day the bacterial suspension was sedimented by centrifugation and processed with the PureLink kit (Invitrogen/Life Technologies) according to manufacturer's protocol. Prior to first preparation 340 μ l of bacterial suspension were mixed with 50 μ l glycerol and stored at -80°C as glycerol stock.

3.2.4 Purification from gel

To isolate dsDNA after purification in gel the QIAQuick Gel Extraction Kit (Qiagen, Hilden, Germany) was applied. The target band was excised from the gel and dissolved in buffer. The spin-column approach provided a quick binding to a silica membrane in presence of high salt content. After washing steps the DNA was eluted in H₂O. The purified DNA was further used in cloning experiments or Sanger sequencing.

3.2.5 RNA isolation and cDNA synthesis

RNA was isolated from tissue, organ sections or cell culture by the RNeasy Kit (Qiagen). In brief: Frozen organs and tissues were disrupted by mortar and pestle prior to the application. Ground tissue/cells were lysed in a guanidine-thiocyanate-containing buffer supplemented with 1 % β -mercaptoethanol. After passing through a shredder column the eluate was mixed with ethanol to enable binding to a silica-based, column bound membrane. Several washing steps and two successive DNase digestion steps were performed prior to eluting the pure RNA in water. After quality check and concentration measurement by NanoDrop the RNA was transcribed via RevertAid Premium Reverse Transcriptase (Thermo Fisher Scientific, Rockford, USA). Transcription performance was monitored by GAPDH PCR. Results shown in Fig. 4.2 were gained from purchased cDNA (Clontech, Saint-Germain-en-Laye, France).

3.2.6 Analysis of proteins

Protein lysate

Depending on the cell type (suspension/adherent) the cells were either scraped with a rubber scraper or sedimented by centrifugation. The cells were washed in PBS to remove any proteins from the serum containing media and lysed in 1x DLB buffer, supplemented with 2 % protease inhibitor cocktail and 1 % phosphatase inhibitor. After heating up the lysate for 5 minutes to 95°C, they were sonicated and finally centrifuged (15 minutes, 16000 xg, 4°C) to sediment cell debris. The supernatant was transferred to a new tube and protein concentration measured via Lowry assay according to manual (Bio-Rad, Munich, Germany). Protein quantification in this assay was based on the work of Lowry *et al.* [178] and composed of a two-step reaction. A Biuret reaction, where copper ions react with peptide bonds in an alkaline milieu under formation of a blue complex was followed by the reduction of Cu(II) to Cu(I) which itself reduced the yellow Folin-Ciocalteu reagent to molybdenum blue. This staining could be measured photometrically at $\lambda=650$ nm. A standard curve based on known BSA concentrations was used to quantify the measurements. Proteins were adjusted to a concentration of 1 $\mu\text{g}/\mu\text{l}$ by adding PBS and 5x sample buffer.

Sodium dodecyl sulfate polyacrylamide gel electrophoresis

Separating proteins according to their molecular weight was achieved by sodium dodecyl sulfate polyacrylamide gel electrophoresis (SDS-PAGEs). This technique was based upon the findings of

Laemmli *et al.* [179]. A SDS-PAGE consisted of two directly consecutive gels. The stacking gel (3 % w/v polyacrylamide) took up the samples and focused them in the applied electric current. The separation gel (7.5 to 15 % w/v polyacrylamide) could be passed faster by proteins with a lower molecular weight. Depending on the system used a full separation of proteins between 15 and 150 kDa was achieved after 120 minutes (300 W, 300 V, 25 mA). Some samples were separated on ice cooled pre-cast TGX gels (Bio-Rad) using following parameters: 500 W, 200 V, and 2500 mA for 45 minutes. If not otherwise specified 7.5 % SDS gels were poured, and run in TBS buffer.

Western blot

To identify the proteins via antibody treatment the proteins had to be transferred from the SDS-gel to a polyvinylidene fluoride (PVDF) membrane. A PVDF membrane was trimmed and activated for 5 seconds in methanol. After washing in distilled water it was incubated in anode-buffer 1. Three Whatman filter (Biomera, Göttingen, Germany) were cut in shape and soaked in anode-buffer 1, 2 or cathode-buffer respectively. The Western blot stack was assembled in following order (cathode-anode): cathode filter, SDS gel, PVDF membrane, anode filter 1, anode filter 2. Blotting was performed in a Trans Blot Turbo (Bio-Rad) with 300 V, 300 W, and 0.8 mA/cm² membrane for 90 minutes. After blotting the membrane was blocked in a 5 % skimmed non-fat milk powder (Bio-Rad) solution. Blocking was followed by incubating the blot in primary antibody, washing in TTBS, incubation for 40 minutes with horseradish peroxidase (HRP)-coupled secondary antibody, washing with TTBS, and finally incubating in ECL plus (GE Healthcare, Freiburg, Germany) solution and developing on x-ray sensitive film.

Mass spectrometry

To investigate the protein composition of lysates and to confirm bands in SDS gels a MS/MS run was performed on a LTQ Orbitrap Velos with ETD Support & UltiMate 3000 nano-HPLC system (Dionex, Germering, Germany). After picking samples from a Coomassie stained SDS gel the samples were separated and analyzed by reverse-phase liquid chromatography. Therefore the samples were loaded on a PrepMap C₁₈ trap column (Dionex), desalted and washed. After eluting proteins to the analytic column Acclaim PepMap100 C₁₈ (Dionex) two eluates (formic acid and formic acid/acetonitrile) were applied in a linear gradient pattern. The eluted peptides were analyzed on a LTQ Orbitrap Velos mass spectrometer (Thermo Scientific) equipped with a

nano-electrospray ion source. The analysis was performed by D. Linke at the Institute of Experimental Medicine (Kiel, Germany) under supervision of Prof. Dr. A. Tholey.

Co-Immunoprecipitation

To elucidate potential protein-protein interactions several Co-Immunoprecipitations were carried out. This method relied on primary antibodies bound to agarose beads. Adding those beads to a cell lysate would result in the binding of the antibody target protein. After sedimentation of the beads, the antibody bound proteins could be purified and stripped off the beads afterwards. The proteins precipitated could be either pure or still binding their interaction partner. This was verified by SDS-PAGE and Western blot, being incubated with an antibody targeting the interaction partner. To enhance specificity and purity several pre-clearing steps and washing steps had to be performed.

3.2.7 Coverslip staining

Cells were seeded into 6 well plates on sterile coverslips, transfected after 24 hours and washed after 48 hours with pre-warmed medium. In the following, cells were incubated with live cell stains, such as Mitotracker (Life Technologies). Fixation was achieved by adding 4 % paraformaldehyde in PBS for 30 minutes, followed by three PBS washing steps. The cells were blocked and permeabilized for 1 hour in PBS supplemented with 0.75 % bovine serum albumine and 0.1 % Triton-X 100 (Carl Roth). Primary antibodies were diluted to their respective concentrations and applied according to Tab. 3.7. The incubation was followed by washing steps and the incubation with secondary antibodies for 45 minutes. The incubation was finalized by three washing steps and a nuclear staining with DAPI if applicable. Coverslips were lifted with forceps and inversely mounted onto a glass slide with Dako Fluorescent mounting medium (Dako, Glostrup, Denmark). Staining and fluorescence were analyzed via Confocal laser scanning microscopy or wide field-fluorescence microscopy. Samples were stored at 4°C in the dark afterwards.

Tab. 3.15: Microscopes. Three different microscopes were used. A confocal laser scanner microscope, a wide field-fluorescence microscope and an inverse light microscope.

type	model	manufacturer
CLSM	TCS SP5	Leica
Fluorescence	AxioImager.Z1	Zeiss
Inverse light	h500	Hund

3.3 Methods of cell biology

3.3.1 Cell culture

All human immortalized cell lines were provided by the "Deutsche Sammlung für Mikroorganismen und Zellkulturen GmbH" (DSMZ, Braunschweig, Germany).

Maintenance of cells

Work on cell lines, both maintaining and experimental, were conducted under a laminar flow bench (HeraSafe, Heraeus Instruments GmbH, Hanau, Germany) under strict observation of germ-free working. All materials, buffer, media, and chemicals were either filtered, autoclaved or thoroughly wiped with 70 % ethanol (or respective commercial available disinfectant) prior to work. For cultivation, cells in media were exposed to 37°C, 5 % CO₂. Cells were visually inspected twice a week via an inverse microscope and split at 80 % confluence. For passaging, the cells were washed with pre-warmed PBS (Gibco/Life Technologies) and trypsinized for 5 minutes with 1x Trypsin/EDTA (Life Technologies). Exceptions were made for either RAW 264.7 cells, which were scraped or confluent cells which were solely centrifuged. The reaction was stopped by adding serum containing media and transferring the suspension to a 50 ml reaction tube. Cells were sedimented by centrifugation at 600 xg for 5 minutes (Heraeus). The cells were resuspended in medium, counted, and diluted 1:4 to 1:6 in a 25 ml cell culture flask (Falcon, Heidelberg, Germany). Cells were passaged maximal 25 times. Cell counts were carried out using a Cellometer Auto T4 (Nexcelom Bioscience, Lawrence, USA).

Isolation of Peripheral Blood Mononuclear Cells (PBMCs)

Peripheral blood mononuclear cells were isolated from human blood samples of voluntary donors. The samples were applied on a Ficoll 400 kDa, poly sucrose 400 d:1.077 g/ml gradient (Biochrom AG, Berlin, Germany). After centrifugation the interphase, containing lymphocytes together with monocytes and platelets (buffy coat) was extracted and transferred to a new tube. Cells were washed with PBS, sedimented and cultivated in RPMI^{+/+}.

Cells in experiments

According to the experimental requirements cells were seeded into 10 ml dishes to 96 well plates according to Tab. 3.16. For coverslip staining cells were seeded in a 6 well format onto a flame disinfected coverslip. Live cell imaging was performed using Lab-Tek chamber slides from Thermo Scientific.

Tab. 3.16: Cell dilution and media volume. According to experimental needs, cells were seeded into following dishes.

format	10 ml	6 well	12 well	24 well	96 well
volume medium [μ l]	10000	2000	1000	500	100
cell count					
transfection	8×10^5	4×10^5	2×10^5	1×10^5	2×10^4
stimulation	1.2×10^6	6×10^5	3×10^5	1.5×10^5	2.5×10^4

3.3.2 Transfection

Plasmid transfection

Plasmids were transfected according to the FuGene 6 protocol (Roche, Basel, Switzerland). In brief: The FuGene transfection reagent was mixed with medium and pipetted upon the plasmid. The mixture was incubated for 30 minutes at room temperature and carefully dispensed upon the cells in their respective media afterwards. Follow up incubation was carried out at 37°C and 5 % CO₂ for 48 hours if not stated otherwise.

RNA interference and siRNA transfection

RNA interference (RNAi) is a process of post-transcriptional gene silencing where the transfection of small interfering RNAs (siRNA) into cells causes the destruction of messenger RNA (mRNA). The RNAi pathway itself occurs naturally in most eukaryotic cells, detecting dsRNA as a marker for i.e. dsRNA-virus intrusion. As the inhibition of gene expression could be achieved by injecting dsRNA directly into the larvae/adults of *Drosophila melanogaster* or *Caenorhabditis elegans*, those organisms became pioneering organisms in gene inhibition studies [180]. The direct injection of dsRNA into human cell culture was a not applicable method due to a strong interferon response [181, 182]. Reducing the size of the siRNA to 21 to 22 nucleotides and designing special complementary sequences resulted in a specific knockdown of genes [183]. If not other specified siRNAs were purchased from the silencer select product line (Life Technologies). Upon arrival the lyophilized siRNAs were solved in RNase free water to a concentration of 10 μ M. The siRNA transfection was carried out according to the siPORT Amine transfection protocol (Life Technologies). In brief: The siPORT Amine transfection reagent was diluted in OPTI-MEM medium, as were the siRNAs. After incubating both solutions for 10 minutes at room temperature they were combined and carefully dispensed onto the cells in their respective media, giving a final concentration of 5 nM siRNA. The plates were gently tilt to reach optimal mixing and incubated at 37°C and 5 % CO₂ for 48 hours if not stated otherwise.

3.3.3 Stimulation

Stimulation experiments were carried out according to Tab. 3.17.

Tab. 3.17: Stimulants. The LPS from the *Forschungszentrum Borstel* (Leibniz Institute) was provided by the group of Prof. Dr. U. Zähringer.

Stimulant	concentration	supplier	remarks
LPS			
Sigma-Aldrich	100 ng/ml	Sigma-Aldrich	L4524 <i>E. coli</i> 055:B5
Invivogen	100 ng/ml	Invivogen	Ultra Pue LPS <i>E. coli</i> K12
Borstel	100 ng/ml	Research Center Borstel	<i>E. coli</i> Nissle 1917 DSMO
various			
2C11	1 µg/ml	Inst. of Immunology	50 µl coating of wells
PHA	1 µg/ml	Sigma-Aldrich	
PMA	10 ng/ml	Sigma-Aldrich	
Ionomycin	200 ng/ml	Sigma-Aldrich	
TNFα	50 ng/ml	Invitrogen	single stimulation
TNFα	20 ng/ml	Invitrogen	co-stimulation
Tunicamycin	10 µg/ml	Calbiochem	

The stimulation experiments were designed in a way to be harvested at a common end point. This ensures, that the cells were all exposed to the same general cell culture conditions for an equal period of time.

3.3.4 Cell fractionation

Cell fractionation was achieved by a differential centrifugation protocol modified after Kwon *et al.* [184]. All buffers were supplemented with phosphatase and protease inhibitors. The cells were harvested and lysed (cell fractionation buffer 1, Tab. 3.9) on ice. The incubation was followed by shearing the cells via a 26G needle on a syringe. The lysate was centrifuged (10 minutes, 1000 xg, 4°C). The nuclei containing sediment was resuspended in cell fractionation buffer 2 and kept on ice for 30 minutes while the supernatant was further separated by centrifugation (45 minutes, 16000 xg, 4°C). The second pellet contained the cell membrane and was resuspended in PBS, while the supernatant provided the cytosolic fraction. All fractions were snap frozen in N₂(l).

3.3.5 Isolation of mitochondria

Mitochondria were isolated via the Abcam Mitochondria Isolation Kit (Abcam, Cambridge, UK) according to manufacturer's protocol. In brief: Cells were harvested, buffered, and lysed by 25

strokes of a Dounce homogenizer. The lysates were differentially centrifuged to receive a purified mitochondrial fraction.

3.3.6 Dual luciferase assay

The dual luciferase assay enables a quantification of NF κ B activation. Therefore the dual luciferase system relied on two plasmids. Plasmid A (pNF κ B-Luc, Clontech, Heidelberg, Germany) contained a luciferase originating from the firefly *Photinus pyralis*, plasmid B (pRL-TK, Promega, Madison, USA) a luciferase from the sea pansy *Renilla reniformis*. While the luciferase from plasmid A oxidized luciferin to oxiluciferin under emission of light with $\lambda=550$ to 570 nm, luciferase from plasmid B catalysed the oxidation of coelenterazine to coelenteramide under the emission of light with $\lambda=480$ nm. The luciferase of pNF κ B-Luc was under control of three NF κ B-consensus-enhancers, thus expressing the luciferase and therefore oxidizing luciferin directly depending to the intracellular NF κ B level. The luciferase of the pRL-TK was under the control of a thymidine-kinase promoter of a Herpes simplex virus. It was constitutively expressed in all transfected cells, thus giving a reliable value for cell viability and cell count. The firefly luciferase values were normalized to the *Renilla* values to achieve comparable results throughout the experiments. As both luciferases relied on different substrates and pH level this system was suitable for an automated read out by a GeniosPRO microplate reader (Tecan, Männedorf, Switzerland). Measurements were done on HEK-293 cells, seeded in 96 well plates and transfected 24 hours after seeding. Stimulation, if applicable, occurred 24 hours after transfection. After incubation the supernatant was discarded and the cells lysed in 1x passive lysis buffer (Promega). Lysate was transferred into a white 96 well plate. The luciferase substrates were mixed and applied according to manufacturer's protocol (Promega). Readout was conducted via a GeniosPRO microplate reader. The quotient of both luciferase activities was calculated and depicted as relative luciferase unit (RLU).

3.3.7 Enzyme-linked immunosorbent assay

Supernatant of stimulated cells were harvested to carry out enzyme-linked immunosorbent assay (ELISA). This antibody based technique facilitated the quantification of i.e. interleukins in the supernatant. In the present experiments CytoSet Kits were used according to manufacturer's protocol (Life Technologies). In brief: Nunc 8 well stripes (Thermo Scientific) were coated with a primary antibody overnight. After a blocking step the cell supernatant was applied for 1 hour, enabling the antibodies to bind their targets. After several washing steps a streptavidin HRP-coupled secondary

antibody was applied, followed by a washing step and the administration of a TMB-substrate solution. After 30 minutes the reaction was stopped by adding HCl. The absorbency at $\lambda=490$ nm was read out photometrically. Quantification was enabled by a standard series of recombinant target proteins processed in parallel.

3.3.8 MTS assay

The MTS assay was a non-radioactive, colorimetric cell-proliferation assay. The chemical 3-(4,5-dimethylthiazol-2-yl)-5-(3-carboxymethoxyphenyl)-2-(4-sulfophenyl)-2H-tetrazolium reacts in the presence of the electron coupling reagent phenazine methosulfate. In viable cells endogenous dehydrogenases were expressed leading to the conversion of MTS to the soluble formazan. The OD could be measured at $\lambda=490$ nm.

3.4 Generation of *Nlrc3*^{-/-} mice

To study the effect of *Nlrc3* in an *in vivo* system a knockout mouse model was generated. Due to a *Nlrc3*-gene size of approximately 38 kb, the deletion of the whole gene was not a suitable option. It has been agreed to target the exons 2 and 3 of *Nlrc3* instead, therefore deleting approximately 2.5 kb (1990 bp of the coding sequence). This deletion results in the loss of 661 aa, containing the potential CARD- and the NACHT-domain. The generation of a constitutive *Nlrc3* knockout was achieved by targeting and inserting a distal *loxP*-site and a FRT-neomycin-FRT-*loxP* cassette into intron 1 and 3. The overall deletion was achieved by two consecutive *in vivo* excisions. A summary of the cloning strategy and recombination events is given in Fig. 3.2.

A more detailed explanation of the homologous recombination and cloning strategy performed by genOway (Lyon, France) is given in the chapter Supplements (chapter 6). Having reached sexual maturity, the highly chimeric males were crossed with Flp deleter C57BL/6N females to enable the *in vivo* excision of the neomycin selection cassette. The heterozygous knockout F1 mice were validated by Southern blot. Therefore the genomic DNA was digested by PspOMI, blotted and hybridized with a 418 bp probe generated by PCR (5'-CTGAAGCAGTAGAACCACAGTAAGACTGAGAGG-3' and 5'-GAAGGTAATGCTCAAGTCAGGGCAGGC-3'). The WT resulted in a 6283 bp, the floxed in a 10512 bp fragment. The gained offspring was bred as constitutive knockout mice. Mice were backcrossed for nine generations onto a C57BL/6N background. The genotype was frequently checked during the breeding process by PCR. An example of the genotyping PCRs, enabling the

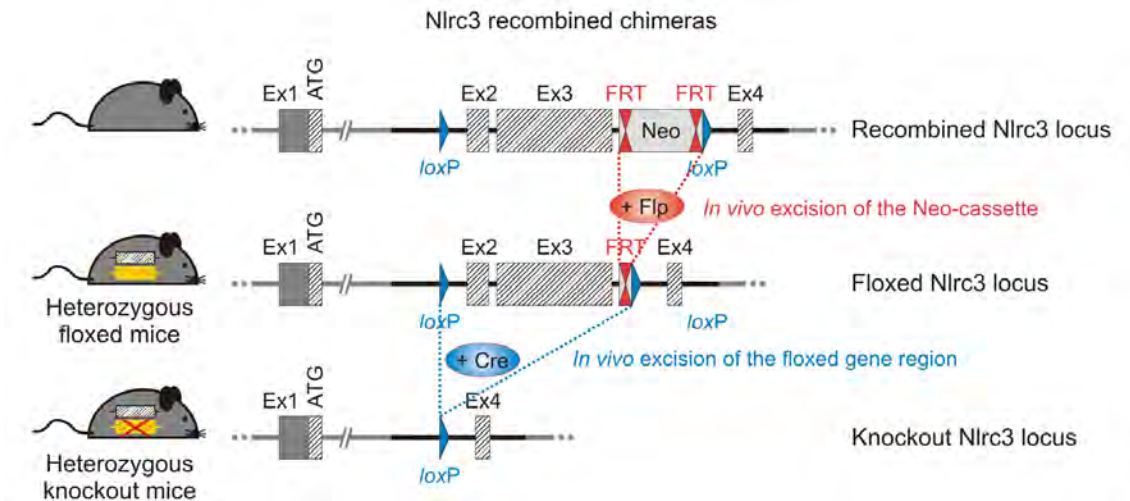


Fig. 3.2: Murine *Nlrc3* gene cloning. A summary of the cloning strategy and recombination events is given. The exons 2 and 3 were flanked by a *loxP*-site and a FRT-neomycin-FRT-*loxP* cassette. The Neo-cassette was excised *in vivo* to generate a floxed *Nlrc3* locus. Mating the floxed mice with Cre-mice resulted in the excision of the floxed gene region. Diagram is not depicted to scale. Boxes represent exons, solid lines intronic sequences.

distinction between WT and KO is given in Fig. 3.1, the oligomers are listed in Tab. 3.5. The mice were housed in a separated facility fulfilling SPF-standards according to Federation of European laboratory animal science associations (FELASA).

3.4.1 Handling of mice

Mice were kept in individually ventilated cages, up to maximal five litter mates per cage. A strict 12 hours/12 hours light cycle with 60 - 400 Lux was established and a temperature between 20 - 24°C maintained. Air humidity was kept at 55 % at a ventilation rate of 8 - 20 fold. IVC cages were bought from Bioscape GmbH (Castrop-Rauxel, Germany) or Tecniplast (Hohenpeißenberg, Germany). Tap water and standard caloric food were given *ad libitum*. Mice were bred in separated cages. After pregnancy of 21 days the offspring was separated from the mother by the age of 4 weeks and genotyped. All experiments were performed on animals aged between eight and sixteen weeks as they were considered adult and homeostatic. Animals were sacrificed by cervical dislocation.

All animal experiments were in concordance with federal law and monitored by an independent animal rights supervisor. Permits were issued by the authorities of the Ministry of Education and Science of Schleswig-Holstein.

3.4.2 Bone marrow derived macrophages

Murine bone marrow derived macrophages (BMDMs) are leukocytes derived from murine femur and tibiae bone marrow. These primary cells were a tremendous, unbiased model to study murine immune system related processes.

The mice were sacrificed by cervical dislocation. After removing femur and tibiae, they were stripped of any adherent material. The joints were cut off and the bone marrow was flushed out with BMDM medium (Fig. 3.4). After suspending the cells they were filtered through a 70 μm cell strainer, plated in 150 mm dishes, and cultivated at 37°C/5 % CO₂. Macrophage medium had to be supplemented with macrophage colony-stimulating factor. This lineage-specific growth factor enabled the proliferation and differentiation of committed myeloid progenitors into cells of the macrophage/monocyte lineage [185]. BMDMs were cultured for three days, than medium was replaced or replenished according to cell development. After about seven days (depending on visual inspection) the adherent cells were harvested, count, and seeded into appropriate cell culture dish according to Tab. 3.18.

Tab. 3.18: Cell density for BMDM experiments. Depending on experimental needs, the BMDMs were seeded according to this table.

format	10 ml	6 well	12 well	24 well	96 well
volume medium [μl]	10000	2000	1000	500	100
cell count	6×10^6	1×10^6	0.5×10^6	2.5×10^5	5×10^4

3.4.3 Mixed splenocytes

Murine mixed splenocytes were employed as a T cell model. Spleen was removed from sacrificed mice and pressed through a 70 μm cell strainer. Cells were suspended in RPMI^{+/+}, supplemented with 1 % of the antifungal agent amphotericin and 1 % glutamine. Cells were counted and plated to culture dishes according the experimental requirements.

3.4.4 Acute dextran sodium sulfate induced colitis

Procedure

Acute dextran sodium sulfate (DSS) colitis was slightly modified after Wirtz *et al.* [186]. Male C57BL/6 Nlrc3^{-/-} and C57BL/6 Nlrc3^{+/+} mice (aged 11 - 13 weeks) were housed in SPF-conditions according to FELASA standards. They were granted unlimited access to food pellets and drinking

water. Animals were kept in groups separated by their genotype but masked to the experimenter (8 WT, 9 KO, 3 KO-Ctrl.). Mice were given autoclaved tap water, supplemented with 4 % (w/v) DSS *ad libitum* for 5 days. The solution was changed once during this time to prevent bacterial growth in the water, water consumption was recorded. After 5 days with DSS administration the drinking water was replaced by pure autoclaved water. Mice were sacrificed upon day 8 or when reaching stop criteria. During the whole experiment three separated mice *Nlrc3^{-/-}* were fed consequently with autoclaved tap water as control.

Stop criteria

The three major features: obvious pain, weight loss >25 %, and death were assigned as stop criteria for each mouse. Upon reaching one criteria the mouse was taken from the experiment, sacrificed by cervical dislocation (if applicable), and further processed.

Daily scoring

Body weight measuring, occult blood in stool analysis, and stool consistence were checked and scored on a daily basis according to the parameters given in Tab. 3.19.

Tab. 3.19: Disease Activity Index (DAI). Rectal bleeding was scored via Haemocult test from Beckman Coulter (Krefeld, Germany).

DAI	weight loss [%]	stool consistency	rectal bleeding
0	0	formed	Hemocult neg.
1	1 - 5		
2	6 - 10	unformed	Hemocult pos.
3	11 - 20		
4	>20	liquid	visible

Final analysis

The mice were anesthetized with ketamine (100 mg/kg bodyweight) and xylazine (16 mg/kg bodyweight) to enable endoscopic examination. The parameters for scoring according the modified murine endoscopic index of colitis severity (MEICS) score [187] are given in Tab. 3.20. After endoscopy the still anesthetized mice were coronary punctured. The blood was kept clotting for 30 minutes and centrifuged for 5 min at 10000 xg to gain serum. The serum was snap frozen in N₂(l). Afterwards the mice were sacrificed by cervical dislocation. Organs were obtained and processed as followed:

- The spleen was weighted and its length measured. Afterwards one half was snap frozen, the other half was preserved in 10 % formaldehyde.
- Liver and mesenchymal lymph nodes were snap frozen.
- Colon was flushed with PBS, its length measured, and photographed. Subsequently the colon was cut longitudinally. A small piece was cut from the distal part and snap frozen. The rest was rolled up from distal to proximal, embedded into a Histo-cassette and stored under 10 % formaldehyde until further processing.
- The ileum was sampled and cut accordingly.

All snap frozen organs were ground and further processed as mentioned in subsection 3.2.5.

Tab. 3.20: Modified murine endoscopic index of colitis severity score. Proxies of the MEICS score modified after Becker *et al.* [187].

Score	Thickening of colon	Changes of vascular pattern	Fibrin visible	Granularity of mucosal surface	Stool consistency
0	transparent	normal	none	none	solid
1	moderate	moderate	moderate	moderate	still shaped
2	marked	marked	marked	marked	unshaped
3	nontransparent	bleeding	extreme	extreme	spread

3.4.5 Histology

The organs and histological rolls were fixed in 10 % neutral buffered formalin, dehydrated, and embedded in paraffin wax. Blocks were cut to 3.5 μm sections on a Leica RM 2255 microtome (Leica Microsystems, Wetzlar, Germany) and collected on microscope slides.

Hematoxylin and eosin staining (HE staining)

The histological sections were deparaffined in a decreasing alcoholic dilution series, stained in hemalum, and dyed in tap water. After staining with Eosin G the sections were dried in an increasing alcoholic series and preserved with Roti Histokit. Hemalum, a complex formed of aluminium ions and oxidized haematoxylin, functions as a DNA independent nuclear stain, which stains the rER, too. The synthetic acidic eosin Y eosinophilic stains structures, such as proteins of the cytoplasm, mitochondria, and sER in different intensities. All solutions were bought from Carl Roth.

DAB staining

The coverslips were prepared as mentioned above. The deparaffining was achieved by substituting paraffin with the xylol substitute Roti-Histol (Carl Roth), followed by incubation in a decreasing alcoholic dilution series, and washing in PBS. After saturating endogenous peroxidases by a 3 % H₂O₂ treatment the sections were blocked with the respective VectorStain Elite serum (VectorLab, Burlingame, USA). Primary antibody was applied in a humidified chamber to the sections and incubated overnight. Following several washing steps in PBS the sections were incubated with the corresponding biotinylated secondary antibody VectorStain (VectorLab) for 45 minutes. Successively the sections were washed, treated with the VECTASTAIN Elite ABC reagent, and finally incubated with a peroxidase substrate solution until the final brownish stain became visible. The reaction was stopped by PBS and aqua dest. washing steps. Counter staining was achieved by bathing the sections in haematoxylin (Carl Roth), blueing under rinsing tap water, drying in an increasing alcohol dilution series and embedding in mounting medium.

Additionally, the IMMT and NLRC3 antibody were tested for histological usage and found to be not suitable for this purpose.

3.4.6 Blood analysis

After sacrificing the mice, blood samples were taken from Nlrc3^{-/-} mice out of the heart or the main abdominal vein. Analysis was performed by ACCU-CHEK (Roche, Mannheim) for blood glucose [188] and by HPLC of EDTA-blood to measure HbA_{1c} levels. Coronal puncture of anesthetized mice was not suitable, as it has been shown, that different agents heavily impact blood glucose level [189].

3.5 Statistical analysis

All quantitative numeric data were tested for statistical outlier, using QuickCalcs Outlier Calculator (GraphPad Software Inc., La Jolla, USA). A value of $\alpha=0.05$ was taken as confidence value. The examined data were corrected for outlier and plotted with MEAN and SEM in GraphPad Prism (GraphPad Software Inc.). In few cases not all data points could be depicted in the shown range of graph, which did not affect the statistics. Statistical analysis was conducted by a two-sided, two parametric Student's *t*-test, where applicable. Significance levels were marked as (*) for $p \leq 0.05$, (**) for $p \leq 0.01$, and (***) for $p \leq 0.001$. Statistical analysis was carried out when applicable.

4 Results

4.1 NLRC3 is differentially expressed in various tissues

To assess questions regarding the function or typical characteristics of NLRC3 it is important to know which tissues/cells express NLRC3 either on mRNA or protein level.

4.1.1 *Nlrc3* is expressed in cDNA of immune related tissues

After sacrificing a *Nlrc3*^(+/+) male and female mouse, organs were obtained, RNA was isolated, translated into cDNA, and analyzed by endpoint PCR. A *Nlrc3*-specific fragment was amplified. The result is shown in Fig. 4.1 in comparison to mGAPDH as housekeeper.



Fig. 4.1: Endpoint PCR on murine cDNA. Mice were sacrificed, organs removed, and lysed. RNA was isolated and transcribed into cDNA. Two samples (skel. muscle and heart) were taken from a Clontech cDNA kit. An endpoint PCR was carried out, using m10 and mGAPDH oligomers. Human plasmid cDNA was used as control resulting in a slightly higher amplicon band and a lack of a mGAPDH signal. Blot shown is representative. The results are shown in inverted gray scales.

The strongest signals were gained for spleen, bone marrow, lymph node, testis, and thymus. The mGAPDH housekeeper showed equal amounts of cDNA in the samples. As a *Nlrc3* containing plasmid was used as positive control no mGAPDH bands were expected here. A representative band was excised, purified and verified by Sanger sequencing.

4.1.2 High transcript level of *NLRC3* and *Nlrc3* are found in immune related tissues, but not in the intestinal tract

To further quantify the expression of *NLRC3* and *Nlrc3* two qPCRs were carried out. The results are shown in Fig. 4.2. The highest expression of human *NLRC3* was observed in spleen, lymph node, thymus, leukocytes, and tonsil (increasing order). Murine tissues showed highest *Nlrc3* expression in spleen, heart, adrenal gland, thymus, and lymph node (increasing order), indicating

distinct similarities between the species.

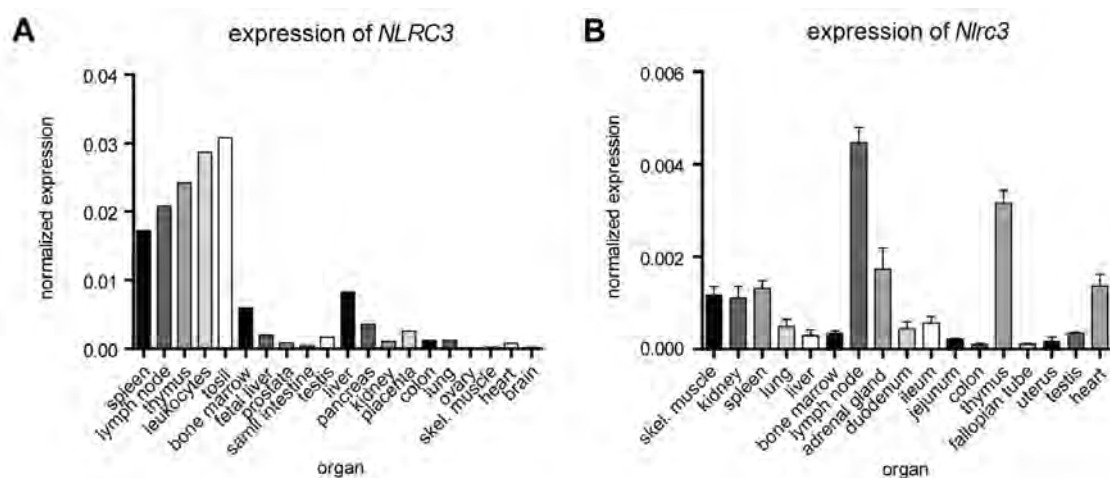


Fig. 4.2: Expression analysis of human and murine *NLRC3/Nlrc3*. Commercial available cDNA samples were analyzed via qPCR. The values were normalized against β -Actin as housekeeper. The x-axis shows the organs of which the cDNA originates, the y-axis depicts the normalized expression. **A** Shows the results from the human samples and **B** the results from the murine samples. All samples were analyzed in two technical replicates. Murine samples contain male/female when applicable.

4.1.3 *NLRC3/Nlrc3* in human and murine cell lines

Established cell lines were checked for their endogenous *NLRC3* protein expression (Fig. 4.3).

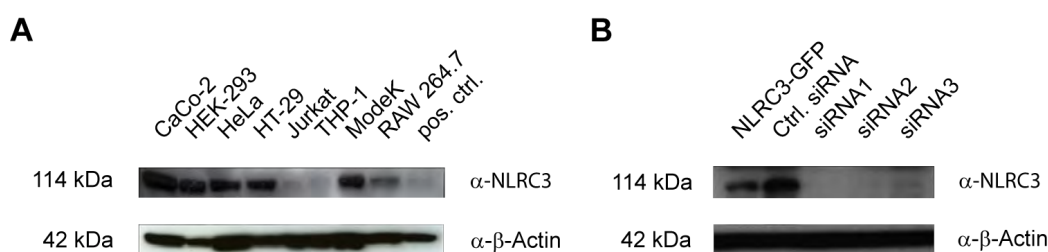


Fig. 4.3: Endogenous expression of *NLRC3* in cell lines. **A** Several cell lines were cultivated and harvested from a 10 ml dish. Cells were lysed with DLB buffer and proteins analyzed via Western blot. **B** *NLRC3*-GFP was overexpressed in HEK-293 cells. The cell were either kept untreated (1st lane) or were transfected with siRNA. The results in the 2nd lane are based on control siRNA transfection, siRNA1-3 represent different *NLRC3* specific siRNAs. The blots were incubated with **A** 1:500 α -*NLRC3*, **B** 1:250 α -*NLRC3*, and 1:10000 α - β -Actin antibodies (**A+B**), detection was performed with HRP linked species specific secondary antibody and ECL.

NLRC3 was expressed in all tested cell lines. Additionally to the human cell lines, two murine cell lines (RAW 264.7 and ModeK) were tested, too, and found to be *Nlrc3* positive. One of the strongest expressions was observed in HEK-293 cells. As HEK-293 cells are well known to be easily transfectable they were used for most of the following *in vitro* experiments. A strong signal was observed in the colon carcinoma cell line CaCo-2 cells, but cDNA analysis failed to show

elevated transcript levels either in end-point PCRs or in qRT-PCR analysis (Fig. 4.1, 4.2). The siRNA experiment (Fig. 4.3 B) proofed the specificity of the primary antibody.

4.1.4 Cell fractions demonstrate the cytosolic localization of NLRC3

After demonstrating a strong signal of NLRC3 in HEK-293 cells and having elucidated a preferred expression in cells of the immune system cell fractionations were carried out. Peripheral blood mononuclear cells isolated from human buffy coats, contained lymphocytes, monocytes, and platelets and therefore a subset of the most important cells of the adaptive and innate immune system. The cell fractions were analyzed via Western blot (Fig. 4.4).

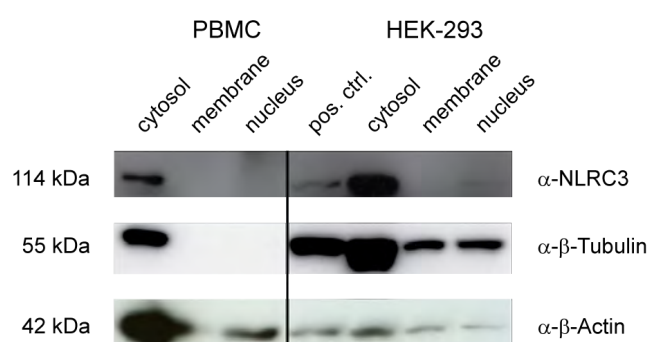


Fig. 4.4: Cell fraction of human PBMCs and HEK-293 cells. Human PBMCs were isolated and fractioned by differential centrifugation. The same protocol was applied to HEK-293 cells from cell culture. The lysates were analyzed by Western blot. The blot was incubated with α -NLRC3 (1:500), α - β -Tubulin (1:1000) as compartment control, and α - β -Actin (1:10000) as loading control.

NLRC3 was solely expressed in the cytosol of the PBMCs and HEK-293 cells tested. The fraction contained a strong tubulin signal, being a specific marker for the cytosol. The NLRC3-signal was even stronger in HEK-293 cells, although the separation was not fully successful according to the tubulin signal. The positive control, being generated from HEK cells overexpressing NLRC3, confirmed the specificity of the NLRC3 signal.

4.2 Analysis of functional interaction and colocalization between NLRC3 and Mitofilin

An early Yeast-2-hybrid screen has been performed by Billmann-Born *et al.* [data not shown], indicating a potential interaction between NLRC3 and the inner mitochondrial membrane protein Mitofilin (IMMT).

4.2.1 Co-immunoprecipitation of NLRC3 and IMMT

Co-Immunoprecipitations were used to test for direct protein-protein interactions (Fig. 4.5).

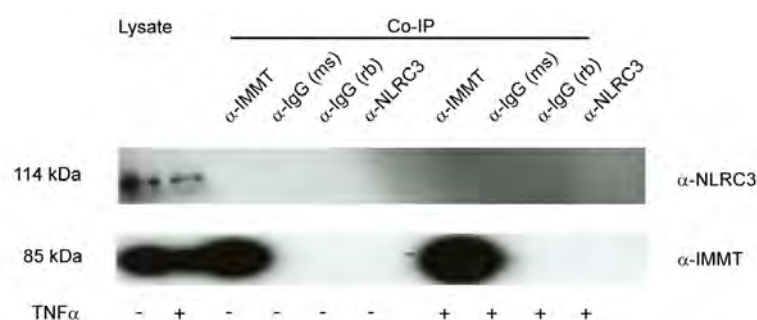


Fig. 4.5: Co-Immunoprecipitation of NLRC3 and IMMT. HEK-293 cells were either stimulated with $\text{TNF}\alpha$ or kept unstimulated. They were lysed and incubated with either, α -IMMT, α -IgG mouse (as IMMT Ctrl.), α -NLRC3 or α -IgG rabbit (as NLRC3 Ctrl.) bound to agarose beads. Precipitates were purified and blotted. Blots were incubated with α -IMMT and α -NLRC3 antibody.

While both, NLRC3 and IMMT, were detectable in the cell lysates of HEK-293 cells, no NLRC3 was detectable in the samples pulled with α -IMMT antibodies. The same holds true for the samples pulled with α -NLRC3 antibody. A positive signal was gained in the IMMT pulled samples for IMMT. The negative controls, consisting of IgGs equal to the species in which the α -NLRC3 (rabbit) or respectively the α -IMMT (mouse) antibody were generated, showed no band. A stimulating effect of $\text{TNF}\alpha$ could not be shown.

4.2.2 Cell staining reveals spatial position of NLRC3

Coverslip stainings were performed to assess the localization and potential interaction of NLRC3 with other proteins or cell structures. All stainings were designed with an IgG control as well as a mock-transfected control. First cells were tested for endogenous NLRC3 and overexpressed NLRC3-flag. Endogenous NLRC3 signals were weak, but overexpressed NLRC3-flag could be successfully detected by either α -NLRC3 or α -flag-antibodies. Both signals appeared close to the Mitotracker signal as seen in the merged pictures. Accordingly, the NLRC3 antibody from Abcam was applied in combination with the mitochondrial dye Mitotracker, and α -IMMT as shown in Fig. 4.7.

Each setup consisting of a NLRC3-flag and a mock transfected sample was stained with Mitotracker, DAPI, and a specific, antibody based AlexaFluor dye. While the stains were kept constant between the setups A-C in Fig. 4.6, the antibody based staining (2nd column) altered. Unspecific binding of the secondary antibody could be excluded, as the IgG control was negative (Fig. 4.7 A

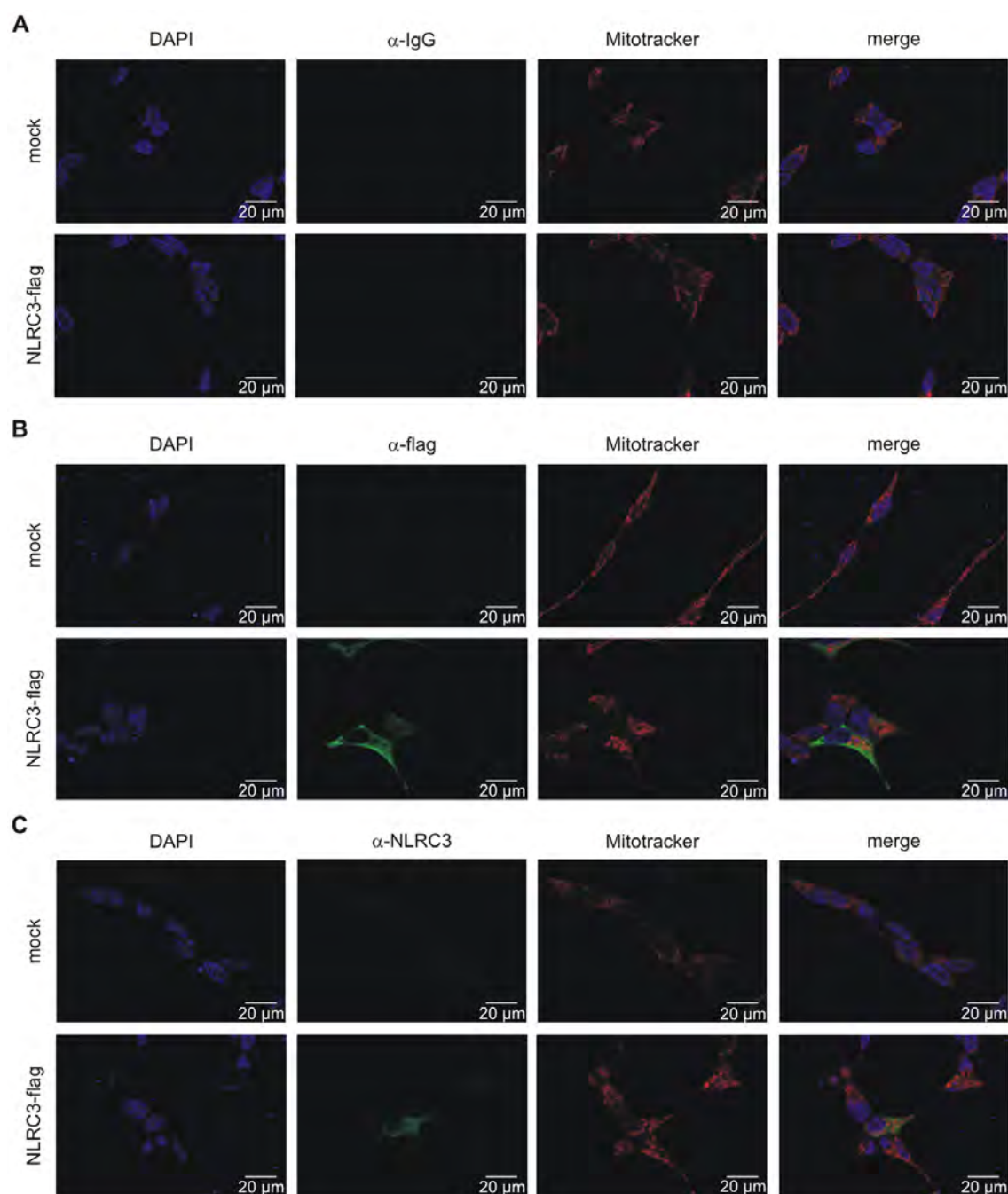


Fig. 4.6: Coverslip staining of HEK-293 cells comparing α -NLRC3 and α -flag-antibody. HEK-293 cells were seeded onto coverslips and transfected either with a mock vector or a NLRC3-flag vector. The cells were cultivated for two days and stained with Mitotracker (red signal). After PFA fixation and permeabilization the cells were incubated with primary antibodies as followed: **A** α -rb-IgG, **B** α -flag, **C** α -NLRC3. The primary antibodies were detected by the respective AlexaFluor-488 coupled secondary antibody, giving a green signal. Finally, the cells were stained with DAPI, resulting in a blue signal for nucleic acid.

and 4.6 A). A rabbit α -IgG was used as primary antibody control. While DAPI and Mitotracker produced distinct signals, no green fluorescence was observed. The α -flag antibody (Fig. 4.6 B) resulted in a strong signal in cells overexpressing NLRC3-flag. When merging all three channels

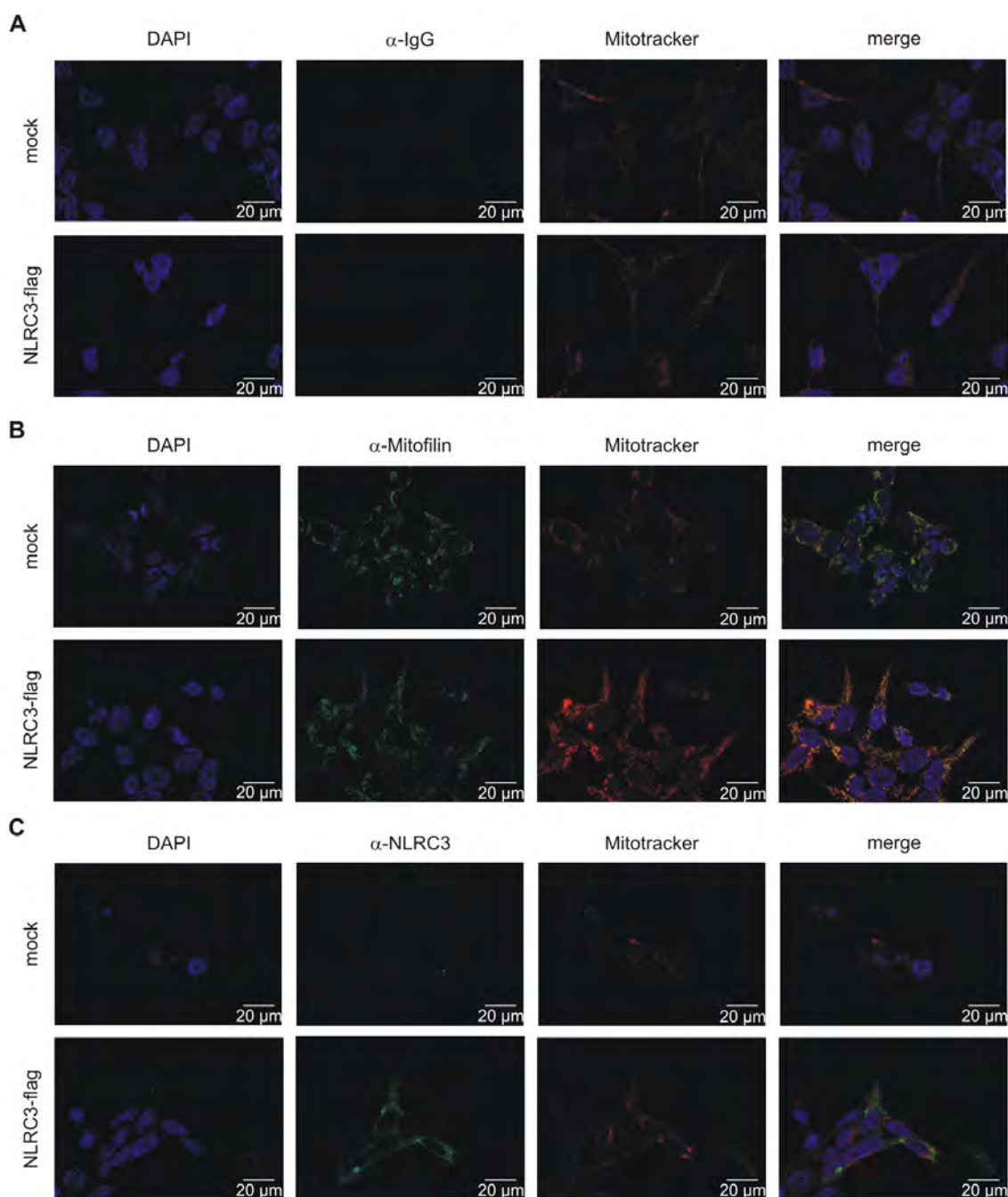


Fig. 4.7: Coverslip staining of HEK-293 cells with α -Mitofilin-antibody. HEK-293 cells were seeded onto coverslips and transfected either with a mock or a NLRC3-flag vector. The cells were cultivated for two days and stained with Mitotracker (red signal). After PFA fixation and permeabilization the cells were incubated with primary antibodies as followed: **A** α -rb-IgG α , **B** α -Mitofilin, **C** α -NLRC3. The primary antibodies were detected by the respective AlexaFluor-488 coupled secondary antibody, giving a green signal. Finally, the cells were stained with DAPI, resulting in a blue signal for nucleic acid.

distinct cell features and yellow areas of overlapping signals became visible. The positive control, using an α -NLRC3 antibody, binding both, endogenous and exogenous, NLRC3 is shown in Fig. 4.6 C. Merging the channels, showed very few antibody specific green signals for endoge-

nous NLRC3 (in the mock control) and a specific overlap in the transfected cells. As expected, the successive incubation with Mitotracker and α -Mitofilin (Fig. 4.7 B) showed colocalization as demonstrated by the wide overlap in the merged picture. This effect appeared to be even increased in the NLRC3-transfected cells. Applying a successive staining with Mitotracker and α -NLRC3 in NLRC3-flag transfected HEK-293 cells resulted in a specific overlap as indicated in the lower merged picture in Fig. 4.7 C.

In a third experiment HeLa cells were transfected with NLRC3-flag matching the previous experimental setup (Fig. 4.8).

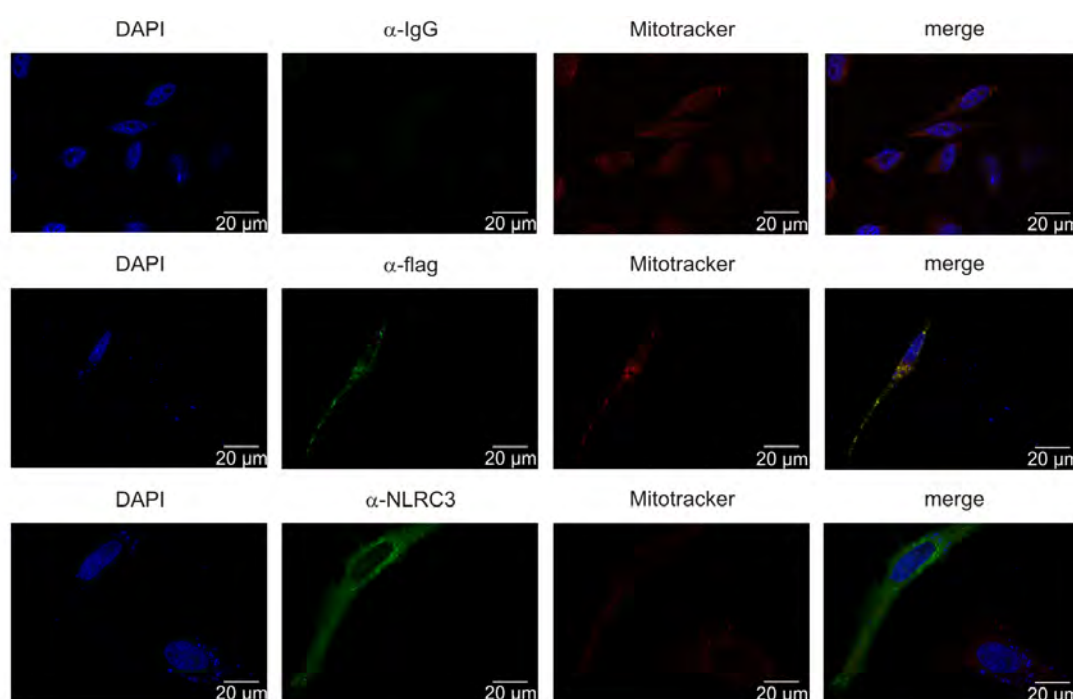


Fig. 4.8: Coverslip staining of HeLa cells. HeLa cells were seeded onto coverslips and transfected with a NLRC3-flag vector. The cells were cultivated for two days and stained with Mitotracker (red signal). After PFA fixation and permeabilization the cells were incubated with primary antibodies as indicated in the pictures. The primary antibodies were detected by the respective AlexaFluor-488 coupled secondary antibody, giving a green signal. Finally, the cells were stained with DAPI, resulting in a blue signal for nucleic acid.

These results indicate a close spatial proximity of NLRC3 and IMMT and are therefore in concordance with the results shown previously (Fig. 4.6). Having shown the same effect independently in two different cell systems strengthens the theory of NLRC3 being in close proximity to mitochondria.

Finally, a staining for CLSM analysis was conducted. HEK-293 cells overexpressing NLRC3-flag were incubated with α -flag and Mitotracker (Fig. 4.9). As shown in Fig. 4.9 A are the signals from α -Mitofilin and mitotracker matching perfectly, resulting in a yellow signal. The white spots

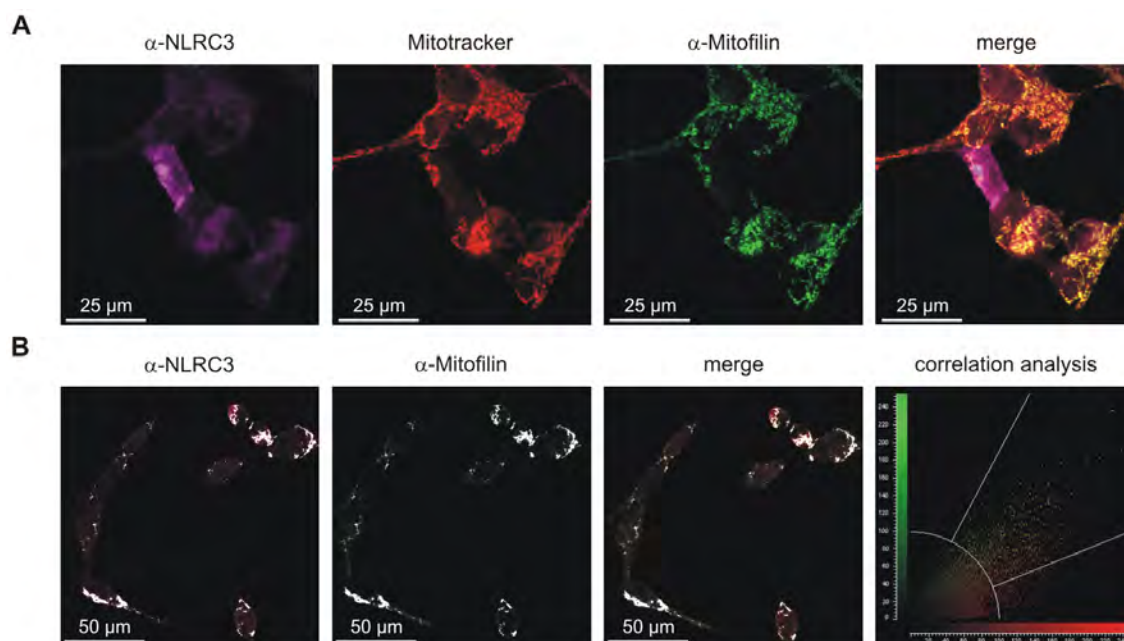


Fig. 4.9: Staining for CLSM analysis. HEK-293 cells were seeded onto coverslips and transfected with a NLRC3-flag vector. The cells were cultivated for two days and stained with Mitotracker (red signal). After PFA fixation and permeabilization the cells were incubated with primary antibodies as indicated in the pictures. The primary antibodies were detected by the respective AlexaFluor-488/-633 coupled secondary antibody, giving a green/purple signal. **A** The merged signals of the secondary antibodies and the mitochondrial stain can be merged to an image, where white areas indicate an overlap of all three channels. **B** The α -NLRC3 signal and the Mitofilin signal of cells were merged and analyzed. The white areas indicate areas of perfect overlap. The last image shows a distribution of the signals. Dots near to the color-axis represent non matching signals, while dots appearing yellow result from overlapping signals. NLRC3 signals are shown in false color here.

in the merged picture indicate the overlap of all three signals, further hinting at a close spatial proximity of NLRC3 and mitochondria. Due to the higher intensity of the stain a new picture was taken for the overlap of Mitofilin and NLRC3 signals (Fig. 4.9 B). The potential correlating signals are indicated in white. A correlation analysis of those signals, as shown in the fourth panel, revealed that most of the signals are indeed overlapping. All signals appearing yellow in the dot plot are considered to be perfect matches. All other dots (red/green), which are located nearer to their respective axes represent non-matching single signals.

4.2.3 NLRC3 was detected in a mitochondrial lysates via MS/MS

Having detected NLRC3 in close spatial proximity of mitochondria (subsection 4.2), mitochondrial lysates and two protein samples from Co-IPs were analyzed via MS/MS. All samples were based on HEK-293 cells, overexpressing NLRC3. While the α -IMMT pulled sample was pre-stimulated with TNF α , the α -NLRC3 pulled sample was kept unstimulated. After Coomassie staining, several bands were extracted (Fig. 4.10) and analyzed (Tab. 4.1).

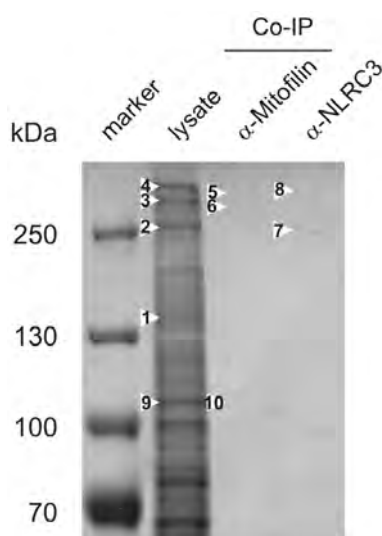


Fig. 4.10: Coomassie stained gel for MS/MS analysis. Lane 1: marker; lane 2: mitochondrial lysates from HEK-293 cells; lane 3: Co-IPs from HEK-293 cells overexpressing NLRC3, stimulated with 50 ng/ml TNF α and pulled with α -Mitofilin; lane 4: Co-IPs from HEK-293 cells overexpressing NLRC3 pulled with α -NLRC3 were separated on a SDS-PAGE and stained with coomassie. The arrows indicate spots sampled for MS/MS analysis.

Tab. 4.1: Excerpt of proteins identified via MS/MS. The sample numbers correlate with those indicated in Fig. 4.10. The accession number refers to the UniProt database. The full list of identified proteins is available on a compact disc attached to this thesis.

ID	size [kDa]	lane	description	accession
1	130	2	NLRC3	B5MDB6
			mHsp 60	B7Z5E7
			keratin	P13655
2	250	2	PRP8 hom.	Q6P2Q9
			keratin	P13645
3	260	2	ELYS	Q8WYP5
			keratin	P13645
4	>260	2	DNA-PKcs	P78527
			keratin	P13645
5	>250	3	keratin	P13645
6	<250	3	keratin	P13645
7	<250	4	keratin	P13645
8	>250	4	keratin	P13645
9	<130	2	<i>uncertain spectra</i>	
10	<130	3	Mitofilin	Q16891
			keratin	P13645

A positive NLRC3 signal was detected in the lysate at approx. 130 kDa, while no NLRC3 was detectable in the α -NLRC3 pulled samples. The α -IMMT sample produced a positive MS hit for IMMT. Further samples were found positive for keratin mainly, an ubiquitous bias of this analysis. High molecular weight bands of the mitochondrial lysate did not reveal NLRC3 as potential constituent of protein complexes. Hits as Q6P2Q9 in sample 2 indicate that this method is suitable even for large proteins, but that the mitochondrial isolation may be biased by small sub-nuclear structures like speckles. Staining and separation experiments did not indicate a nuclear localization of NLRC3. The full list of hits is available in the electronic supplements (see chapter 6).

4.2.4 *In silico* prediction of probability of NLRC3 being imported into mitochondria

To calculate the probability of the import of NLRC3 into mitochondria the protein sequence was analyzed by two different algorithms. The MITOPROT algorithm has been published by Claros *et al.* [190] and has been provided by the Institute of Human Genetics at the Helmholtz Center Munich (Tab. 4.2 A). The Predotar algorithm was provided by the French National Institute for

Agricultural research (Tab. 4.2 B) [191]. Both algorithms aimed at the identification of a putative N-terminal targeting sequence. The predictions are summarized in Tab. 4.2, while a graphic overview of the isoforms mentioned is given in the supplements of this thesis (chapter 6).

Tab. 4.2: Probability of NLRC3/Nlrc3 to be imported into mitochondria. **A** The results are based on calculations by MitoProt II - v1.101 and **B** Predotar v. 1.03. The human inner mitochondrial membrane protein Mitofilin was calculated as positive control.

protein	isoform	size [kDa]	A	B
			probability	value of export into mitochondria
human NLRC3	1	114.658	0.0445	0.01
	2	119.415	0.1095	0.0
	3	83.456	0.06	0.01
	4	111.634	0.09	0.01
Mitofilin	1	83.678	0.9825	0.63
murine Nlrc3	1	115.993	0.0811	0.26
	2	80.819	0.0041	0.0
	3	41.669	0.8004	0.0
	4	32.882	0.788	0.0
	5	25.538	0.061	0.0

The positive control Mitofilin showed a high probability to be imported into mitochondria. The calculated values for NLRC3 were lower, varying between the different isoforms. Depending on the algorithm a quite high probability has been predicted for the murine Nlrc3 isoforms 3 and 4. They are both missing the NACHT domain, but still express several LRRs. This is true for isoform 5 as well, although the algorithm computed a more than tenfold lower probability. This demonstrates the sensitivity of the algorithm, which calculates a probability based on 47 different parameters. A conserved signal recognition protein, comparable to those discovered by Blobel *et al.* has yet not been described for mitochondria [192]. Instead, a variety of cleavable presequences and noncleavable targeting and sorting signals were published, indicating a complex protein sorting system [193].

4.2.5 NLRC3 influences the ERSE mediated unfolded protein response

Having strong support for an interaction of NLRC3 and mitochondria, especially with IMMT it was interesting to follow up a potential functional trait. Cellular stress may result in misfolding or unfolding of proteins. The unfolded protein response (UPR) has been described for the ER [194, 195, 196]. The UPR controls the activation of i.e. molecular chaperones or enzymatic sets to

refold or dispose the incorrect folded proteins. The endoplasmic reticulum stress element (ERSE) which is inducible by ATF6, XBP1, and p50 is a central promoter in the upregulation of unfolded protein response related proteins like the glucose regulated proteins (grp) [197]. A significant activation of UPR should therefore be detectable by an increased ERSE promoter activity.

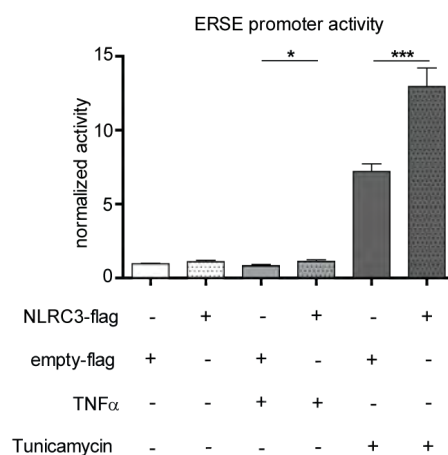


Fig. 4.11: Impact of NLRC3 on tunicamycin induced ERSE promoter activity. HEK-293 cells were either transfected with 5 ng NLRC3-flag or a flag-vector. An ERSE-Luc and a pRLTK were also transfected. The total DNA amount was kept constant by the use of an empty vector. A stimulation regime with 50 ng/ml TNF α , 10 μ g/ml tunicamycin, and cell culture medium as negative control was applied. Each bar summed up from 2 experiments, n=10 samples prior to statistical correction. Significance levels were evaluated by Student's *t*-test.

The data shown in in Fig. 4.11 are based on repeated experiments, which have been normalized to the unstimulated controls. The ERSE promoter activity was not affected by TNF α , but highly upregulated after tunicamycin stimulation. NLRC3 overexpressing cells exhibited a higher ERSE promoter activity after tunicamycin stimulation. An increased activation of ERSE indicated the activation of the downstream UPR cascade. The cell fate depends upon the further regulation of this cascade [198].

4.3 NLRC3 and its impact on NF κ B activation

As the NF κ B pathway is well known to be interconnected with inflammatory processes, a potential impact of NLRC3 was tested. One of the most convenient readouts at hand was a dual luciferase assay, enabling the direct quantification of NF κ B activation in relation to a housekeeper.

Following experimental procedures, described by Conti *et al.* [50], several luciferase experiments were conducted. Utilizing the same amounts of plasmid as mentioned in the publication failed to produce reliable data [data not shown]. Decreasing the total amount of plasmid to a maximum of 50 ng per sample resulted in the data shown in Fig. 4.12.

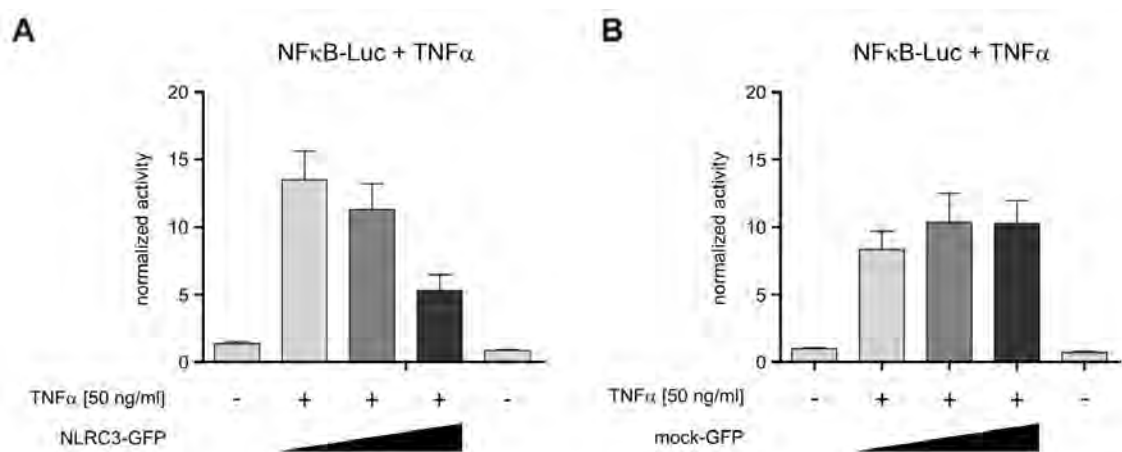


Fig. 4.12: Dual luciferase assay in HEK-293 cells. HEK-293 cells were transfected with a NFκB-Luc and a pRLTK-Luc construct. Additionally, different amounts of NLRC3-GFP (5, 17.5, and 35 ng) were transfected. The total amount of plasmid was kept constant by the addition of an empty vector. Half of the cells were stimulated with TNFα for eight hours, the other cells were kept unstimulated. The unstimulated negative controls were transfected with 5 and 35 ng NLRC3-GFP respectively. The 17.5 ng transfected control is not depicted and did not show any elevated values. The data shown are a summary of four independent results, with each n=10 samples per column.

A strong increase in NFκB activation was observed following TNFα treatment. The activation was strongest in a 5 ng NLRC3 transfection setup. The unstimulated transfections did not respond with an increased NFκB-Luc activity. The mock transfected controls showed a general response to TNFα, which had to be considered as physiologic response.

4.4 Stimulation and downstream signaling

4.4.1 NLRC3 in response to TNFα stimulation

To investigate the fate and distribution of NLRC3 upon TNFα stimulation, an experiment with different time points and an Western blot read-out was established (Fig. 4.13).

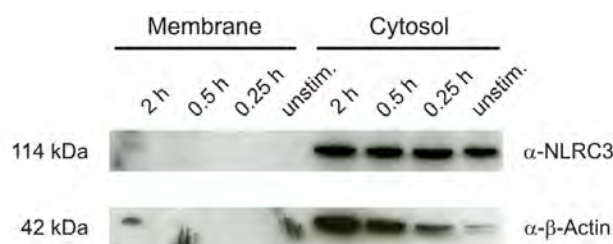


Fig. 4.13: Cell fractionation of HEK-293 cells. HEK-293 cells were stimulated with 50 ng/ml TNFα for different time periods and fractionated by differential centrifugation afterwards. The lysates were analyzed by Western blot. The blot was incubated with α-NLRC3 and α-β-Actin as loading control.

Incubating the membrane with α-NLRC3 and α-β-Actin as control showed a strict localization of NLRC3 in the cytosolic compartment. Normalizing the NLRC3 bands to the β-Actin bands

showed a decrease of NLRC3 with time. The cell fractioning was successful leaving only marginal amounts of β -Actin in the membrane fraction.

4.4.2 TRAF6 and NLRC3

TRAF6 is a member of the TNF receptor associated factor (TRAF) protein family, which takes part in the downstream signaling of TNF α . The E3 ligase TRAF6 functions downstream of TNFR and TLRs as an adapter molecule leading to the CD40-mediated activation of NF κ B and c-Jun [199, 200]. TRAF6 is known to be involved in the production of pro-inflammatory cytokines via the TLR/MyD88/TRIF pathway and in the activation of NF κ B signaling [201]. To investigate the impact of TNF α stimulation upon NLRC3 signaling, a NF κ B-Luc assay was established. A close connection between NLRC3 and TRAF6 was published by Schneider *et al.* recently [51].

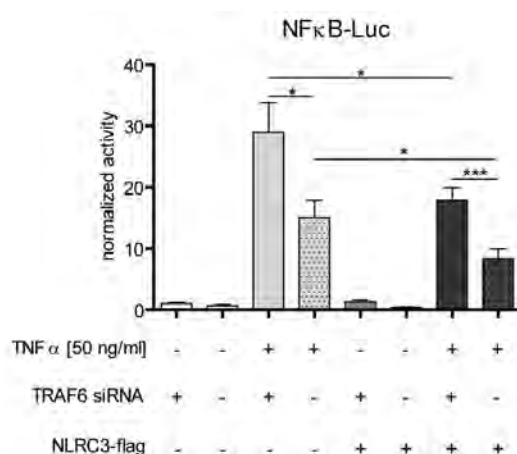


Fig. 4.14: Dual luciferase assay in HEK-293 cells. HEK-293 cells were transfected with a NF κ B-Luc, a pRLTK-Luc construct, and either 5 ng NLRC3 or an empty flag vector. The total amount of plasmid was kept constant by the addition of an empty vector. Simultaneously, the samples were either transfected with TRAF6 siRNA (+) or control siRNA (-). Half of the setup was stimulated with TNF α for eight hours, the other part was kept unstimulated. The data were gained in two independent experiments, with each n=10 per column. Statistical significance was calculated by Student's *t*-test.

Stimulating the cells with TNF α increased the NF κ B response. Focusing on the effect of TRAF6 siRNA it was shown, that a down regulation of TRAF6 is accompanied by a significant increase of the NF κ B activity. A simultaneous transfection of TRAF6 siRNA and NLRC3-flag in HEK-293 cells significantly decreased the NF κ B activity (Fig. 4.14). This experiment demonstrates, that the signaling pathways of NLRC3 and TRAF6 are interconnected.

4.4.3 Human peripheral blood mononuclear cells show distinct transcript patterns after stimulation

Human peripheral blood mononuclear cells were isolated from a healthy donor, cultivated, and stimulated. The cells were harvested, the RNA extracted, and transcribed to cDNA. The cDNA was analyzed via TaqMan qRT-PCR.

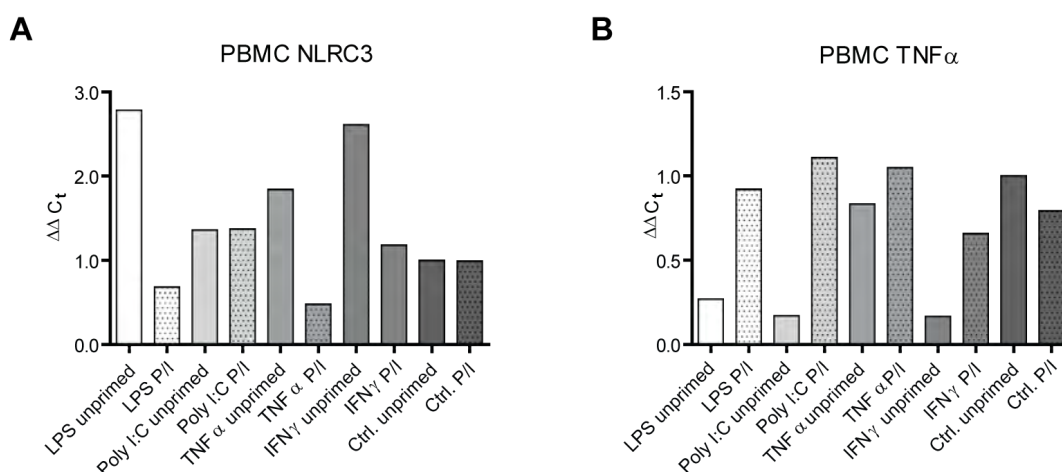


Fig. 4.15: TaqMan qRT-PCR analyses of PBMCs. PBMCs were either kept unprimed or were pre-stimulated with PMA/ionomycin (P/I). After 18 hours priming the main stimulus was added (LPS, PolyI:C, TNF α , IFN γ). Transcript level for **A** NLRC3 and **B** TNF α were evaluated. The stimulation was carried out in two independent wells for each treatment, quantification utilized two technical replicates each.

Responsiveness of PBMCs to a variety of stimuli was assessed on transcript level (Fig. 4.15). NLRC3 transcript levels were upregulated especially after LPS, TNF α , and IFN γ stimulation (Fig. 4.15 A). The transcript level of NLRC3 were decreased after co-stimulation of P/I. P/I stimulation alone did not alter NLRC3 expression. With respect to the TNF α transcript level it has to be mentioned, that co-stimulation generally increased the transcript level (Fig. 4.15 B).

4.5 Nlrc3^{-/-} mice do not exhibit a spontaneous phenotype

4.5.1 Basal phenotyping

The offspring of Nlrc3^{+/+} and Nlrc3^{-/-} mice was alive and development appeared normal. Neither an optical phenotype, nor differences in behavior and life span were detectable between WT and KO. In a basal aging experiment four Nlrc3^{+/+} and five Nlrc3^{-/-} mice were housed and fed *ad libitum*. They all survived more than 18 month, outliving the observation period. For a basal phenotyping, organs with known Nlrc3 expression were sampled from sacrificed Nlrc3^{+/+} and Nlrc3^{-/-} mice and stained with HE (Fig. 4.16, 4.17).

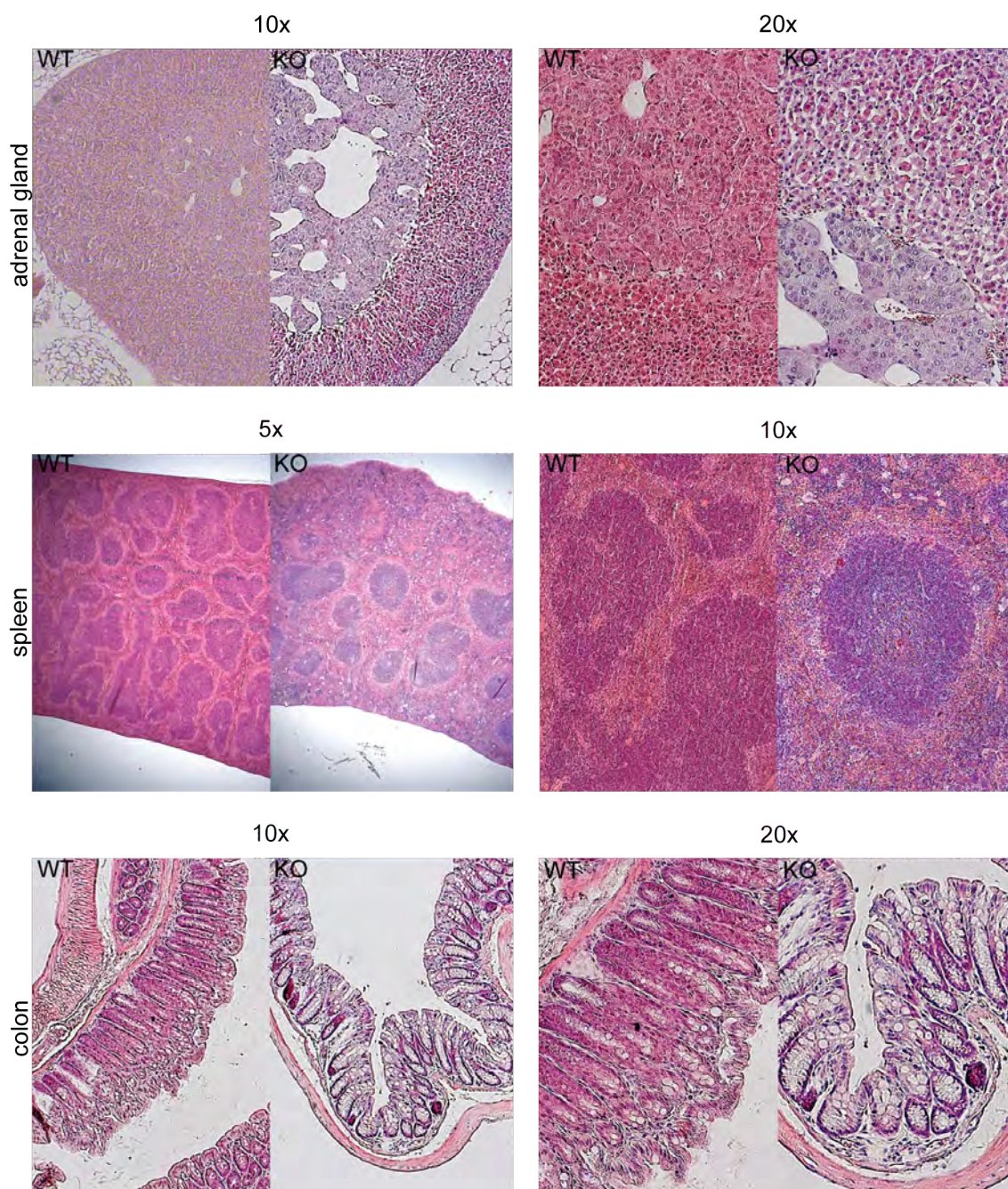


Fig. 4.16: Basal phenotyping of murine adrenal gland, spleen, and colon. Adrenal gland, spleen, and colon tissue were HE-stained. The magnification is given for each pair of pictures. WT and KO are directly opposed for each organ in both magnification steps.

Adrenal gland The tissue of the adrenal gland was composed of the inner medulla, engulfed in the cortex, and finally covered by the outer capsule. The most obvious difference were less dense packed chromaffin cells in the medulla of the KO animals. Several larger holes appeared, which might be an artifact due to the cutting. The surrounding *zona fasciculata* seemed to be more permeable, too (Fig. 4.16, 1st row).

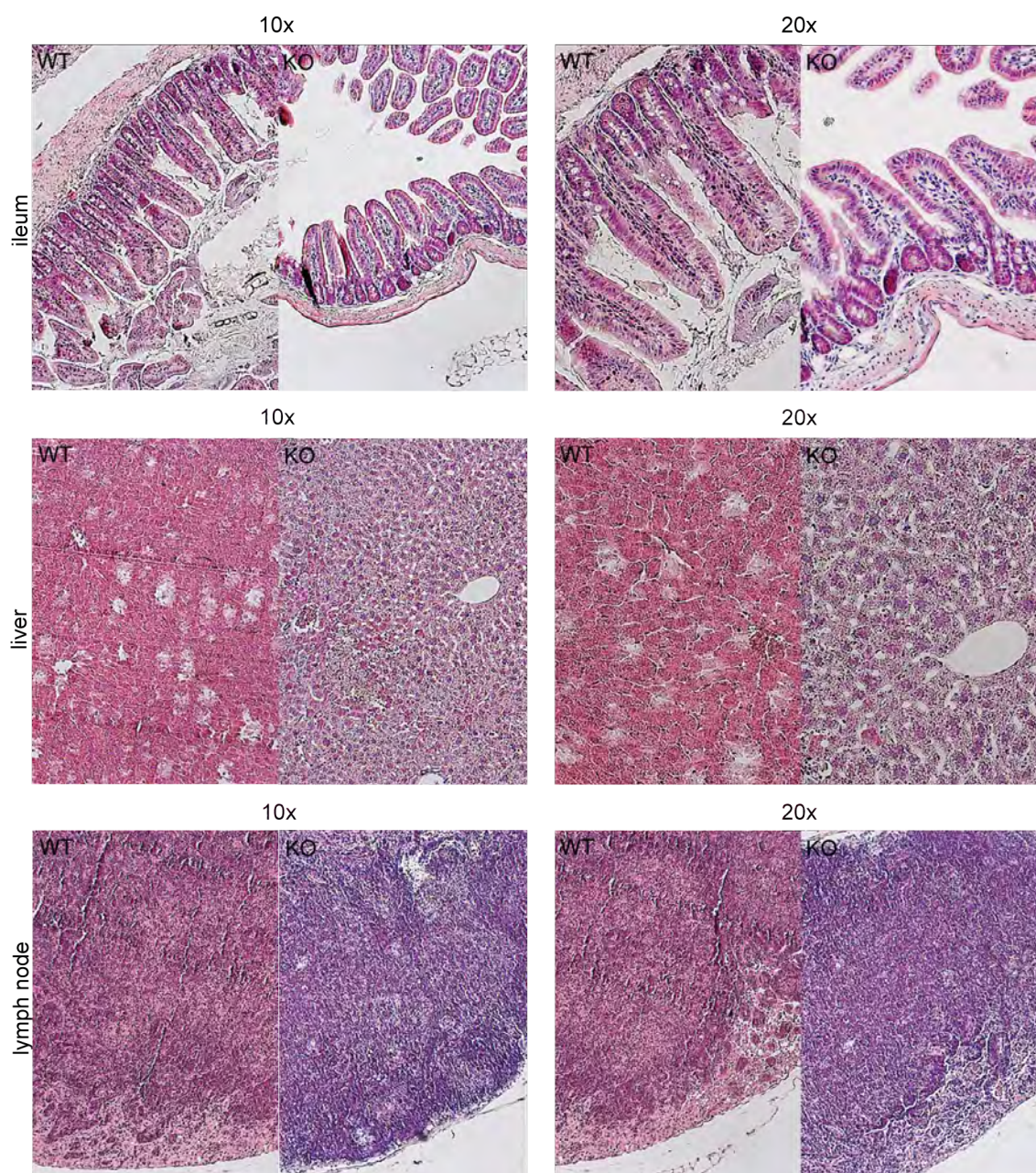


Fig. 4.17: Basal phenotyping of ileum, liver, and lymph nodes. Ileum, liver, and lymph node were HE stained. The magnification is given for each pair of pictures. WT and KO are directly opposed for each organ in both magnification steps.

Spleen A healthy WT spleen displayed two easily distinguishable patterns - the red and white pulp. The white pulp appeared blue after HE staining, while the red pulp, a host to monocytes [202], appeared red. The surrounding capsule commenced in a comparable thickness in WT and KO samples, indicating no latent inflammation (Fig. 4.16, 2nd row).

Colon The sections showed the three clearly distinguishable parts of the colon structure, the outer

muscularis, followed by a thin submucosa, and the inner mucosa. The mucosa consisted of villi columnar cells including absorptive cells and the goblet cells. Goblet cells are glandular cells, secreting mucin. All structures were identifiable in both, the WT and KO sections and did not show any genotype-related abnormalities (Fig. 4.16, 3rd row).

Ileum A striking feature of this sections were the large crypts between muscularis and villi, appearing as intensively stained round structures. The *Lamina propria mucosa* was well structured. There was no obvious disturbance in the KO samples compared to WT (Fig. 4.17, 1st row).

Liver The liver sections revealed a homogeneous structure of hepatocytes, being separated by sinusoids. Hollow, round shaped structures were veins (Fig. 4.17, 2nd row).

Lymph node The encapsulated lymph node is mainly composed of two regions, the outer cortex and the inner medulla with the medullary sinuses. According to the microscopic inspection no alterations between WT and KO were visible (Fig. 4.17, 3rd row).

4.5.2 Murine blood analysis

As earlier experiments showed elevated blood glucose level in *Nlrc3*^{-/-} compared to WT mice [data not shown], a new glucose test and analysis of HbA_{1c} levels was performed (Fig. 4.18).

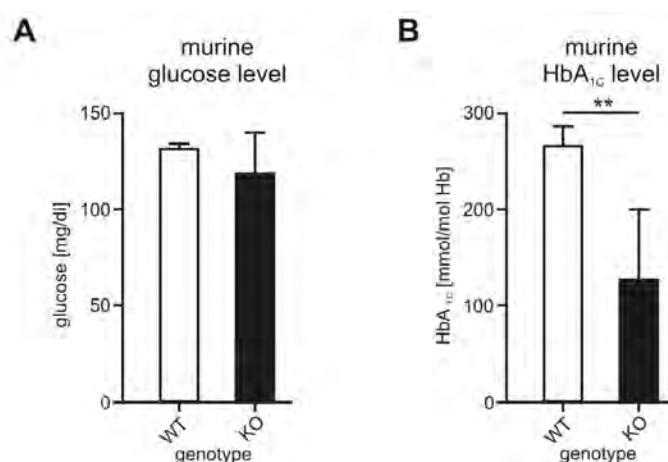


Fig. 4.18: Basal blood glucose and HbA_{1c} evaluation. Blood was drawn from eight freshly sacrificed mice of each genotype (4 male and 4 female each) and analyzed for blood glucose level and HbA_{1c} level.

The blood glucose level showed no significant differences between WT and KO. HbA_{1c} is a long term sugar proxy as hemoglobin is able to bind glucose to its N-terminus of the β -chain via *Amadori rearrangement*. The value increases linear to the time of exposure to high sugar environment and persists for the lifetime of the erythrocyte. The HbA_{1c} value is increased in diabetic patients. In case of the *Nlrc3*^{-/-} mice the HbA_{1c} levels were significantly decreased compared to

the WT. The mice did not show any other signs of diabetes, e.g. an abnormal water consumption. Pregnancy may interfere with the HbA_{1c} level, but is not applicable here, as the mice were kept separated by gender. Malfunctions of the liver, were not identifiable by structural changes (Fig. 4.17). Dietary differences could be excluded as well, as all mice were fed with the same food pellets. It might be hypothesized, that an increased red blood cell turnover of yet unknown reason caused the genotype related differences.

4.6 Response of *Nlrc3*^{-/-} BMDM to lipopolysaccharide stimuli

As the main stimulus for *Nlrc3* activation remained unknown, a general LPS stimulation was applied to determine the impact of *Nlrc3* on the pro-inflammatory IL-6 (Fig. 4.19). Therefore BMDMs were isolated from *Nlrc3*^{-/-} and *Nlrc3*^{+/+} mice and stimulated with three different LPS preparations (Invivogen, Sigma-Aldrich, and FZ Borstel, see Tab. 3.17) for 8 hours.

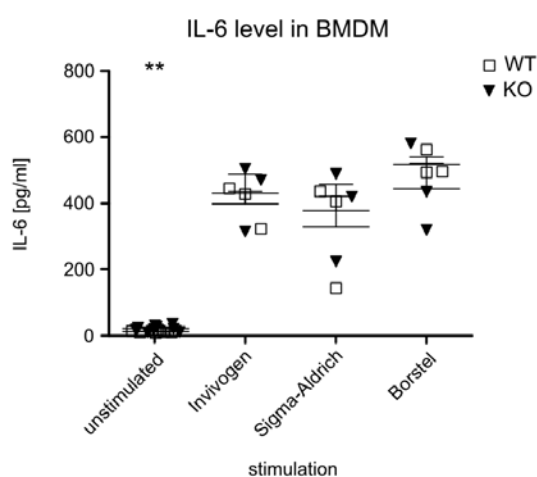


Fig. 4.19: Responsiveness of BMDMs to LPS stimulation. An IL-6 ELISA was performed to measure the IL-6 level secreted by the BMDMs prior and after eight hours stimulation. Significance levels were evaluated by Student's *t*-test.

The pro-inflammatory cytokine IL-6 was upregulated in all stimulated samples after 8 hours. To further investigate the time-dependency, also with regard to different ILs, a second experiment on BMDMs was performed. BMDMs were cultivated and stimulated with the ultrapure LPS provided by the Research center Borstel. The transcript level of IL-2, IL-6, and IL-10 were monitored.

IL-2 transcript levels were below the detection limit. IL-6 transcripts steeply increased after 30 minutes stimulation, with values being significantly higher in KO cells. The IL-10 transcript levels were increasing after 30 minutes as well, peaking after 60 minutes, to decrease afterwards (Fig. 4.20). To further assess the transcript regulation in BMDMs a new experiment was designed, utilizing *n*=6 mice of each genotype. BMDMs were isolated and stimulated with three different

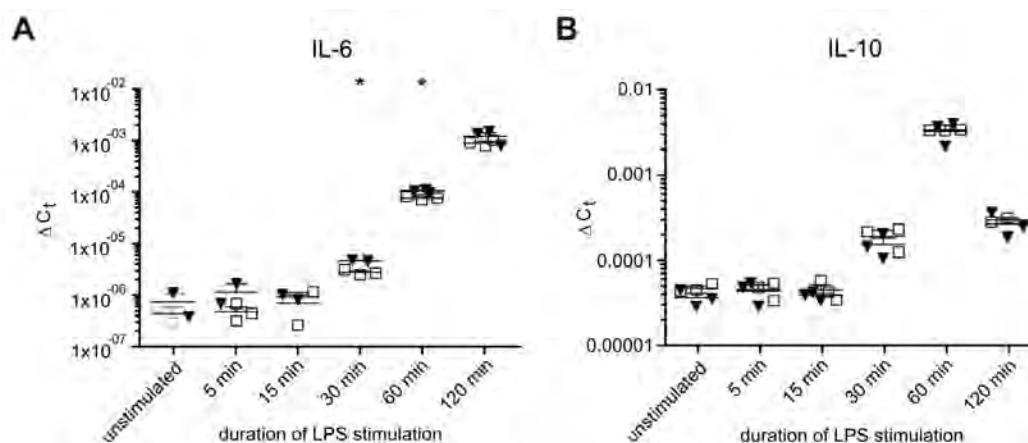


Fig. 4.20: Transcript analysis in BMDM. Murine BMDMs were isolated from 3 *Nlrc3*^{+/+} (WT, hollow square) or 3 *Nlrc3*^{-/-} (KO, filled triangle) mice and stimulated with LPS. The transcript level of **A** IL-6 and **B** IL-10 were quantified via TaqMan assay in two technical replicates each. IL-2 was not detectable.

LPS for 2 to 8 hours, governed by an unstimulated control. IL transcript levels were assessed via qPCR analysis. The results are depicted for the interleukins IL-1 β , IL-6, and IL-10 in Fig. 4.21 and for IL-12, IL-18, and the murine IL-8 homologue CXCL1 in Fig. 4.22.

IL-1 β levels were slightly higher in KO than in WT unstimulated BMDMs. This trend persisted throughout the whole stimulation time, showing a stronger response to LPS from Sigma-Aldrich and Borstel. The induction with the Sigma-Aldrich and Borstel LPS resulted in a 1000-time fold-change after 8 hours, while the foldchange in Invitrogen LPS samples was lower. As a tendency the induction seemed to peak between 2 and 8 hours to decrease afterwards (Fig. 4.21 A).

IL-6 levels were significantly higher in untreated KO cells. After LPS stimulation the transcript level increased dramatically, promoted strongest by the ultra-pure Borstel LPS. In general were the transcript levels, expressed as foldchange, significantly higher in KO cells (Fig. 4.21 B).

Although the transcript level of **IL-10** were much lower than in case of IL-6 the general course appeared to be similar. IL-10 transcript levels were slightly elevated in unstimulated KO cells and were still exceeding the WT values after stimulation (Fig. 4.21 C).

The transcript level of **IL-12 β** displayed a heterogeneous response to LPS stimulation. While a general induction was clearly visible after LPS stimulation, peaking after 2 hours, KO and WT samples were indiscriminative (Fig. 4.22 A).

IL-18 was the least inducible cytokine in this set. The transcript levels merely did not changed after 2 hours of LPS stimulation. As a trend the WT seemed to transcribe lower amounts of IL-18, being weakly significant after 2 hours of Sigma-Aldrich LPS stimulation (Fig. 4.22 B).

CXCL1 displayed the highest variation even in unstimulated cells, with a significant trend to

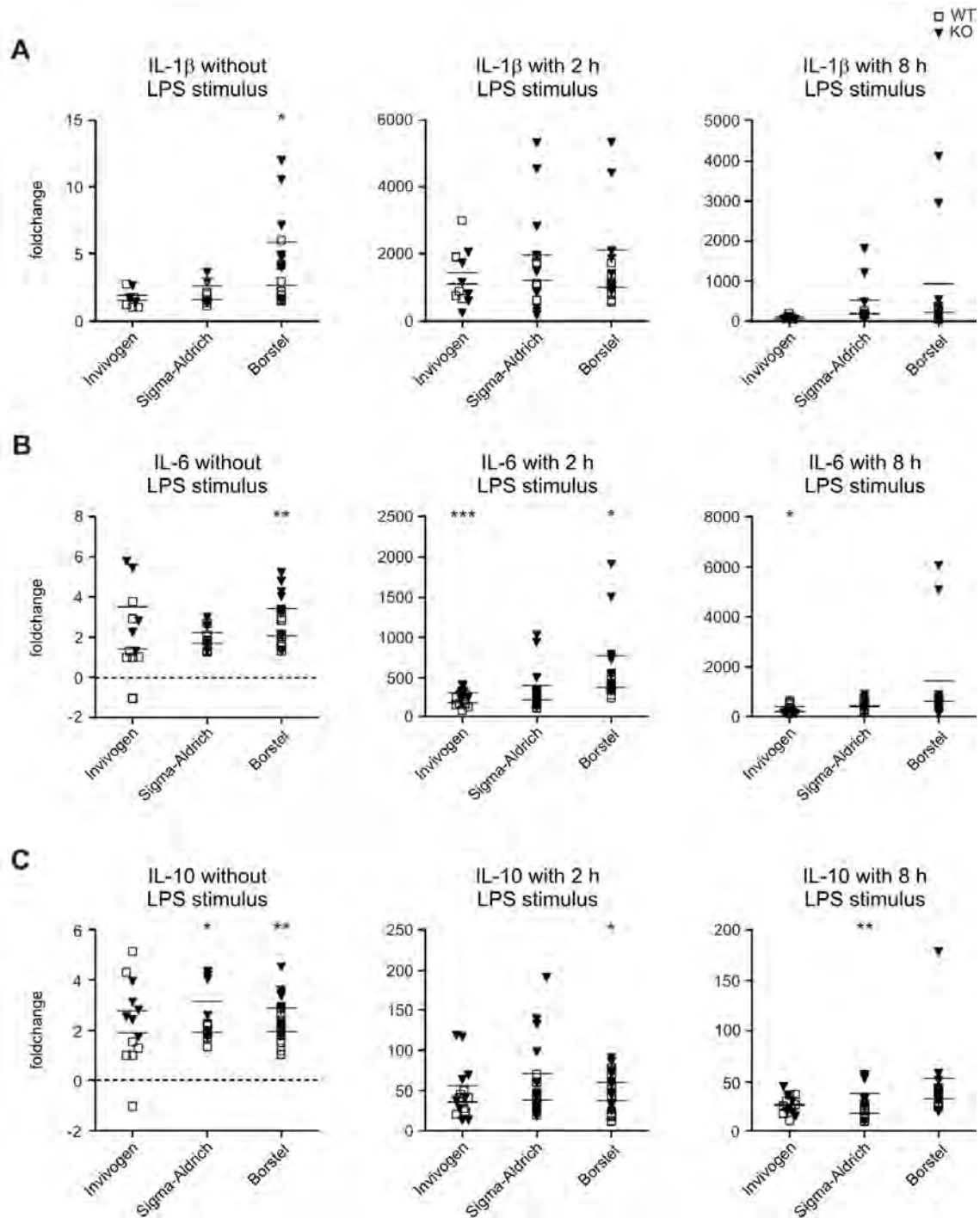


Fig. 4.21: TaqMan analysis of LPS stimulated BMDMs. BMDMs were stimulated with three different LPS for three different periods each. RNA was isolated, transcribed to cDNA, and analyzed via TaqMan. The cytokine expression of **A** IL-1 β , **B** IL-6, and **C** IL-10 was measured in unstimulated BMDMs and 2 and 8 hours after LPS stimulation. WT is indicated by hollow squares, KO by black triangles. Six mice of each genotype were used. Significance level were evaluated by Student's *t*-test.

a higher transcript level in KO cells. The stimulation with LPS induced a boost after 2 hours, extinguishing any significant difference between KO and WT (Fig. 4.22 C).

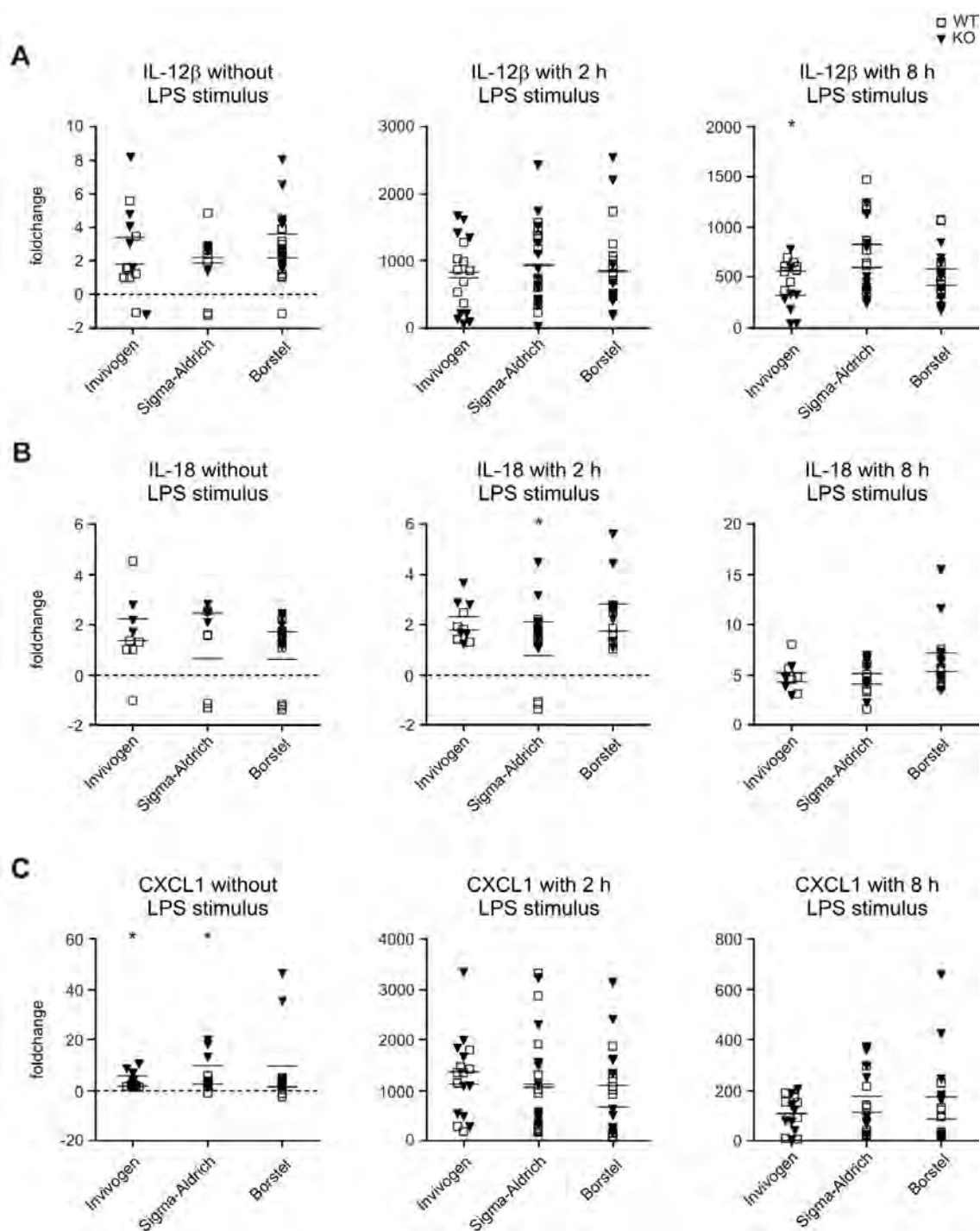


Fig. 4.22: TaqMan analysis of LPS stimulated BMDMs. BMDMs were stimulated with three different LPS for three different periods each. RNA was isolated, transcribed to cDNA, and analyzed via TaqMan. The cytokine expression of **A** IL-12 β , **B** IL-18, and **C** CXCL1 (murine IL-8 homologue) was measured in unstimulated BMDMs and 2 and 8 hours after LPS stimulation. WT is indicated by hollow squares, KO by black triangles. Six mice of each genotype were used. Significance level were evaluated by Student's *t*-test.

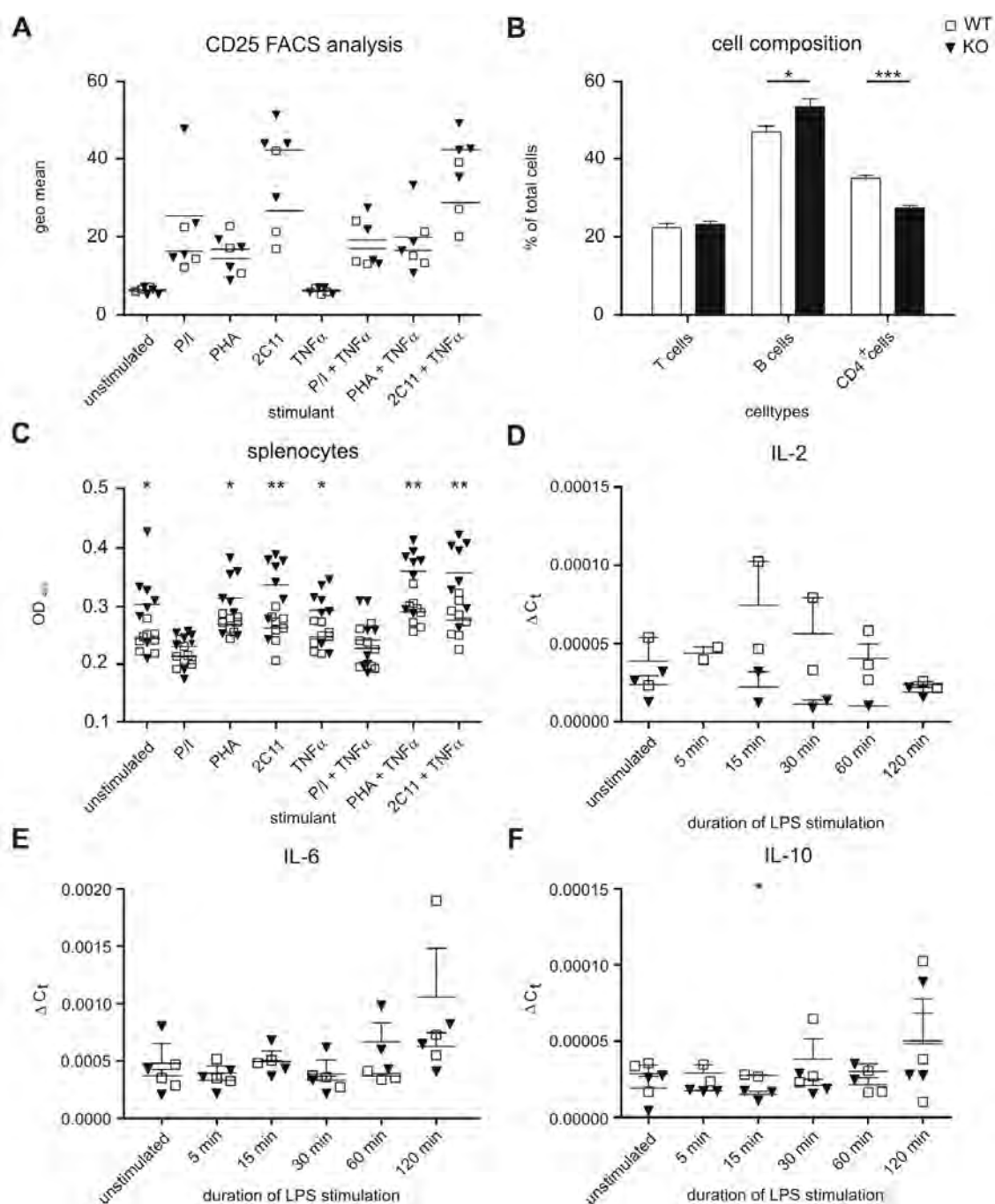


Fig. 4.23: Activation, responsiveness, composition, and IL-transcript level of murine mixed splenocytes. Murine mixed splenocytes were extracted from four $Nlr3^{+/+}$ (WT, hollow square) and $Nlr3^{-/-}$ (KO, filled triangle) mice each. **A** Cell composition of mixed splenocytes was assessed by FACS analysis. **B** The activation of T cells included in the mixed splenocytes was measured by FACS α CD25 staining. **C** Cell viability was tested by MTS assay. The transcript level of **D** IL-2, **E** IL-6, and **F** IL-10 were quantified via TaqMan Assay (three mice per genotype, two technical replicates). Significance levels were evaluated by Student's *t*-test.

4.6.1 Murine splenocytes as *in vitro* model for immune cells

Mixed splenocytes were isolated from $Nlr3^{-/-}$ and $Nlr3^{+/+}$ mice. The cell composition was evaluated, and cells were incubated with a set of stimuli quantifying activation by binding to α -CD25

via flow cytometry. Additionally, a viability assay was carried out (Fig. 4.23).

The isolated splenocytes were composed of about 20 % T cells, and 40 % B cells. Up to 30 % of the cells were CD4⁺. While B cells were significantly increased in KO mice, CD4⁺ cells were strongly decreased compared to WT mice (Fig. 4.23 A). Analysis of CD25 after stimulation revealed a strong activation effect for 2C11, being a T cell activator by binding to the CD3 ϵ of murine T cells. In comparison to WT splenocytes, KO cells displayed elevated CD25 marker levels (Fig. 4.23 B). *Nlrc3*^{-/-} mice had a significant higher viability in nearly all tested stimulation regimes. A stimulation or co-stimulation with P/I resulted in a lower viability, compared to unstimulated controls (Fig. 4.23 C). Additionally, a stimulation with LPS was conducted to achieve a more detailed time resolution of the splenocyte response. Assessing the transcript levels of *Nlrc3* and three of the major cytokines showed a decrease in IL-2 transcript levels, being stronger in WT cells. The IL-6 increase was nearly insignificant and indistinguishable between WT and KO. The transcript level of IL-10 increased slightly over time (Fig. 4.23 D-F).

4.7 Implication of NLRC3 in autoimmune and chronic inflammatory diseases

4.7.1 Wegener's granulomatosis/granulomatosis with polyangiitis

Wegener's granulomatosis (WG) is an autoimmune disease resulting in early stages in a local inflammation of the nasal mucosa [203]. Expression level of the NLRC3 protein were measured in patient samples (Fig. 4.24).

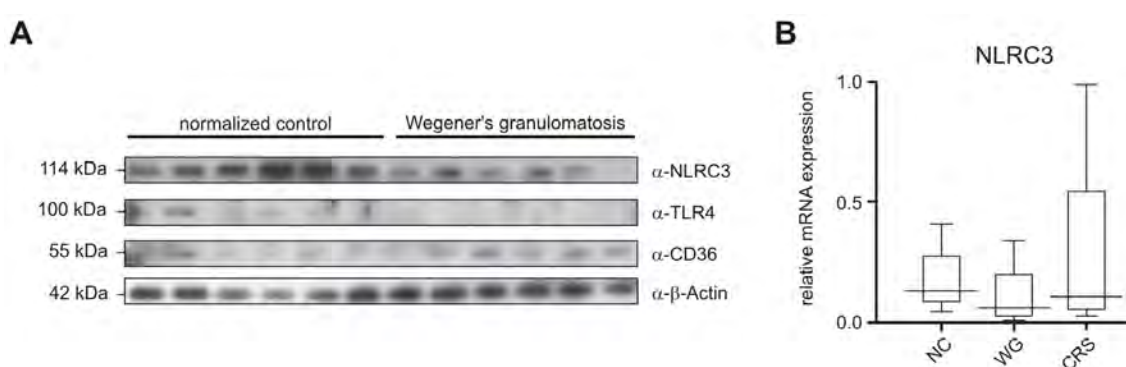


Fig. 4.24: NLRC3 protein level and relative mRNA expression in Wegener's granulomatosis. **A** Western blot of NLRC3 and other proteins of interest in samples from normal controls (NC) and WG patients (WG). **B** Relative mRNA expression of NLRC3 transcripts in NC, WG, and chronic rhinosinusitis with nasal polyps (CRS) patients. Box plots represent the 25th, 50th, and 75th percentile, whisker plots display 5th and 95th percentile. Asterisks highlights transcript which resulted in a p-value ≤ 0.05 and false discovery rate of the induction of $\leq 5\%$ when compared with WG.

While no histological abnormalities were detectable in biopsies taken from WG and normal con-

trols (NC) the NLRC3 protein level differed significantly. NLRC3, detected by the α -NLRC3 antibody showed a decrease in the protein levels of WG patients. The transcription levels of mRNA, assessed by qPCR analysis supported this trend (Fig. 4.24 B). The differences were based on specific disease associated mechanisms as general inflammation markers were not affected [203]. Several publications are referring to WG now as granulomatosis with polyangiitis (Wegener's) [204].

4.7.2 Crohn's disease

As NOD2, a member of the NLR family group, is highly relevant for Crohn's disease (CD) a qPCR test was performed on relevant samples, testing for altered NLRC3 expression. Biopsies from non-inflamed tissues were compared for 18 Crohn's disease, 11 Ulcerative colitis (UC), 15 diseased controls (DC), and 28 hospitalized normal (HN) patients. NLRC3 in CD was 1.3 times elevated compared to NC ($p=0.0324$) and 1.8 elevated with respect to inflamed disease specific controls ($p=0.0315$).

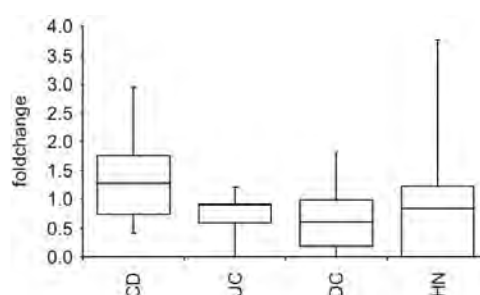


Fig. 4.25: Quantification of NLRC3 transcript level in IBD patients. Non-inflamed samples of Crohn's disease (CD), Ulcerative colitis (UC), diseased controls (DC), and hospitalized normal (HN) patients were analyzed via TaqMan. All samples were age and gender matched.

4.8 Impact of acute dextran sodium sulfate induced colitis on WT and KO mice

An acute murine colitis was induced by 4 % DSS. The experimental setup included only male $Nlrc3^{+/+}$, $Nlrc3^{-/-}$ mice, and an untreated $Nlrc3^{-/-}$ control group. The course of disease was scored via the proxies united in the disease activity index (DAI). Additionally, the mice were scored endoscopically on the final day. After sacrificing the mice the colon length was measured and normalized to the body weight and spleen weight was determined. Serum was sampled and selected organs were prepared for histological staining.

4.8.1 DSS-induced colitis heavily affects the colon

Prior to sacrificing the mice an endoscopic examination was carried out, resulting in the pictures displayed in Fig. 4.26 and the MEICS score as shown in Fig. 4.28 B.

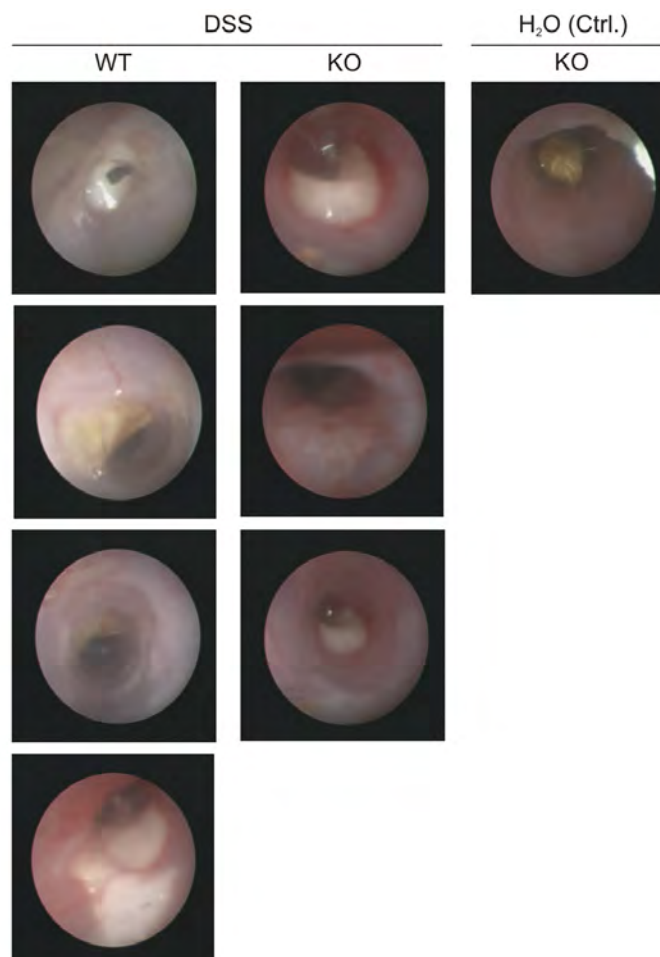


Fig. 4.26: Selected exemplary pictures of murine coloscopy. Prior to sacrificing the mice, they were anesthetized and examined by coloscopy. The coloscopy data were the basis for the MEICS score. Pictures shown are demonstrating the most striking features found during the endoscopy of all mice in the experiment.

An exemplary colon from a water treated control mice is shown in the control column (Fig. 4.27). The mucosa was found to be intact, the stool was formed and no plaques were seen. The blood vessels appeared normal. A different state was observed in the DSS treated mice. While the stool consistency was more like a smear several white fibrin patches were visible. Blood vessels were prominently seen in several directions and the mucosa was strongly eroded. As shown in Fig. 4.28 D the colons of DSS treated mice were significantly shortened. The exact measurements of colon length is given in Tab. 4.3.

A significant shortening of colon was observed when comparing water and DSS treatment. Both

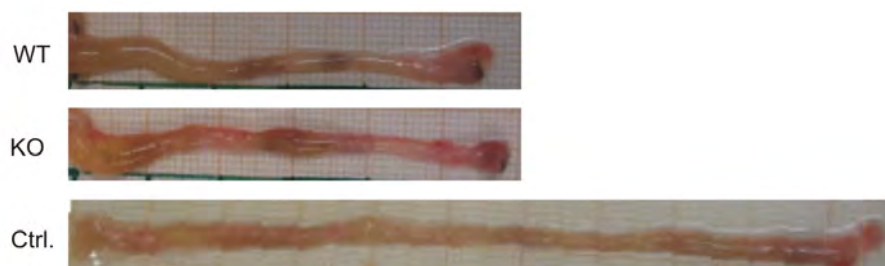


Fig. 4.27: Selected exemplary pictures of murine colons. The colon was flushed and measured. The proximal end is on the left side.

Tab. 4.3: Measured colon length of animals included in this study. Length is given in mm. Values in brackets were measured in animals which died during the experiment. Those values were not considered for Fig. 4.28 D.

genotype	colon length [mm]								
WT	55	47	52	50	55	50	51	42	
KO	(54)	50	(65)	53	(51)	58	50	70	60
Control	78	103	88						

genotypes were affected, displaying additional heavily inflamed distal parts and occasional patches of clotted blood.

4.8.2 DAI and MEICS score

The disease progression was monitored via DAI and finally via MEICS. Increasing index values represent a more severe disease progression. The results are summarized in Fig. 4.28.

While the untreated animals remained visibly healthy during the experiment, both treated groups showed a significant onset of disease at day three. The onset of disease was comparable in WT and KO during the first days, worsening significantly for *Nlrc3*^{-/-} animals on day six (Fig. 4.28 A). The experiment was stopped on day eight, with most mice reaching the critical cut off bodyweight of 75 % as depicted in Fig. 4.28 C. An endoscopic examination of the mice prior to scarification showed a significant difference between the DSS treated animals and the control, but not between WT and KO mice (Fig. 4.28 B). As a proxy for DSS-induced disease severity colon length was measured. After flushing the colon, it was measured and the length normalized to the body weight on day eight. While the untreated mice displayed a colon length of up to 103 mm, the colon was shortened down to 42 mm in DSS treated mice independent of the genotype.

Weighting the spleen resulted in weights between 34.9 and 106.1 mg, but gave no strict trend or significant different results between the genotypes or the treatment (Fig. 4.28 E). Additionally, the spleen length was determined, resulting in sizes between 12 - 17 mm. A significant difference

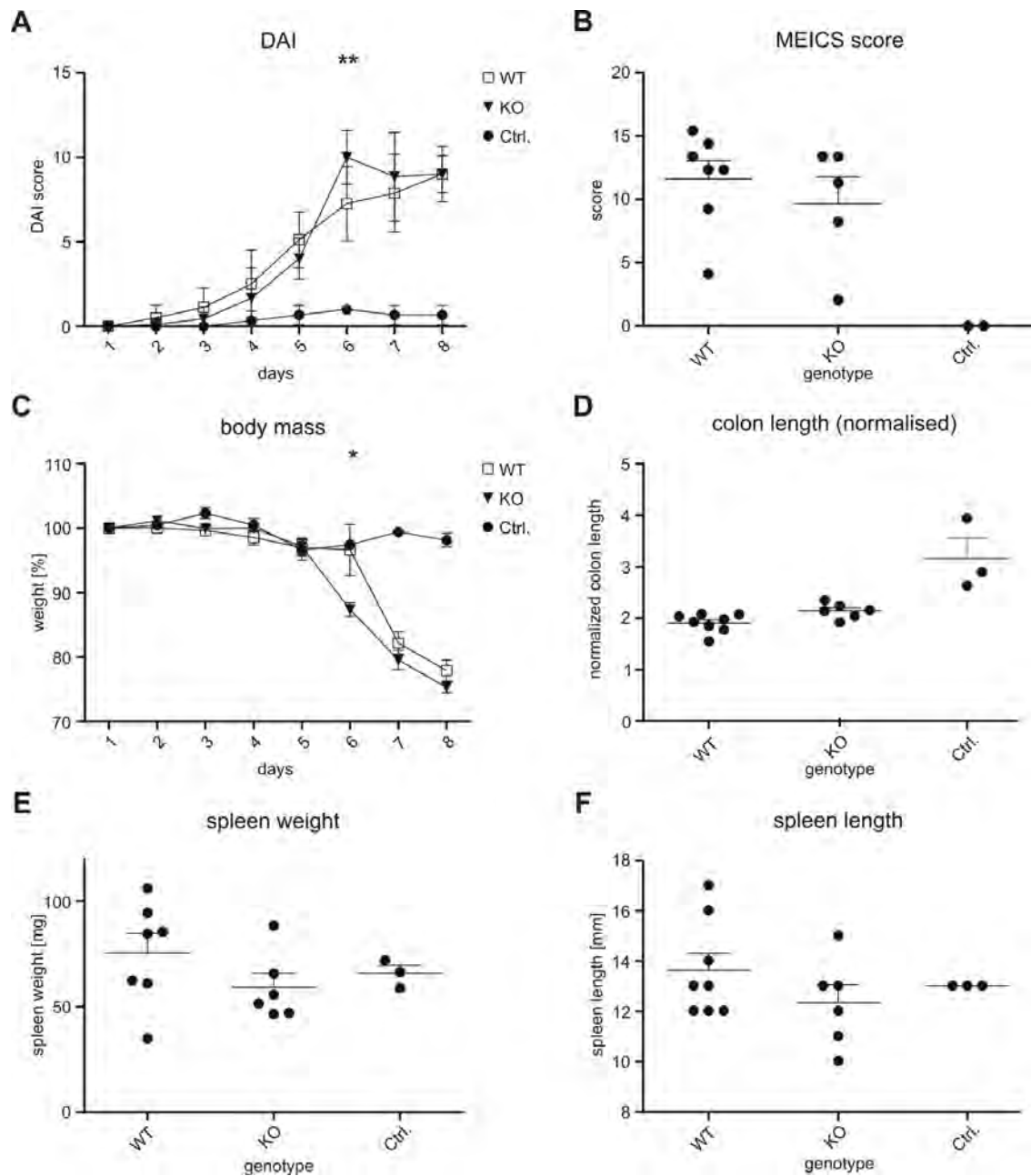


Fig. 4.28: DAI and MEICS score of acute DSS colitis. **A** The disease activity index (DAI) is an artificial numeric score, summed up from evaluation of weight loss, stool consistency, and intensity of rectal bleeding. The DAI was assessed on a daily basis. **B** The modified murine endoscopic index of colitis severity (MEICS) consists of five parameters and was assessed according to Becker *et al.* [187]. **C** Body weight was measured daily and is expressed in percent normalized to individual starting weight. **D** Colon length was measured and normalized to starting bodyweight of the respective mouse. Additionally, the spleen was weighted **E** and measured along its largest extent **F**. Initially 8 WT, 9 KO, and 3 Ctrl.-KO mice were used in this experiment. Due to disease progression, technical limitations or experimental procedures do not all graphs contain data from each mouse. All values of $Nlrc3^{+/+}$, $Nlrc3^{-/-}$, and an untreated $Nlrc3^{-/-}$ control group were corrected for statistical outliers and were finally analyzed by Student's *t*-test.

between the genotypes or a general response to the DSS treatment was not measurable (Fig. 4.28 F).

4.8.3 *Nlr3*^{+/+} mice are less affected of tissue damage and infiltration by immune cells

To visualize morphological changes in colon and ileum, microsections of fixed tissues were stained with HE. A HE score was evaluated in a blinded manner to grade the severity of tissue damage (Fig. 4.29 A). Therefore the two proxies "infiltration of immune cells" and "tissue damage" were scored with zero (unaffected) to three points (heavily affected) each. Summing up the points for each sample gave the HE score and therefore an indicator of the severity of DSS-induced colitis [205].

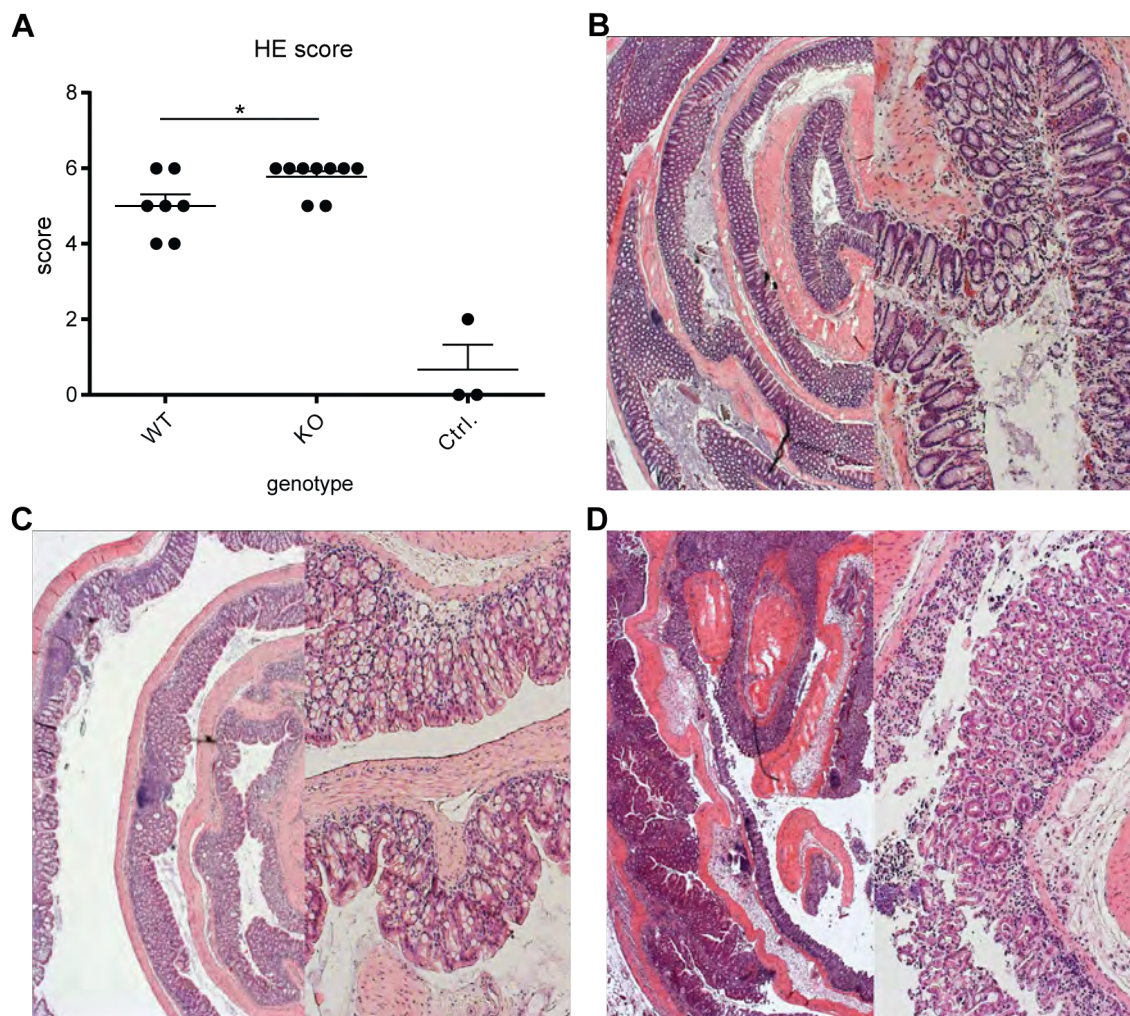


Fig. 4.29: Histological scoring of HE stained colon sections. The colon was flushed and cut longitudinally. After rolling it from distal to proximal, fixation in 10 % formalin, and embedding in paraffin, it was cut and stained with HE. **A** The scoring was performed in blinded manner, taking mucosal damage and invasion of immune cells into account. HE stained sections were microscopical inspected and scored, giving 0-3 points each for mucosal damage and immune cell invasion, with 0 being a non visible and 3 being a thoroughly visible effect. A Student's *t*-test was performed. **B-D** Exemplary microscopic pictures were taken for **B** Ctrl., **C** WT, and **D** KO, each showing a 5x magnified overview and a 10x magnified detailed photo. Due to disease progression, technical limitations or experimental procedures were not all mice represented in the graph.

Comparing the HE score of *Nlrc3*^{+/+} and *Nlrc3*^{-/-} mice showed a significant lower score for the WT. Both scores were highly elevated when compared to the untreated control mice (Fig. 4.29 A). The numerical scoring is based on microscopic evaluation. In Fig. 4.29 B-D exemplary pictures of the three groups are shown. Compared to the untreated controls in Fig. 4.29 B, both DSS treated samples displayed a severe change in cellular structure and organization. While the crypts were neatly aligned in the control, they seemed to lack any structure in the DSS treated samples. Crypts were closed or displayed no regular structures at all. Mucosal surfaces were eradicated and the *lamina propria* was infiltrated by immune cells. Additionally, some crypt abscesses were found. Those structures were manifested mostly in the distal part of the colon and were significantly increased in the *Nlrc3*^{-/-} samples. As seen in Fig. 4.30 those abscesses were characterized by a decrease of goblet cells and a reduced cell count per structure compared to healthy crypts.

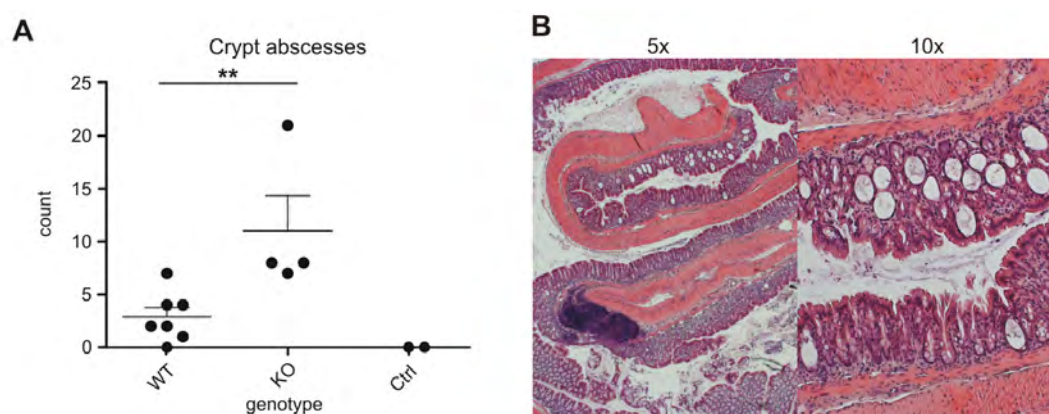


Fig. 4.30: Crypt abscesses in colon tissue of DSS treated *Nlrc3*^{-/-} mice. The colon was flushed and cut longitudinally. After rolling it from distal to proximal, fixation in 10 % formalin, and embedding in paraffin, it was cut and stained with HE. **A** The vacuolar like structures were counted in a sample blinded manner in all samples suitable. Some samples had to be excluded due to eradicated colon structure or cutting artifacts. **B** Two microscopic images are demonstrating the observed structures. The left side shows the general appearance in the distal colon. The 10x close-up on the right reveals the detailed morphology. Due to disease progression, technical limitations or experimental procedures were not all mice represented in the graph.

4.8.4 Serum and transcript level of interleukins

Additionally to the morphological analysis of tissue sections and organs, several molecular analyses were carried out. Murine blood was gained by coronal puncture. After clotting and centrifugation the serum was snap frozen. Due to the limited volume of serum available, three ELISA were performed, quantifying the serum level of IL-6, CXCL1, and IL-10 (Fig. 4.31).

The serum levels of neither IL-6 nor IL-10 were significantly altered comparing either WT vs. KO or the treatments. The same held true for a comparison of samples from DSS treated animals and

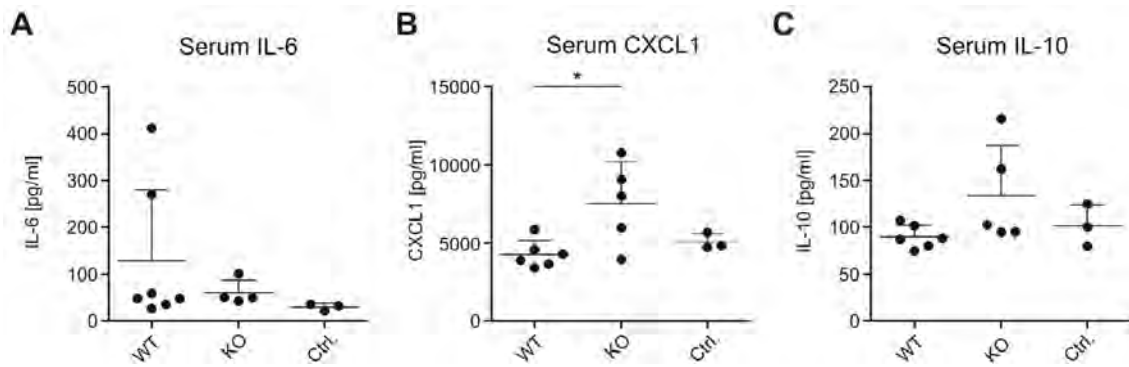


Fig. 4.31: Serum analysis of DSS treated mice. Serum concentrations of interleukins were measured by ELISA. All levels are given in pg/ml. Mean and standard deviation are indicated. **A** IL-6, **B** CXCL1, and **C** IL-10 levels of $Nlrc3^{+/+}$, $Nlrc3^{-/-}$, and an untreated $Nlrc3^{-/-}$ control group were assessed. A Student's *t*-test was performed after calculating values distribution and correcting for outliers. Due to disease progression, technical limitations or experimental procedures were not all mice represented in the graph.

the water control. The CXCL1 level was significantly increased in $Nlrc3^{-/-}$ mice treated with DSS. As the secreted interleukin levels were quite low, spleen, colon, and mesenchymal lymph node were tested for their IL-6 and IL-10 transcript level.

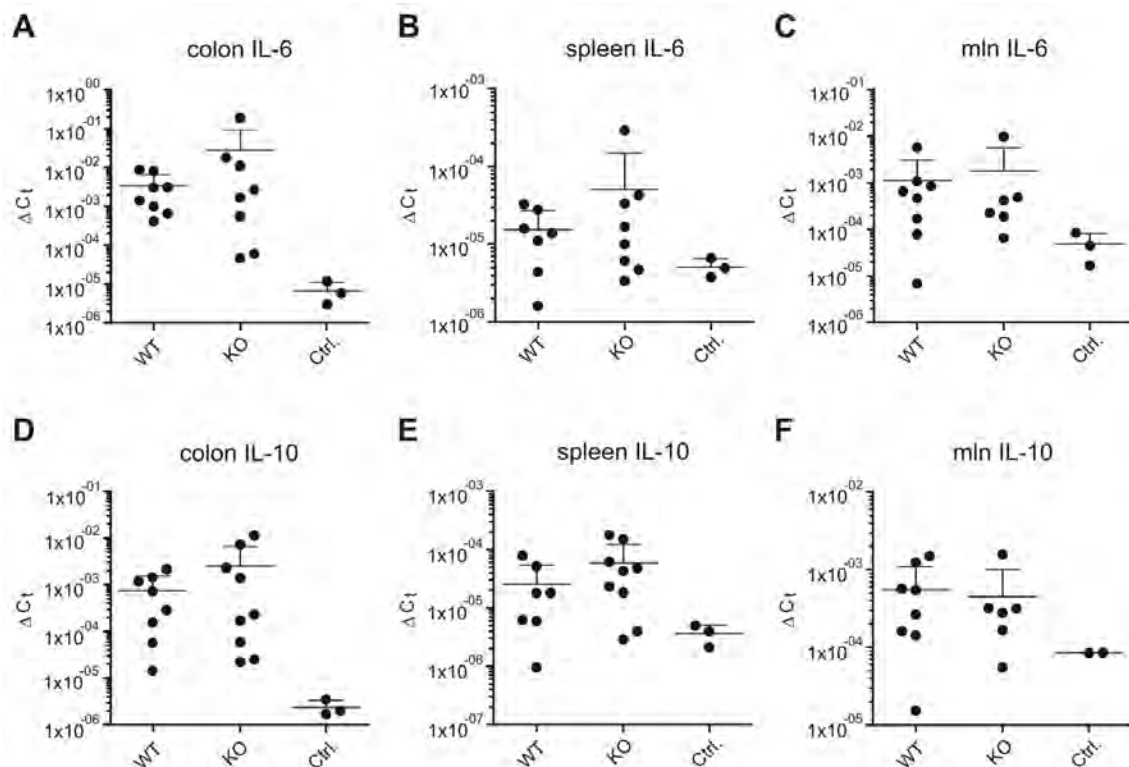


Fig. 4.32: TaqMan analysis of DSS tissue cDNA. RNA was isolated from colon, spleen, and mesenchymal lymph node (mln), processed and analyzed by TaqMan. Transcript levels of **A-C** IL-6 and **D-F** IL-10 were assessed in samples of DSS treated $Nlrc3^{+/+}$ and $Nlrc3^{-/-}$ mice, as well as in mice of the untreated $Nlrc3^{-/-}$ control group. A Student's *t*-test was performed.

In general only small ΔC_t values were gained (Fig. 4.32). The IL-6 level were increased in all

DSS treated samples compared to the untreated KO, revealing no significant difference between the treated WT and KO (Fig. 4.32 A-C). The mean value of the KO samples exceeded the WT values. The IL-10 levels were increased in all DSS treated samples as well, showing no distinctness between WT and KO (Fig. 4.32 D-F).

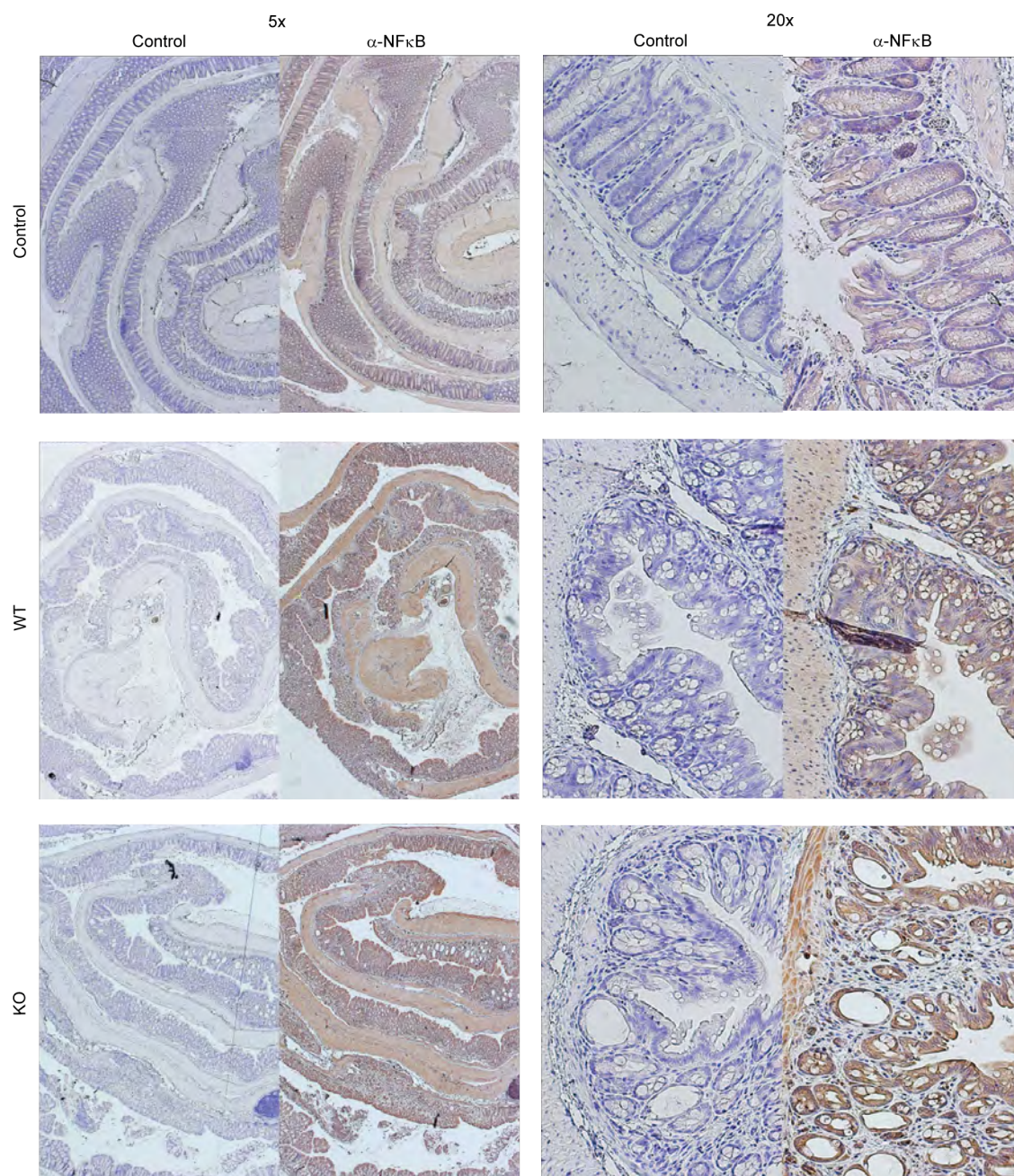


Fig. 4.33: NFκB activation in DSS treated *Nlr3*^{-/-} knockout mice. Mice were treated with DSS. After scarification the colon was rolled from distal to proximal and prepared for histological staining. Staining was carried out by using an α-NFκB antibody, being detected by the DAB system. Pictures were taken in two different magnifications, each comparing the secondary antibody only control (left) with the antibody based staining (right).

4.8.5 NF κ B is upregulated in DSS treated mice

Following the luciferase results, showing an impact of NLRC3 on the NF κ B pathway, colon sections of DSS treated mice were stained with an α -NF κ B antibody, using the DAB system. The comparative results are depicted in Fig. 4.33.

The untreated controls exhibited the weakest expression of NF κ B in the histological staining. Stained colon microsections from DSS treated mice showed a general increase in NF κ B, obviously strongest in the KO samples (Fig. 4.33). A treatment without the primary antibody was used as control. Thus the blue counter staining was predominant, showing no unspecific staining of the DAB system. As NF κ B was nearly ubiquitous expressed in cells a negative control including a first antibody was not suitable. All results are therefore to be seen in relation to the control animals.

4.8.6 Mitochondrial stress markers are not affected in colonic tissue after DSS treatment

Consistent with the idea of a mitochondrial stress reaction and a potential impact of unfolded protein response governed by Nlrc3 the transcript level of three described proxies (*grp78*, *cpn60*, and *pkf* [206]), were quantified via SYBRGreen analysis (Fig. 4.34).

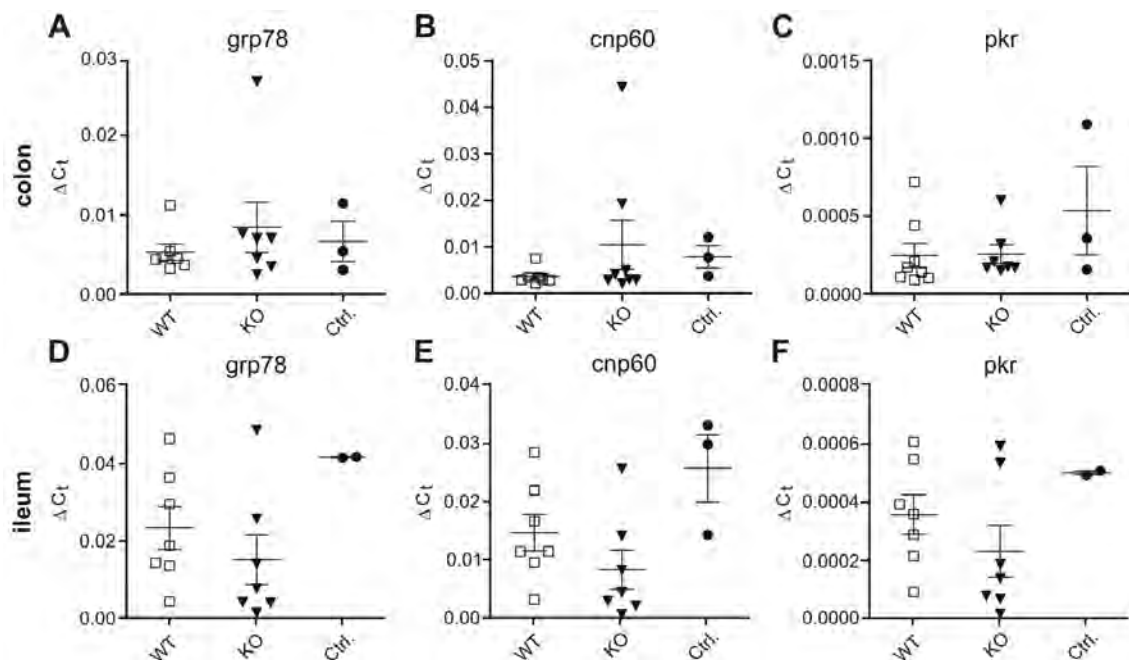


Fig. 4.34: SYBRGreen analysis of DSS tissue cDNA. RNA was isolated from colon and ileum, processed, and analyzed by quantitative qPCR. Transcript levels of *pkf*, *cpn60*, and *grp78* were assessed. **A-C** Colon and **D-F** ileum samples of Nlrc3^{+/+}, Nlrc3^{-/-}, and an untreated Nlrc3^{-/-} control group were analyzed. A Student's *t*-test was performed.

Comparing the expression level of *grp78* between WT and KO did not reveal any significant dif-

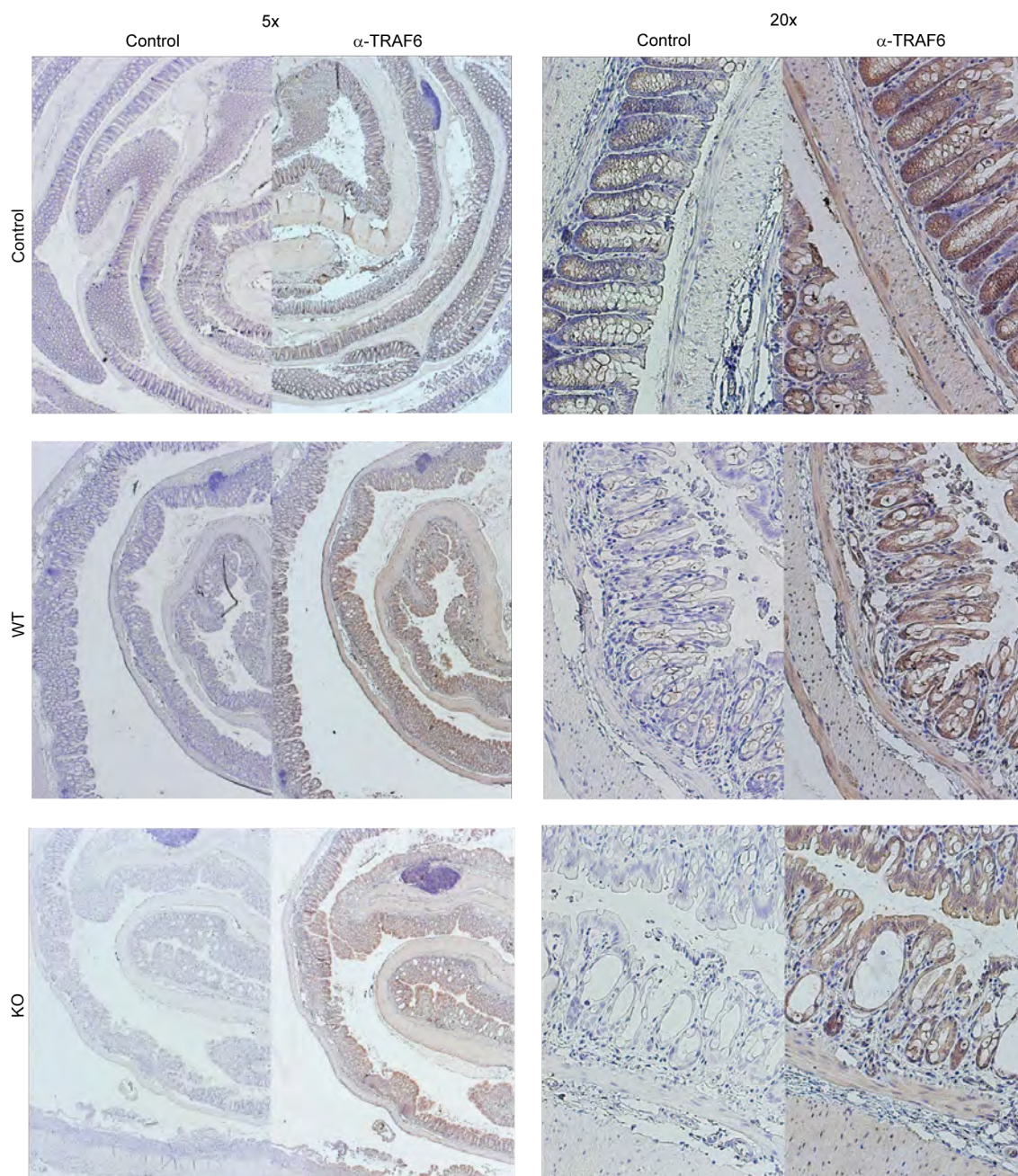


Fig. 4.35: TRAF6 staining in DSS treated colon samples. Mice were treated with DSS. After scarifying, the colon was rolled from distal to proximal and prepared for histological staining. Staining was carried out by using a α -TRAF6 antibody, being detected by the DAB system. Pictures were taken in two different magnifications, each comparing the secondary antibody only control (left) with the antibody based staining (right).

ferences between neither both genotypes nor the genotypes and the controls. The variation was remarkably low in colon samples, while it showed an interesting trend in ileum. The grp78 level were generally lower after DSS treatment, independently of the genotype, although the level in KO tended to be lowest. With regard to cpn60 level it has to be mentioned, that colon samples seemed to be unaffected, while the level were decreased in DSS treated ileum cells. Nevertheless

did no statistical significances occur. The pkr levels were the lowest in the whole experiment with regard to their ΔC_t value. Neither the level in colon nor in ileum samples showed a statistically relevant difference.

4.8.7 TRAF6 is diminished in DSS treated mice

As TRAF6 is a member of the downstream signaling in the NF κ B pathway it was tracked by histological staining in microsections from DSS mice.

The TRAF6 control showed a widely distributed staining. Compared to the control the villi and muscularis were stained brownish, indicating a TRAF6 localization. The intensity of staining decreased in WT an even more in KO samples (Fig. 4.35). The crypt abscesses shown in Fig. 4.30 were visible in this samples, too. The inner lining of the structures seemed to be thoroughly stained.

5 Discussion

5.1 NLRC3/Nlrc3 is localized in immune relevant tissues

The expression level of NLRC3/Nlrc3 were assessed in human and murine cDNA samples (Fig. 4.2). Human NLRC3 was found to be highest expressed in tonsil, leukocytes, thymus, lymph node, and spleen (Fig. 4.2 A). These findings are supported by the study of Yin *et al.* although they found a markedly higher expression in placenta cDNA [207].

Results shown in Fig. 4.1 and 4.2 B present an extended picture for mice. Immune relevant organs, such as lymph node, thymus, and spleen show an increased expression of Nlrc3. These findings are in concordance with the results from human samples, with slight differences according to their relative values. The high expression in thymus is supported by earlier findings, describing NLRC3 as a negative regulator for T cells [50]. Combined with a low expression of NLRC3 in hematopoietic stem cells the results suggested that NLRC expression occurs in cells that have undergone thymic maturation and induction. Samples obtained from organs of the gastrointestinal tract display a low expression of NLRC3/Nlrc3 in both, human and mouse. The respective organs were not assessed in the gene microarray published by Conti *et al.* [50]. Additionally, only weak NLRC3 expression was measured in healthy brain samples, which supports the theory of suppressed NLRs in immune privileged sites [208].

Comparing these results to previously published data by Conti *et al.* reveals a high overlap in mouse data. The human samples exhibit a comparable NLRC3 expression profile with additional high NLRC3 transcript levels in leukocytes, spleen, and tonsil. The latter two were not tested by Conti *et al.*. In general, the expression level of NLRC3 in bone marrow and lymph node samples is higher in the experiments conducted for this thesis. Higher NLRC3/Nlrc3 transcript levels were found in types of immune relevant tissues, indicating a lack of NLRC3 in most other tissues.

Differences between the current data and those found by Conti *et al.* may occur due to different sampling strategies. The data in this thesis are based on pooled cDNA samples, while Conti *et al.* mined different microarrays and compared them to a murine profile to validate the data sets. Their data might be stratified due to the fact that every sample originated from a different individual, bearing the danger of different health/immune states of each donor. This indicates the importance of standardized sampling and processing procedures to avoid contamination, activation or induction.

The NLRC3 expression in kidney and spleen is matched by an earlier study in channel catfish *Ictalurus punctatus* [48]. Sha *et al.* additionally found increased level in the intestine, a feature which seems to be specific for fish. This might indicate a difference in NLRC3 distribution between systematic classes, such as mammals and pisces. Overall, tissues involved in the generation of immune relevant cells seem to express NLRC3/Nlrc3.

5.2 NLRC3 in mitochondria associated immune functions

To address localization and the functional role of NLRC3 in cell signaling pathways, HEK-293 cells were used, which express endogenous levels of NLRC3 (Fig. 4.3 A). Additionally, the adherent HEK-293 cells allow the transfection of recombinant NLRC3 and luciferase-based reporter assays and a reliable visualization in microscopic studies. HeLa cells were used to confirm the microscopic results.

In Fig. 4.4 the localization of endogenous NLRC3 in HEK-293 cells, as well as in primary culture of PBMCs, was detected in the cytosolic fraction only. This finding was confirmed by microscopy in antibody-tagged NLRC3 coverslip staining (Fig. 4.6). One of the general features of NLR proteins seems to be their cytosolic or intracellular localization [209]. Y2H approach revealed the mitochondrial protein Mitofilin/IMMT as a potential interactor for NLRC3. The cytosolic localization of NLRC3 would allow an interaction with mitochondria. During a MS/MS analysis NLRC3 was detected in mitochondrial lysates (Fig. 4.10).

5.2.1 Mitochondria in innate immunity

Mitochondria are considered to be crucial hubs for the immune system. An overview of mitochondrial associated proteins involved in innate immunity is given in Tab. 5.1. NLRX1 has been the only member of the NLR family known to localize to mitochondria so far. Although the N-terminal HA-tagged version of NLRX1 was not observed inside the mitochondria, most likely due to an additional tag, it was proposed to interact with mitochondria via a mitochondria associated viral sensor (MAVS) [210]. MAVS has been shown to have a critical effect in the activation of antiviral host response, by spanning the outer mitochondrial membrane and activating the NF κ B pathway [211]. A MAVS mediated apoptosis was shown, including viral strategies to evade apoptosis by inhibiting host response [212]. This interaction might prove valuable for further NLRC3 studies since initial Y2H results indicated NLRC3 to interact with the mitochondrial protein Mitofilin (IMMT).

Tab. 5.1: Mitochondrial proteins associated with immune related signaling. ASC: Apoptosis-associated speck-like protein containing a CARD; c: cytosol; cs: cell surface; ECSIT: Evolutionary conserved signaling intermediate in Toll pathway; IFN: Interferon; IRGM: Immunity-related GTPase family M protein; loc: localization; MAP: Mitogen-activated protein; MAPK: MAP kinase; MAVS: Mitochondria associated viral sensor; MDA5: Melanoma differentiation associated gene 5; NEMO: NF κ B essential modifier; RIGI: Retinoic acid-inducible gene gene I; RLR: RIGI like receptor; ROS: Reactive oxygen species; tl: translocates; TANK: TRAF family member-associated NF κ B activator; TBK: TANK binding kinase; TLR: Toll like receptor; TRAF: TNF receptor associated factor; UQCRC2: Ubiquinol-cytochrome c reductase core protein II.

PRR	trigger	adapter	signaling	loc	source
NLRX1	<i>indirect?</i>	UQCRC2	MAVS	tl	[210, 213]
NLRP3/ NALP3	mitoROS?	ASC	Inflammasome/ Caspase-1		[214, 215, 216]
RIGI like/ MDA5	viral ss/ds RNA	MAVS	TRAF3&6/ TBK1-NEMO/ NF κ B	c	[211, 217, 218, 219]
TLR1/2/4 IRGM	ROS intracellular pathogens	TRAF6/ECSIT cardiolipin	NF κ B, MAPK HMGB1	cs	[220] [221, 222]

To evaluate whether NLRC3 interacts with the mitochondrial protein IMMT, a three-step microscopic sequence was established. As shown in Fig. 4.6, HEK-293 cells were transfected with flag-tagged NLRC3. The α -flag antibody detected the overexpressed flag-tagged NLRC3, while the α -NLRC3 antibody detected both the endogenous and overexpressed NLRC3. The nucleus and mitochondria were stained with DAPI and Mitotracker, respectively. The merged pictures showed an overlap of the mitochondrial and NLRC3 signals indicating the spatial localization of NLRC3 with mitochondria. To confirm the potential interaction between NLRC3 and IMMT, a specific α -IMMT antibody was used. The perfect overlap of the IMMT and mitochondrial staining (Fig. 4.7) demonstrate the specificity of the detection. An overlap of Mitotracker and NLRC3 signals was detectable. These finding were confirmed in transfected HeLa cells (Fig. 4.8). A higher resolution and a correlation analysis were gained by CLS microscopy (Fig. 4.9). The merged picture indicates a broad overlap of the NLRC3-, IMMT- and Mitotracker signals. A second approach without Mitotracker was used for a correlation analysis, further confirming the overlap of signals. Co-immunoprecipitations performed, did not show an interaction of NLRC3 and IMMT, probably due to technical limitations of the α -NLRC3 antibody (Fig. 4.5). A tandem mass spectrometry (MS/MS) analysis of the mitochondrial lysates was conducted, confirming NLRC3 in mitochondria lysate. However, in the same study NLRC3 was not detected in the α -NLRC3 immunoprecipitation from the same mitochondrial lysate, reassuring the limitations of the NLRC3 antibody (Tab. 4.1).

The difficulty to show a direct interaction between NLRC3 and mitochondria raises the possibility of an induced re-localization. Upon stimulation, cytosolic NLRC3 might be recruited to the mitochondria. After TNF α stimulation NLRC3 did not migrate to the membrane, but decreased over time in the cytosolic compartment (Fig. 4.13). No accumulation of NLRC3 was detected in the membrane fraction. The close spatial proximity of NLRC3 and IMMT may involve a yet unknown adapter similar to the interaction of NLRX1 (Tab. 5.1). Factors like mitochondrial membrane potential and conformational changes after ligand binding might influence this translocation as well [210, 223].

Subsequently, in a bioinformatic approach probabilities of mitochondrial localization of NLRC3 were calculated. These *in silico* analyses predicted low values for the human NLRC3 isoforms (max. 0.11), but increased probability values for the murine Nlrc3 isoforms 3 and 4 (Tab. 4.2). A different analysis by Moore *et al.* calculated lower values for mitochondrial localization. As the exact location of NLRC3 within the mitochondria or mitochondrial complex remains unknown it is interesting to note significant differences in the mitochondrial import probability of the Nlrc3 isoforms. While the human variants and the murine consensus isoform were calculated to have a low probability to be imported into mitochondria, the results for isoform 3 and 4 are much more promising. Both isoforms are truncated and are lacking the NACHT domain. This is true for the murine isoform 5 as well. Taking the electric charge of the isoforms into account does not solve the problem either. It becomes obvious, that mitochondrial targeting is an interplay of a variety of different molecular and biophysical factors [190, 193]. Additionally, the integration of NLRC3 into the outer membrane of the mitochondria might be a feasible mechanism to enable NLRC3 and IMMT interaction [92].

5.2.1.1 Supramolecular mitochondrial structures

Several α -NLRC3 Western blots showed additional and distinct bands at high molecular weight (>250 kDa) in cellular lysates following stimulation [data not shown]. Although NLRC3 is not known to multimerize, dimerization is a common feature in members of the NLR family [36]. High molecular weight complexes have been published for mitochondrial constituents, such as IMMT [82, 224]. To determine whether the high molecular weight protein bands correspond to complexes of IMMT with NLRC3, the lysates were analyzed by MS/MS. Comparable to a variety of recently described signalosomes, an IMMT containing multi-protein complex would offer several possibilities for NLRC3 association. Matrix and membrane spanning elements could bridge

the spatial distance, while functional complexes, such as Optic atrophy 1 (Opa1) and DISC could provide effector activities. A yet hypothetical model could be considered as followed:

The coiled-coil-helix-coiled-coil-helix domain containing protein 3 (Chchd3) is a peripheral protein of the inner mitochondrial membrane facing the intermembrane space. It closely interacts with the IMMT and Opa1, which are both located in the mitochondrial cristae and are involved in cristae morphology [80, 91, 225]. Downregulation of those proteins leads to mitochondrial fission and cristae morphology loss [80, 84]. This complex interacts with Sam50, being an outer mitochondrial membrane protein regulating import [224]. As Chchd3 has been proposed as a protein that preserves cristae integrity and mitochondrial stabilization, it would be an ideal interaction partner for an NLRC3 mediated signaling, relayed through IMMT. Chchd3 has been shown to be part of a 340 kDa mitochondria organizing complex that has not been fully sequenced yet [226]. A variety of human pathologies are associated with alterations of these complexes, ranging from Epilepsy to diabetic cardiomyopathy [82, 227, 228]. The MS/MS results presented in this thesis did not identify a complex, neither in the lysate nor in the pull down assay. This indicates the need of further effort to induce and stabilize the high molecular weight complexes in order to characterize them.

5.2.1.2 Mitochondrial unfolded protein response (mtUPR)

The mtUPR is characterized as a cellular stress response activating nuclear-encoded mitochondrial chaperone genes in order to restore organelle protein homeostasis [229]. Similar to the UPR generally known from the ER, the mtUPR facilitates the refolding of mis- or unfolded proteins by the use of heat shock Hsp70 family members. The mitochondrial matrix includes chaperones for the general import and folding of proteins. Failures in this machinery might be corrected by proteases in the inner membrane by degrading misfolded proteins [230]. This process can be modified according to the needs of the cell. In this cause, the mitochondrial import efficiency is monitored as a proxy for mitochondrial overall performance [231, 232]. However, the complete signaling pathway is still under investigation. In a first attempt to unravel the molecular processes, an ER targeting stress test was performed. The ERSE was cloned into a dual luciferase system. ERSE is one out of three *cis*-acting elements which are capable of binding the transcription factor ATF6 [196, 233]. ER bound molecular chaperones are activated downstream to relieve the UPR burden. As shown in Fig. 4.11, HEK-293 cells were transfected with an ERSE-promoter responsive luciferase. The effect of NLRC3 overexpression and stimulation with either TNF α or tunicamycin

was quantified. Tunicamycin is a known stressor and inducer of UPR, which ultimately can lead to apoptosis [234, 235, 236]. Results show that tunicamycin stimulation successfully induces the ERSE activity. Additionally, a significant increase in ERSE activity in the NLRC3 overexpressing cells was observed (Fig. 4.11). An upregulated activation of ERSE reflects the physiological cell response to decide upon the cell fate. Depending on the downstream signaling the cell may either upregulate molecular chaperones to counteract unfolded protein response, or activate apoptotic pathways, when the unfolded protein burden overpowers the repair mechanisms of the cell [198]. Overexpressing NLRC3 alone does not induce ERSE. In combination with a stressor like tunicamycin is the ERSE promoter activity significantly increased. An increased NLRC3 level leading to higher ERSE activation may therefore result in a protective function of NLRC3.

The hypothesis of NLRC3 being involved in mitochondrial apoptotic processes is further supported by the fact that CARD domains have been originally described to be in close relation to mitochondria dependent apoptotic signaling [237]. Furthermore, the translocation of the TNF α receptor 1 (TNFR1/CD120a) triggered by TNF α administration to mitochondria has been observed [238]. This is of importance as the DISC formation is TNF dependent and TNF α decreases the cytosolic NLRC3 expression (Fig. 4.13; [239]). Further *in vivo* studies of Nlrc3 effect on mtUPR are discussed in chapter 5.6.

5.3 NLRC3 is involved in central immune signaling pathways

5.3.1 NLRC3 is involved in the NF κ B signaling pathway

HEK-293 cells overexpressing different levels of NLRC3 and stimulated with TNF α had an increased NF κ B reporter gene activity. NLRC3 transfections were performed with 10-fold lower DNA than used by Conti *et al.* which should keep the effect on destabilizing luciferin to a minimum and mimic a more physiological range [50, 68]. A notable increase in NF κ B activity in response to TNF α and overexpression of NLRC3 was observed. Increasing the amount of NLRC3 showed the contrary effect by decreasing the NF κ B activity (Fig. 4.12). The results suggest that NF κ B activation is governed by a threshold of NLRC3 expressed and a resulting negative feedback loop.

Conti *et al.* showed a decrease of NF κ B reporter activity with increasing NLRC3 level. Their time-course kinetics showed a reduced degradation of I κ B α after overexpression of NLRC3 demonstrating that NLRC3 may negatively regulate T cells via the canonical NF κ B pathway [50]. An increasing I κ B α level in a time-course stimulation study indicated a downregulation of the NF κ B

pathway in the presence of NLRC3 [51]. The validity of luciferase assays was questioned by Ling *et al.*, who stated that the overexpression of NLRC3 resulted in an artificial inhibition of NF κ B [68]. To address this concern we employed in this study a dual luciferase assay with a second luciferase under a thymidine-kinase promoter of Herpes simplex virus.

5.3.2 NLRC3 mediated NF κ B signaling pathway is modulated by TRAF6

Rising evidence suggests a close crosstalk between TLR and NLR pathways, although it still remains poorly understood. Of special interest is a recently published paper by Schneider *et al.*, showing that NLRC3 inhibits the K63-ubiquitination of TRAF6 and the TLR mediated NF κ B signaling [51]. Experiments showed, that the overexpression of 5 ng NLRC3 during a TNF α stimulation increases the NF κ B promoter activity. Increasing the amount of NLRC3 led to a contrary result (Fig. 4.12). The activation of the NF κ B promoter could be generally shown in Fig. 4.14, too. Interestingly, the presence of TRAF6 siRNA interferes with this result. As TRAF6 is known to be an activator of NF κ B, one would expect an additive effect of NLRC3 and TRAF 6 [201]. Nevertheless, in the experiments presented here is the NF κ B promoter activity increased, when TRAF6 is downregulated. This holds true for experiments with and without overexpressed NLRC3. Additionally, the normalized activity in samples containing NLRC3 and TRAF6 siRNA is significantly lower than in samples containing TRAF6 siRNA and a mock vector (Fig. 4.14).

A downregulation of TRAF6 mediated NF κ B signaling has been described in connection with an Epstein-Barr virus infection or microRNA miR-146 transfection [240, 241]. Schneider *et al.* observed an inhibition of TLR mediated NF κ B activation by NLRC3, proposing a negative feedback loop. Still, the significant difference without overexpressing NLRC3 is not answered. Those effects were not significantly detectable in unstimulated cells (Fig. 4.14). An upregulation of NF κ B in response to TNF α stimulation was expected and the effect mentioned above might be the result of the TRAF6 and NLRC3 interplay, which is not fully understood yet. There is an apparent overlap in the signaling of TLRs and NLRs converging at the same signaling cascades [242, 243, 244]. This convergence may either potentiate the signals or trigger a common inflammatory response to different stimuli. Additionally, TRAF6 forms the linkage between the TLR receptor and the evolutionary conserved signaling intermediate in TOLL pathway (ECSIT) [245]. TRAF6 translocates to the mitochondria upon activation resulting in mitochondrial ROS and localization of ECSIT to mitochondria where it is crucial for the assembly of complex 1 of the respiratory chain [146, 220]. It has been shown that TRAF6- Δ T mice displayed an increased IL-17 level during DSS-induced

colitis, indicating a beneficial effect on disease progression in absence of TRAF6 [246]. IL-17 is mainly produced by T cells in the lamina propria and has a protective effect by inducing tight junctions and mucin expression [247, 248].

A Y2H screen and Co-immunoprecipitation [data not shown] did not reveal a direct interaction between NLRC3 and TRAF6 which is confirmed by others [51]. A histological staining shown in Fig. 4.35 was performed in sections of intestinal tract of *Nlrc3^{-/-}* mice after an acute DSS colitis. The results suggest a decrease of TRAF6 in *Nlrc3^{-/-}* mice after colitis. The strong TRAF6 staining in the untreated control, which were mainly located at the villi surface, was not detectable in the DSS treated *Nlrc3^{-/-}* mice. This may be due to the heavily rearranged colonic structure. Overall, the DSS-treated mouse show an increased TRAF6 level in wildtype *Nlrc3^{+/+}* mouse tissues and decreased level in *Nlrc3^{-/-}* samples. These findings are supported by recent work from Shen *et al.*, who showed that TRAF6 expression is significantly increased in serum, PBMCs, and inflamed intestine mucosa of IBD patients [249].

Besides the *in vivo* data from DSS colitis experiments TRAF6 was assessed in *in vitro* cell culture experiments. Dual luciferase assays were conducted with expression of NLRC3 and knockdown of TRAF6 via specific siRNA. The results are shown in Fig. 4.14. As expected, the normalized activity of the NF κ B-Luc reporter was increased in response to TNF α stimulation. In TNF α stimulated HEK-293 cells, a knockdown of TRAF6 upregulates NF κ B, an effect which is significantly decreased by the addition of NLRC3.

Unstimulated cells showed the same trend although less notable. The results indicate that the overexpression of NLRC3 enhances the NF κ B downregulation. The general impact of NLRC3 on the NF κ B pathway was shown to be dependent on the amount of NLRC3 overexpressed (Fig. 4.12). High amounts of NLRC3 downregulate NF κ B, which is in concordance with the hypothesis by Schneider *et al.*, that NLRC3 inhibits TRAF6 mediated NF κ B signaling. Lower amounts of NLRC3 seem to activate NF κ B signaling. The main discrepancy between studies was found when comparing the basal GFP-luciferase assays with the TRAF6 knockdown. Overexpressing even low amounts of NLRC3 seems to decrease the NF κ B signaling. This effect may occur due to different tags, although the findings by Conti *et al.* seemed to be less affected [50]. In the results presented here, a TRAF6 knockdown led to an increase in NF κ B. Combining a TRAF6 knockdown with a NLRC3 overexpression resulted also in a decrease of NF κ B activity. This combination might prove critical in mediating inflammation in affected tissues.

5.4 Interleukins

The mediation of interleukin level is of utter importance in a regulated cell response and aims at re-establishing homeostasis. An interleukin level is a suitable proxy to determine the current state of an inflammatory process and to identify variations caused by genetic knockouts. Experiments in this thesis utilized bone marrow derived macrophages, mixed splenocytes, and serum from DSS treated animals to study interleukin levels. The *in vivo* studies are discussed in subsection 5.6.3. BMDMs are widely used for immunological studies as they exhibit a long lifespan, yield high RNA/protein levels, high homogeneity, and a strong proliferative capacity [185, 250].

The BMDM based stimulation experiments rely on a LPS concentration of 100 ng/ml incubated for two to eight hours to assess early and late responses. The induction of NF κ B in response to LPS (10 μ g/ml) within 0.5 h has been shown for cell lines, indicating the temporally framework for these experiments [145]. LPS of different quality grades was used - LPS from the FZ Borstel and Sigma-Aldrich (Tab. 3.17). First is ultra pure and considered to solely activate the TLR4 pathway, while the less pure Sigma-Aldrich preparations might provide low amounts of alternative stimuli.

5.4.1 Pro-inflammatory cytokines are elevated in Nlrc3^{-/-} BMDMs

All LPS preparations applied induced an IL-6 secretion in WT and KO (Fig. 4.19). Transcript levels of the pro-inflammatory cytokines IL-1 β , IL-6, and CXCL1 were increased (Fig. 4.20, 4.21, and 4.22).

IL-1 and IL-6 can induce acute phase proteins and are generally considered to be pro-inflammatory [251, 252]. IL-1 has been shown to be increased in inflammatory bowel disease during the active phase [253]. Additionally, those values are expected to be high shortly after colonic injury and during tissue repair [254]. The higher IL-1 β levels therefore indicate that the BMDMs from Nlrc3^{-/-} mice are more effected by the LPS stimulation, indicating a protective effect of Nlrc3 in murine BMDMs. The finding for IL-6 agrees with published findings in THP-1 cells [51] and indicates a negatively regulatory role of Nlrc3 in signaling. Preventing a high pro-inflammatory IL-6 level is furthermore in concordance with the hypothesis of a protective Nlrc3 behavior. Plasma level of IL-1 β and IL-6 have been studied in connection with IBD [255]. IL-1 levels were elevated during flares of acute disease, fitting well to the higher values in Nlrc3^{-/-} BMDMs. Hiscott *et al.* published that NF κ B is a potent inducer of IL-1 [256] giving a further potential connection to Nlrc3. The CXCL-1 level dramatically increased after 2 hours and remained elevated throughout the next six hours, a behavior which is in concordance with earlier findings [168]. The higher chemokine

level in *Nlrc3*^{-/-} is indicating an increased macrophage recruitment, which could lead to a stronger immune response. IL-12 was induced by LPS administration, but shows no significant pattern or distinction between *Nlrc3*^{-/-} and *Nlrc3*^{+/+}. Schneider *et al.* confirmed that the expression of pro-inflammatory cytokines is increased in LPS-treated *Nlrc3*^{-/-} macrophages [51].

5.4.2 Anti-inflammatory cytokine IL-10 is upregulated in *Nlrc3*^{-/-} BMDMs

Since NLRC3 has been described as negative regulator for T cell function [50] it was tempting to speculate on the effect on IL-10 as both seemed to signal along the same direction. The results show that IL-10 is upregulated in LPS stimulated BMDMs of *NLRC3*^{-/-} mice after two hours. Compared to IL-6 the effect is weaker and shorter (Fig. 4.21). It is therefore hypothesized that IL-10 acts as a mediator, modulating the cytokine induced response, but that cellular capacity was out-ruled after 2 hours of LPS administration. Even though the delineation between acute and late phase interleukin are not fully defined, these results suggest, that *Nlrc3* is involved in the mediation of the acute phase interleukins.

IL-10 is mainly produced by macrophages, T cells, and B cells [257], and acts as a potent suppressor of macrophage and T cell function. IL-10 inhibits the production of cytokines such as IL-1, IL-6, and TNF α after LPS stimulation [258]. IL-10 deficiency in mice resulted in a lack of regulatory T cells responsible for controlling the inflammatory response in the intestine [259]. The use of IL-10, or IL-10 producing bacteria as treatment for IBD patients is controversially discussed [260, 261, 262, 263]. Goblet cells and mucus do not seem to differ between IL-10 WT and KO mice, but IL10 deficient mice produce a mucus penetrable for bacteria sized beads [7]. IL-10-null mice develop a severe colitis driven by the microbiota [159]. Having determined a higher IL-10 level in *Nlrc3*^{-/-}-BMDMs after LPS stimulation we expected to see an increased effect in a DSS-induced colitis.

5.4.3 Translation of murine results to human systems

A high susceptibility of BMDMs for LPS stimulation and a strong reaction with respect to IL-6 and IL-12 were observed (Fig. 4.21, 4.22).

Wang *et al.* published recently a comparison of different macrophages with respect to their cytokine expression, capacity for proliferation, and phagocytosis [250]. Their data showed, that bone marrow derived macrophages possess a high basal IL-10 expression, which decreased after LPS stimulation and a vice versa IL-6 and IL-12 expression. Although their results were gained in

BALB/c mice they are supporting the data evaluated for this thesis. Schneider *et al.* used peritoneal macrophages of Nlrc3^{-/-} to analyze the cytokine response to a LPS stimulus. These data confirm the strong increase in IL-6 and IL-12 level. This includes the tendency of Nlrc3^{-/-} to express higher levels than the WT in early stages of the experiment and an approximation in later stages [51]. The work of Wang *et al.* and of Schneider *et al.* differ with respect to the IL-10 expression. The BALB/c mice of Wang *et al.* behaved opposite to the findings presented here, while IL-10 expression was not tested by Schneider *et al.* [51, 250].

It might be questioned in how far the results gained in a mouse model are representative for human applications. Arrifin *et al.* reviewed this question with regard to NLRs and pointed out, that genetic divergence is relatively low in NLRs. Although the amount of presently known receptors differs between the species, the biological outcome initiated by DAMPs is highly conserved [264].

5.5 Splenocytes exhibit surprising behavior upon stimulation

Splenocytes do require a 24 h pre-stimulation with P/I to respond to further stimuli. The composition of the splenocytes has been assessed via FACS analysis. Nlrc3^{-/-} splenocytes showed a significant elevated B cell level, while CD4⁺ were depleted. In general T helper cells (CD4⁺), cytotoxic T cells (CD8⁺), Memory cells (CD4⁻ or CD8⁺) or T_{regs} (mostly (CD4⁺)) were expected. Additionally, Nlrc3^{-/-} splenocytes seemed to cope better with pro-inflammatory stimuli (Fig. 4.23), resulting in a better survival. This is a still puzzling result, compared to the vast amount of data suggesting a cytoprotective feature of Nlrc3.

5.6 DSS colitis

A DSS-induced colitis in mice is a suitable model for severe intestinal inflammation. Although NLRC3 was not highly expressed in the intestinal tract during normal conditions, the proposed immune receptor activity might be elucidated during severe inflammation.

5.6.1 Nlrc3^{-/-} mice display a stronger onset of disease

The current experiment facilitated three groups of animals, an untreated control group, Nlrc3^{+/+}, and Nlrc3^{-/-} mice, which received 4 % DSS solved in the drinking water. All animals were male as they were described to be slightly more susceptible for DSS colitis [167]. The severity of the DSS-induced etiopathology was measured as the disease activity index. The DAI can value between

0 and 15 points, increasing with disease progression. As shown in Fig. 4.28 A both, WT and KO, displayed an increasing DAI. A significant difference was detectable on day six, showing a peak for the KO animals. The difference disappeared in the following two days. The weight loss and obviously the whole disease progression continued after the DSS containing drinking water was replaced by pure autoclaved tap water. This seems to be an intrinsic feature of the C57BL/6 background [265].

The *Nlrc3*^{-/-} mice displayed a stronger onset of disease, marked by an earlier body weight loss (Fig. 4.28 C). Day five has been the critical turning point in disease progression. Both genotypes were heavily affected by DSS treatment (Fig. 4.28 A-C). The MEICS score is based on observations exemplary depicted in Fig. 4.26. The marks seen in both genotypes resemble the expected signs as published by Becker *et al.* [187].

The colon length has been normalized to the body weight. A general shortening of the colon was observed when compared to the untreated controls, but the genotypes showed the same trend (Fig. 4.27) This is supported by earlier findings [160]. The spleen weight, which would be expected to be increased in heavily inflamed state showed no significant difference even when compared to the control. The same observation holds true for the spleen length. These findings are supported by recently published data, stating that the spleen size could not be expected to be increased prior day 12 [265]. This proxy would accordingly be interesting for longer or chronic DSS experiments. The histological staining were checked for signs of neoplasia, but the indication was negative. The tissue samples of DSS treated mice displayed a severe alteration in tissue structure and organization. The mucus layer seems to be eradicated, crypts lost, and the general tissue structure wrecked. Additionally, the HE-score was assessed, giving an indicator for the severity of colonic tissue damage [205]. As seen in Fig. 4.29 both genotypes are heavily affected, displaying heavy tissue integrity loss, restructuring, and immune cell invasion. The *Nlrc3*^{-/-} mice were affected most (Fig. 4.29 D). The HE score was evaluated in a blinded setup and revealed a significant higher value for the *Nlrc3*^{-/-} samples. Additionally, a yet not described change in the colonic structure of *Nlrc3* WT and KO mice was observed. The DSS treated animals displayed crypt abscesses in the villi. Comparing representative count of those structures, revealed a significantly increased amount in the *Nlrc3*^{-/-} animals (Fig. 4.30). Summarizing the basal disease values it has to be stated that *Nlrc3* seems to have a cytoprotective effect.

5.6.2 NF κ B increased in DSS treated mice

Following the earlier findings of NLRC3 being involved in NF κ B signaling, colon tissue was prepared and stained with an α -NF κ B specific staining (Fig. 4.33). The NF κ B level were increased in all DSS treated samples, showing a clear response to the administration of strong pro-inflammatory drugs. This finding is in concordance with NF κ B activation in human IBD [266]. In comprehension with the comparable disease progression in both genotypes, the NF κ B level seem to be equal. A deletion or decrease of NF κ B could lead to apoptosis of colonic epithelial cells, impaired expression of antimicrobial peptides and translocation of bacteria into the mucosa [267].

5.6.3 Interleukin levels are altered in DSS treated *Nlrc3*^{-/-} mice

As shown in the interleukin screening of LPS stimulated BMDMs IL-10 seems to be elevated in *Nlrc3*^{-/-} mice (Fig. 4.21). Kühn *et al.* suggested, that the absence of IL-10 is associated with gut inflammation [159]. Several of the above mentioned experimental results indicated a protective role of NLRC3. To solve this contradicting data the interleukin level were assessed on transcript and expressed cytokine level. The transcript level of IL-6 and IL-10 were determined in colon, spleen, and mesenchymal lymph node cDNA (Fig. 4.32), while the cytokine concentration of IL-6, CXCL1, and IL-10 was measured in serum (Fig. 4.31). It is interesting to mention that IL-10 interferes with the NF κ B pathway, by inhibiting it [268, 269], therefore signaling along with NLRC3.

The transcript level showed no significant difference between WT and KO, but were generally elevated compared to the control. The highest increase compared to the control was measured in the colon, which is the organ most affected by DSS colitis. The trend which has been visible in the LPS stimulated BMDMs was affirmed here. A study in colonic tissue homogenates by Melgar *et al.* showed, that the cytokine level of IL-1, IL-6, and IL-18 rapidly increased within their first days of DSS colitis compared to healthy mice. The IL-6 values showed a 513 fold difference after 5 days [265], which is confirmed by the findings shown in Fig. 4.32. The *Nlrc3*^{-/-} mice seem to have slightly elevated IL-6 and IL-10 values compared to the wildtype, but drastically increased values compared to the untreated controls. The expression pattern of cytokines over time might interfere with these results, as it has been shown, that e.g. IL-10 expression alters greatly after the critical point in disease progression [270]. The upregulation of IL-6 is consistent with findings in IBD [271]. This implicates, that *Nlrc3* mediates or downregulates the production of interleukins as an indirect response to several inflammatory stimuli, such as LPS and DSS. It

has been recently published, that IL-10 seems to have an inhibiting effect in colitis [272]. The IL-10 transcript level in all three tested tissues was increased in DSS treated animals, but no such effect was measured in serum samples. A positive effect of the anti-inflammatory cytokine IL-10 is therefore plausible, but could not be affirmed by the current experiments. The serum level of IL-6 and IL-10 revealed a statistic significant difference in CXCL-1. The CXCL-1 trend is partly in concordance with the findings in LPS stimulated BMDMs. The CXCL-1 levels boosted after two hours not discriminating between the genotypes. Nevertheless the levels tended to remain higher in KO animals. It has to be highlighted that both experiments facilitated different cell types and that the DSS samples were taken at an uncertain point in time after the primary stimulus (bacterial contact to exposed *lamina propria*). The experiment showed clearly, that a disruption of the colonic mucus as a result of DSS administration contributes to a severe inflammation. The exact moment of the first contact and therefore the possible peak of CXCL1 release *in vivo* could technically not be monitored. CXCL-1 has been described as a neutrophil chemoattractant KC. CXCL1 deficient mice exhibit increased susceptibility to DSS-induced colitis [168].

5.6.4 Nlrc3 influences mtUPR marker

The transcript level of pkr, cpn60, and grp78 were monitored as hallmarks for mtUPR (Fig. 4.34). The mitochondrial cpn60 is responsible for the refolding of proteins after mitochondrial stress events [273]. A SYBR Green assay in ileum samples of DSS treated mice, showed a slight decrease of cpn60 and grp78 level, compared to the untreated control. A significant and overall alteration of mtUPR marker was not detectable in this study design, recommending a screen in more tissues and after longer exposure to DSS.

Rath *et al.* published a potential link between mtUPR and inflammatory bowel diseases as cpn60 and pkr were induced in intestinal epithelia cells of murine colitis models and in human inflamed IBD samples [206]. The data were gained in mice on a 129SvEv background, in two consecutive 7 day 1 % DSS cycles. Especially the double-strand RNA activated protein kinase PKR seems to be a central link between sensing and inflammatory response [274]. They stated further, that pkr^{-/-} mice failed to induce cpn60 under a short-term DSS feeding protocol [206]. As the pkr values do not significantly alter in the DSS experiment presented here, a cpn60 alteration seems to be unlikely, resulting in no accelerated disease progression due to pkr induced cpn60.

5.6.5 Final conclusions on DSS experiment

Concluding the results gained from the 4 % acute DSS colitis it has to be stated, that the *Nlrc3*^{-/-} mice were doing worse than the wildtypes. This is demonstrated by a higher DAI, HE score, altered CXCL1 serum level, and a significant increase in tissue damage/crypt abscesses. The DSS colitis experiment therefore supports the hypothesis of a protective *Nlrc3* function. Some proxies assessed, such as the spleen size, might be different or more distinct after a longer exposition of the mice to DSS. It might therefore be useful to establish a chronic colitis experiment with a lower DSS-dose. Additionally, some values indicate strong tendencies, without being statistical significant. This might be overcome by an experimental setup utilizing a higher number of animals. For future experiments variations between DSS lots have to be mentioned. It has been published, that the ability to induce colitis varies between lots, requiring an experimental approach for the best concentration [168]. The chosen 4 % DSS in this thesis induced a severe colitis resulting in two spontaneously fatal outcomes prior to the termination of the experiment. A dose of 2.5 % DSS might be more suitable and reveal a more distinct difference between WT and KO.

It has been shown, that immunodeficient mice are able to develop DSS colitis, indicating that the pathology is independent of B and T cells and therefore mostly driven by the innate immune system [164]. Mice therefore provide a stable and convenient model for IBD and general inflammatory processes. Nevertheless, it has to be considered that different strains might impact the experiments. The mice for this thesis were back crossed to a C57BL/6 background. A back crossing to the also very common BALB/c background may have resulted in slightly variable results, with respect to interleukine levels or T cell composition [167, 275, 276, 277]. A comprehensive work comparing the results of DSS administration to C57BL/6 and BALB/c mice has been given by Melgar *et al.*. It was shown that both strains developed the clinical symptoms of colitis, but that the outcome and molecular response e.g. the cytokine production somehow differs. Additionally, it was shown that a single 5-day DSS administration was capable to induce a chronic colitis in C57BL/6 mice, while BLAB mice recovered [265].

5.7 Relevance of NLRC3 in several diseases

The results shown in this thesis demonstrate a participation of NLRC3 in inflammatory processes. Thus far, no disease has been directly linked to a mutation or lack of NLRC3. The *Nlrc3* knockout mouse model employed in this thesis showed no visible alterations or basal changes in histology (Fig. 4.16, 4.17) and is shown to be non-lethal. However ongoing research on several diseases

found altered transcript levels of NLRC3.

5.7.1 NLRC3 is downregulated in Wegener's granulomatosis patients

We were able to show that NLRC3 is downregulated on protein level in Wegener's granulomatosis patients Fig. 4.24. The same holds true for the transcript level where NLRC3 is downregulated two-fold compared to normal controls. The altered expression of NLRC3 in WG samples indicates a possible protective role in the context of inflamed respiratory mucosa. As tissue defects or an increased infiltration of immune cells were not detectable [203], it might be concluded, that the protective effect is independent of mucosal integrity. The gene regulation seems to be due to a yet unknown mechanism.

5.7.2 Phase II dasatinib study: NLRC3 is downregulated, while NF κ B2 is increased

A previous study by Amrein *et al.* showed that patients in a phase II study of the drug dasatinib (N-(2-chloro-6-methylphenyl)-2-[[6-[4-(2-hydroxyethyl)-1-piperazinyl]-2-methyl-4-pyrimidinyl]amino]-5-thiazole carboxamide monohydrate) in response to relapsed or refractory chronic lymphocytic leukemia developed signs of brisk apoptosis. Enriched peripheral blood lymphocytes consisting of B cells mostly were sampled and RNA extracted. A microarray gene expression profiling 6 hours prior and after dasatinib application showed a significant downregulation of NLRC3, while NF κ B2 was significantly up regulated [278]. The NF κ B2 upregulation might be useful to evade apoptosis [278, 279]. Due to a parallel downregulation of NLRC3 it is tempting to speculate on a pro-apoptotic feature of NLRC3. It has to be questioned whether this represents a protective effect in the complex interplay controlling apoptosis and a possible involvement of mitochondrial processes. Although the statistical power in the latter study is relative low and enriched peripheral blood lymphocytes were not used in the work presented here, the findings provide another suggestion of the involvement of NLRC3 in NF κ B signaling. In 2005 Conti *et al.* proposed [50], and was later supported [51], that NLRC3 is indeed involved in T cell receptor mediated signaling to NF κ B.

5.7.3 NLRC3 is downregulated during aging

Additionally, it was shown that NLRC3 is downregulated during aging processes in peripheral and intestinal leukocytes [280]. Rosenstiel *et al.* assumed that a downregulation of effectors of the innate immune system diminishes the capabilities of the immune system with age, resulting

in lower pathogen recognition and aberrant immune response which ultimately leads to morbidity and mortality. A protective role of NLRC3 could be inferred, although the direct mechanisms still remain unknown.

5.8 Summary

NLRC3 is a cytosolic protein with direct connections to signaling events of the innate immune system. The main interactors of NLRC3 remain unidentified, but a mere TNF α stimulation decreases NLRC3 in HEK-293 cells on protein level. LPS stimulation of WT and KO BMDMs resulted in a distinct cytokine profile.

Cell fractionation and microscopic imaging indicated a close interaction of NLRC3 with mitochondria. Mitochondria are a central hub for immune regulation and cellular response, which would further strengthen the impact of NLRC3 on immunomodulatory effects, without the necessity of a single inducing PAMP. A theoretical model might follow the example of NLRX1 interacting with mitochondria [19, 281, 282]. Initial work has been done in the field of mtUPR in connection with NLRC3.

Whether the detection of PAMPs via NLRC3 is a direct ligand-receptor interaction or whether complexes or cofactors are required is still elusive. NLRC3 has previously been shown to interact with the E3 ligase TRAF6, modulating a NF κ B response. Current results of a dual luciferase assay are questioning the direction of regulation induced by TRAF6, but were able to show a significant impact of NLRC3 on NF κ B signaling. A cooperation between TLRs and NLRs might distinguish between pathogen and commensal bacteria or modulate an immune response. Analysis of localization, expression level, modulator capacity of the NF κ B pathway and interleukin expression profiling was ultimately followed by an acute DSS-induced colitis model. It could be shown that the *Nlrc*^{-/-} mice fared worse than the WT with respect to survival, tissue damage, and previously undescribed crypt abscesses. NLRC3 has been described to be regulated in a variety of diseases, a connection to WG could be shown in the cause of this thesis.

Reviewing all data gained, it has to be stated, that NLRC3 exerts a cytoprotective effect by modulating immune response. NLRC3 is closely connected to mitochondria, especially the inner mitochondrial membrane protein IMMT and members of the mitochondrial unfolded protein response. This thesis is one of the first systematic works on NLRC3, revealing new data and prospective insights of the molecular function of NLRC3.

5.9 Outlook

This thesis aimed to characterize the yet underrepresented NLRC3 protein. As neither its biological function, nor its molecular signaling has been fully described previously, a broad spectrum of analysis were conducted to assess these open questions. In the course of analysis several new questions and possible connections arose, which could not all be followed up during this thesis. Therefore the most striking of these questions are presented here, which might be interesting hints for further research.

Mitochondrial UPR has been shown to interact directly with erUPR via common signaling molecules, such as eIF2 α and cJun [206]. Taking the current findings of ERSE activation and colitis linked mitochondrial stress into account, this might prove an interesting read out for acute and chronic DSS experiments. Another potent inducer of mitochondrial stress are thapsigargin-induced sepsis models [283]. The breeding of a *Nlrc3*^{-/-} x *Pkr*^{-/-} double knockout mice could be taken into consideration. Beside the alternative induction of mitochondrial stress it would be useful to further monitor cellular responses, such as ATP level and mitochondrial membrane potential. Latter has been shown to be decreased by cytokine-induced ROS generation [284]. The ERSE experiments showed, that an impact of nuclear signaling could not be ruled out, and mtUPR pathways are known to facilitate mitochondria to nucleus signaling [71]. Finally, estrogen has been shown to be an inducer of *nlrc3* in the bony fish gilthead seabream [285]. It has been shown that estrogen receptor mediates UPR resulting in an upregulation of proteasomal degradation and activation of a cytoprotective response [286, 287]. These findings might further prove the hypothesis of protective features of NLRC3.

Acid alpha-glucosidase, which is responsible for the lysosomal degradation of glycogen to glucose has been found as a potential interaction partner of NLRC3 in a Y2H screen [data not shown]. Stimulation of dendritic cells with TLR agonists resulted in a switch to glycolytic ATP metabolism, indicated by higher expression of glucose transporter while simultaneously decreasing the oxygen consumption [288]. With regard to the close connection between NLR and TLR pathway this might be interesting as a first indication has been given that glycolysis might act as a protective mechanism in inflammation [289, 290].

Additionally, it would be interesting to investigate the time laps of disease progression of *Nlrc3*^{-/-} mice in a more detailed way. The present experiments showed, that day five marks the critical turning point in disease progression. The necessarily preceding depletion of mucin, mucin wash out due to diarrhea [291] finally resulting in an exposed lamina propria could not be monitored in

Nlrc3^{-/-} mice yet. Experiments should additionally include an analysis of the impact of different DSS (molecular weight and lot), the mucin, the colonic wet weight to determine collagen increase, and the cytokine production including the pro-inflammatory TNF α [265, 270, 292, 293, 294]. Although the visual inspection of the caecum [data not shown] did not show any obvious signs of inflammation it might be worthy to include them into analysis [167, 295]. Following the results of Baer *et al.* it might be interesting to assess the mucosal ATP level [296]. Together with the finding that NF κ B up regulates mitochondrial respiration, this might be a fruitful way to further connect Nlrc3 with mitochondrial processes and inflammation if applicable [297]. Taking into consideration, that NLR deficient mice host a different microbiota than the respective WT [14] it seems to be urgent to test this hypothesis on NLRC3 animals to evaluate a possible cytokine profile alteration due to immunomodulatory activities of the gut bacteria [298]. An assay of transepithelial electric resistance might reveal, whether Nlrc3^{-/-} animals provide an increased intestinal permeability [299, 300], which might correlate with one of the main effects of DSS [161]. Crossing Nlrc3^{-/-} mice with TRAF6^{-/-} mice, could further clarify the interactions of TLR and NLR pathway. Stimulation of TLRs may further lead to an interaction between p62 and TRAF6, resulting in TRAF6 autoubiquitination, NF κ B activation, and finally inducing pro-inflammatory cytokines [301]. It has been stated that p62 accumulates upon selective disruption of the proteasomal degradation pathway, resulting in altered cellular distribution patterns [302]. Early experiments with NLRC3 indicated a proteasomal degradation of NLRC3 (Fig. 4.13), but initial experiments with proteasom inhibitors failed to show a direct connection [data not shown]. The interactions between TRAF6, NF κ B, and p62 can be linked to protein kinases c, which itself is involved in the same signaling pathways [303]. It has been proposed that the PKC ι in the intestinal epithelium protects against DSS-induced colitis [304]. Although the connection between NLRC3 and p62/pkc is yet not experimentally verified, research in this direction might further extend the knowledge of the NLR signaling pathways.

6 Supplement

6.1 Isoforms of NLRC3

Several isoforms of NLRC3 have been published and deposited in public databases. The proposed isoforms are partly lacking experimental confirmation. A graphical overview is given in Fig. 6.1.

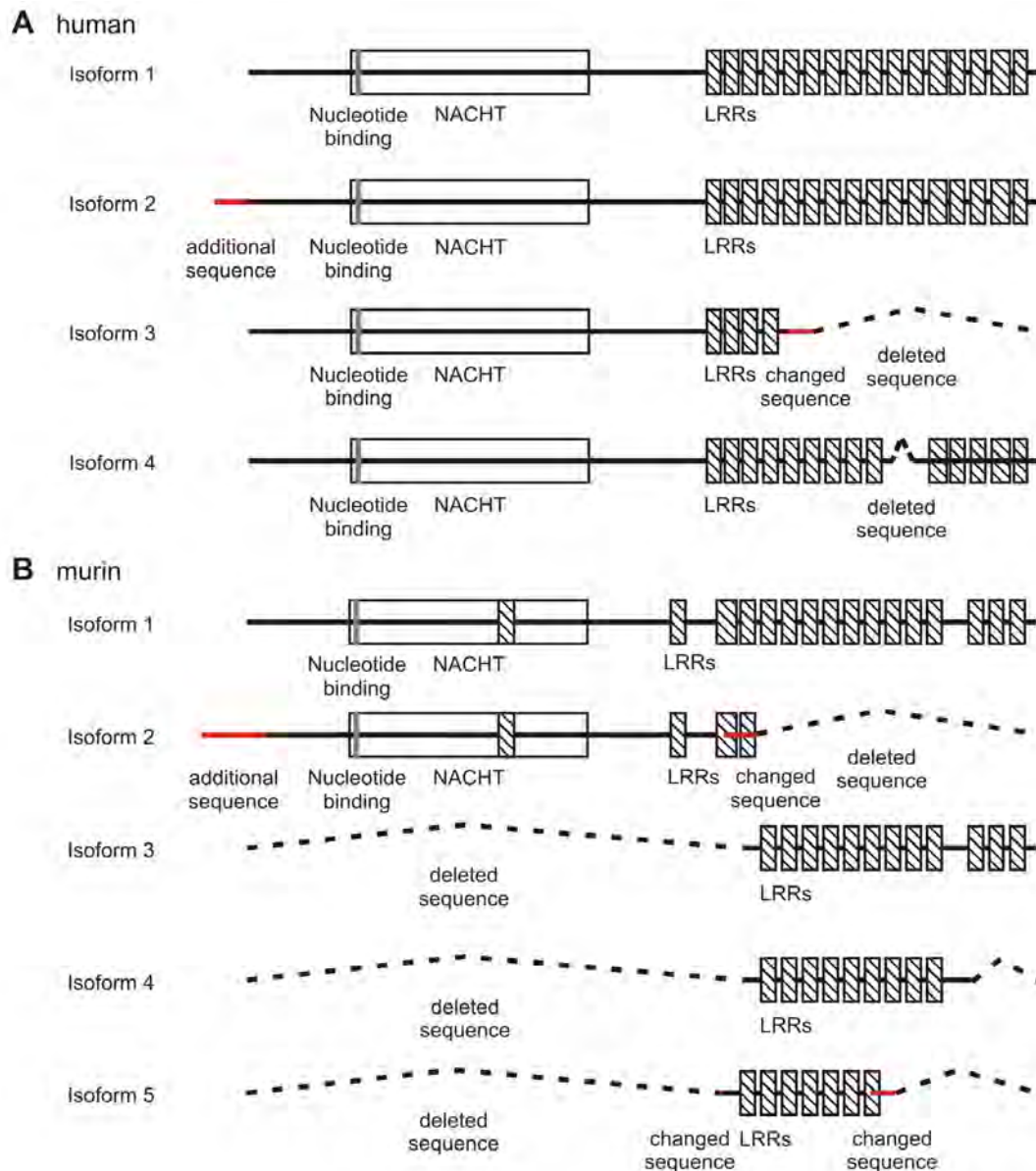


Fig. 6.1: Proposed isoforms of human NLRC3 and murine Nlr3. A Human and B murine isoforms of NLRC3 are shown. Squares symbolize exonic and lines intronic regions. deleted sequences are indicated by a broken line, additional or altered sequences are marked in red. Isoform 1 has been chosen as canonical.

6.2 Generation of mice

The cloning and generation of mice was performed by genOway in close agreement with Prof. Dr. Rosenstiel.

As depicted in Fig. 6.2 the homologous sequences were cloned as three independent fragments obtained by PCR through the use of genomic 129Sv ES cell DNA. The oligomers are given in Tab. 6.1.

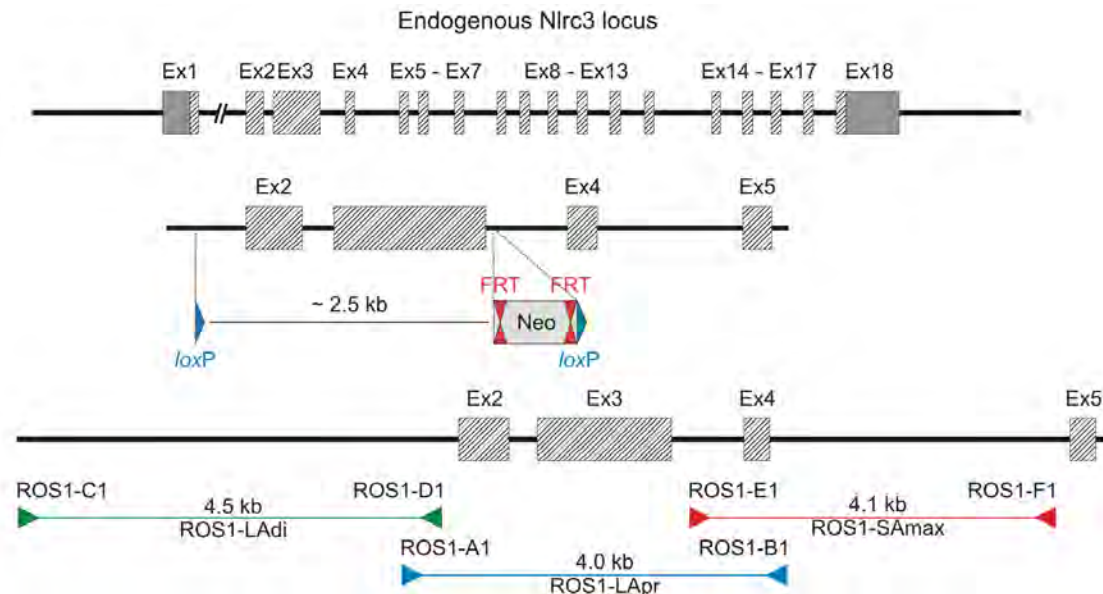


Fig. 6.2: Murine *Nlrc3* gene cloning. Diagram is not depicted to scale. Boxes represent exons, solid lines intronic sequences. The approximate locations of oligonucleotides hybridization sites that were used for the amplification of the homologue DNA fragments are indicated by arrows. The resulting fragments, their names and the respective expected sizes are given.

Tab. 6.1: Oligomers for amplifying murine *Nlrc3*.

subclone	oligo name	sequence 5'-3'	fragment size [bp]
ROS1-LAdi	ROS1-C1	ATCATGCACACATAGAACAACACTCAG	4499
	ROS1-D1	CTGAGGGTCTTCATGTAACAAATGC	
ROS1-LApr	ROS1-A1	GTGACTGGTTTCTGCCTACGAGTCC	4040
	ROS1-B1	CAGGTTCACTAGGGGCTGTGTTACC	
ROS1-Samax	ROS1-E2	GCTCTATTGTCAAAGCCTCAGGTGG	4090
	ROS1-F2	GGAAGGGAGAAAAGGAGAGAGTGC	

The resulting product was cloned into pCR4-TOPO vector (Stratagene) via TA cloning. Several subclones of each fragment were sequenced. The sequences were aligned against the C57BL/6 based consensus sequence available in the public database to determine polymorphisms between C57BL/6 and 129Sv. The polymorphism rate was found to be less than 0.02 %. Several subsequent

cloning steps were utilized to correct single point mutations, inserting the *loxP*-sites, the FRT-Neo-FRT-*loxP* cassette and finally the Diphtheria Toxin A cassette (Fig. 6.2).

The resulting targeting vector named ROS1-HR was homogenic with the embryonic stem cell line 129Sv and contained the exons 2 and 3 of the *Nlrc3* gene and was validated by sequencing. The *loxP*-sites enable the deletion under the action of a Cre recombinase, Diphtheria Toxin A was chosen as negative selection marker. The targeting vector ROS1-HR was linearized by restriction digestion via PacI. The resulting 15.6 kb targeting fragment was purified, transfected by electroporation in 129Sv ES and positively selected after 48 hours by the aminoglycoside G418. The positive selected clones were validated by a PCR screen, additionally the recombination was confirmed by Southern blot. Recipient blastocysts were isolated from pregnant C57BL/6 females (SPF conditions). Based on the screening results positive ES cell clones were injected in C57BL/6 blastocysts. The blastocysts were reimplanted into OF1 pseudo-pregnant females (SOPF status). The pups gained were screened for their chimerism.

6.3 MS/MS

A full list of the MS/MS hits is available on the compact disc attached to this thesis.

6.4 Abbreviations

Abbreviations used in this thesis are enlisted in the following tables:

Tab. 6.2: Abbreviations. SI units were not enlisted.

aa	amino acid
AD	Acidic transactivation domain
AIM	Absent in melanoma
ALP	Absent in melanoma-2-like receptors
AP-1	Activator protein 1
ATF6	Activating transcription factor 6
b	bases
BIR	Baculovirus inhibitor of apoptosis protein repeat
BMDM	Bone marrow derived macrophages
bp	base pair
BSA	Bovine serum albumine
CIITA	Class II transcription activator
CARD	Caspase recruitment domain
CD	Crohn's disease
Chchd3	coiled-coil-helix-coiled-coil-helix domain containing protein 3
cpn60	chaperonin 60

Tab. 6.3: Abbreviations - continued.

Cre	Cre Recombinase
CRS	chronic rhinosinusitis with nasal polyps
CTL	C-type lectin
CXCL1	Chemokine (C-X-C motif) ligand 1
Da	Dalton
DAB	3,3'-Diaminobenzidine
DAI	Disease activity index
DAMP	Danger/damage associated molecular pattern
DAPI	4',6-diamidino-2-phenylindole
DC	diseased controls
ddNTP	2',3' dideoxynucleotides
DLB	Denaturing lysis buffer
DNA	Deoxyribonucleic acid
DSS	Dextran sodium sulfate
ECL	Enhanced chemiluminescence
EDTA	Ethylenediaminetetraacetic acid
ELISA	Enzyme linked immunosorbent assay
(s/r)ER	Endoplasmatic reticulum (smooth/rough)
ERSE	ER stress-responsive cis-acting elements
ESCIT	Evolutionary conserved signaling intermediate in Toll pathway
FELASA	Federation of European laboratory animal science associations
FIIND	Function to find
FCS	Fetal calf serum
FLP	RMCE Recombinase
FRT	FLP recognition target
g	g force
GAPDH	Glyceraldehyde 3-phosphate dehydrogenase
GFP	Green fluorescent protein
grp	glucose regulated protein
h	hours
HEPES	4-(2-hydroxyethyl)-1-piperazineethanesulfonic acid
HN	hospitalized normal
HRP	Horseradish peroxidase
IBD	Inflammatory bowel disease
IVC	Individually ventilated cages
IFN	Interferon
Ig	Immunoglobuline
IKK	I κ B kinase
IL	Interleukin
IMMT	Inner mitochondrial membrane protein, Mitofilin
JAK/STAT	<i>signaling pathway</i> Janus kinase/signal transducer and activator of
IP	Immunoprecipitation
	transcription
k	kilo
KO	constitutive knockout
λ	wavelength
LB medium	Luria-Bertani medium
LPS	Lipopolysaccharides

Tab. 6.4: Abbreviations - continued.

LRR	Leucine rich repeats
m	milli
MAVS	Mitochondria associated viral sensor
M-CSF	Macrophage colony-stimulating factor
MEICS	Murine endoscopic index of colitis severity
min	minutes
mln	mesenchymal lymph node
mRNA	Messenger ribonucleic acid
ms	mouse
n	nano
NAD	NACHT-associated domain
NACHT	<i>domain present in NAIP, CIITA, HET-E and TP-1</i>
NALP	NACHT, LRR and PYD domains-containing protein
NBD	Nucleotide-binding domain
NC	normal controls
NCBI	National Center for Biotechnology Information
NLR	NOD-like receptors
NOD	Nucleotide-binding, oligomerization domain and leucine-rich repeat containing protein
NFκB	nuclear factor kappa-light-chain-enhancer of activated B cells
NLRC3	human NOD-like receptor CARD domain containing 3
Nlrc3	murine NOD-like receptor CARD domain containing 3
Opa1	Optic atrophy 1
PAMP	Pathogen associates molecular pattern
PBMC	Peripheral blood mononuclear cell
PBS	Phosphate buffered saline
PCR	Polymerase chain reaction
PHA	Phytohaemagglutinin
P/I	PMA/Ionomycine
pkR	double strand RNA-dependent protein kinase
PMA	Phorbol 12-myristate 13-acetate
poly(I:C)	Polyinosinic:polycytidylic acid
PRR	Pattern recognition receptor
PRR	Pattern recognition receptor
PVDF	Polyvinylidene fluoride
PYD	Pyrin domain
qPCR	quantitative real time polymerase chain reaction
rb	rabbit
RIG	Retinoic acid inducible gene
RLR	Retinoic acid inducible gene like receptors
RLU	Relative luciferase unit
RMCE	Recombinase-mediated cassette exchange
RNA	Ribonucleic acid
RNAi	Ribonucleic acid interference
ROS	Reactive oxygen species
R protein	Resistance protein
RT	Room temperature
siRNA	Small interfering RNA

Tab. 6.5: Abbreviations - continued.

SPF	Specific pathogen free
STAND	Signal transduction ATPases with numerous domains
Taq	polymerase from the bacterium <i>Thermus aquaticus</i>
TaqMan	<i>probes for real-time PCR</i>
TLR	Toll-like receptor
TMB	3,3',5,5'-tetramethylbenzidine
TNF	Tumor necrosis factor
TNFR	TNF receptor
TOM	Translocase of the outer membrane
TRAF	TNF receptor associated factor
TTBS	Tris-Tween buffered saline
U	Unit
UC	Ulcerative colitis
UPR	Unfolded protein response
UTR	Untranslated region
V	Volt
W	Watt
WB	Western blot
WT	wildtype
w/v	weight per volume
XBP1	X-box binding protein 1
Y2H	Yeast two-hybrid system

Bibliography

- [1] T. D. Luckey, "Introduction to intestinal microecology.," *Am J Clin Nutr*, vol. 25, pp. 1292–1294, Dec 1972.
- [2] D. C. Savage, "Microbial ecology of the gastrointestinal tract.," *Annu Rev Microbiol*, vol. 31, pp. 107–133, 1977.
- [3] G. Yosipovitch, A. Maayan-Metzger, P. Merlob, and L. Sirota, "Skin barrier properties in different body areas in neonates.," *Pediatrics*, vol. 106, pp. 105–108, Jul 2000.
- [4] G. C. Hansson, "Role of mucus layers in gut infection and inflammation.," *Curr Opin Microbiol*, vol. 15, pp. 57–62, Feb 2012.
- [5] G. Diamond, N. Beckloff, A. Weinberg, and K. O. Kisich, "The roles of antimicrobial peptides in innate host defense.," *Curr Pharm Des*, vol. 15, no. 21, pp. 2377–2392, 2009.
- [6] R. L. Gallo and T. Nakatsuji, "Microbial symbiosis with the innate immune defense system of the skin.," *J Invest Dermatol*, vol. 131, pp. 1974–1980, Oct 2011.
- [7] M. E. V. Johansson, J. K. Gustafsson, J. Holmen-Larsson, K. S. Jabbar, L. Xia, H. Xu, F. K. Ghishan, F. A. Carvalho, A. T. Gewirtz, H. Sjoevall, and G. C. Hansson, "Bacteria penetrate the normally impenetrable inner colon mucus layer in both murine colitis models and patients with ulcerative colitis.," *Gut*, Feb 2013.
- [8] S. E. Degn and S. Thiel, "Humoral pattern recognition and the complement system.," *Scand J Immunol*, vol. 78, pp. 181–193, Aug 2013.
- [9] B. Beutler, "Innate immunity: an overview.," *Mol Immunol*, vol. 40, pp. 845–859, Feb 2004.
- [10] R. Medzhitov and C. A. Janeway, Jr, "Decoding the patterns of self and nonself by the innate immune system.," *Science*, vol. 296, pp. 298–300, Apr 2002.
- [11] L. Ferrero-Miliani, O. H. Nielsen, P. S. Andersen, and S. E. Girardin, "Chronic inflammation: importance of nod2 and nalp3 in interleukin-1beta generation.," *Clin Exp Immunol*, vol. 147, pp. 227–235, Feb 2007.

- [12] G. C. Ramos, "Inflammation as an animal development phenomenon.," *Clin Dev Immunol*, vol. 2012, p. 983203, 2012.
- [13] S. Akira, S. Uematsu, and O. Takeuchi, "Pathogen recognition and innate immunity.," *Cell*, vol. 124, pp. 783–801, Feb 2006.
- [14] S. J. Robertson and S. E. Girardin, "Nod-like receptors in intestinal host defense: controlling pathogens, the microbiota, or both?," *Curr Opin Gastroenterol*, vol. 29, pp. 15–22, Jan 2013.
- [15] A. Geremia, P. Biancheri, P. Allan, G. R. Corazza, and A. Di Sabatino, "Innate and adaptive immunity in inflammatory bowel disease.," *Autoimmun Rev*, Jun 2013.
- [16] C. A. Janeway, Jr and R. Medzhitov, "Innate immune recognition.," *Annu Rev Immunol*, vol. 20, pp. 197–216, 2002.
- [17] M. Schnare, A. C. Holt, K. Takeda, S. Akira, and R. Medzhitov, "Recognition of cpg dna is mediated by signaling pathways dependent on the adaptor protein myd88.," *Curr Biol*, vol. 10, pp. 1139–1142, Sep 2000.
- [18] R. Medzhitov, "Recognition of microorganisms and activation of the immune response.," *Nature*, vol. 449, pp. 819–826, Oct 2007.
- [19] T. P. Monie, "Nlr activation takes a direct route.," *Trends Biochem Sci*, vol. 38, pp. 131–139, Mar 2013.
- [20] C. J. Kirschning and R. R. Schumann, "Tlr2: cellular sensor for microbial and endogenous molecular patterns.," *Curr Top Microbiol Immunol*, vol. 270, pp. 121–144, 2002.
- [21] P. Ahmad-Nejad, H. Haecker, M. Rutz, S. Bauer, R. M. Vabulas, and H. Wagner, "Bacterial cpg-dna and lipopolysaccharides activate toll-like receptors at distinct cellular compartments.," *Eur J Immunol*, vol. 32, pp. 1958–1968, Jul 2002.
- [22] B. M. Buchholz and A. J. Bauer, "Membrane tlr signaling mechanisms in the gastrointestinal tract during sepsis.," *Neurogastroenterol Motil*, vol. 22, pp. 232–245, Mar 2010.
- [23] K. H. G. Mills, "Tlr-dependent t cell activation in autoimmunity.," *Nat Rev Immunol*, vol. 11, pp. 807–822, Dec 2011.

- [24] M. Yoneyama and T. Fujita, "Cytoplasmic double-stranded dna sensor.," *Nat Immunol*, vol. 8, pp. 907–908, Sep 2007.
- [25] J. W. Jones, N. Kayagaki, P. Broz, T. Henry, K. Newton, K. O'Rourke, S. Chan, J. Dong, Y. Qu, M. Roose-Girma, V. M. Dixit, and D. M. Monack, "Absent in melanoma 2 is required for innate immune recognition of francisella tularensis.," *Proc Natl Acad Sci U S A*, vol. 107, pp. 9771–9776, May 2010.
- [26] W. I. Weis, M. E. Taylor, and K. Drickamer, "The c-type lectin superfamily in the immune system.," *Immunol Rev*, vol. 163, pp. 19–34, Jun 1998.
- [27] G. Chen, M. H. Shaw, Y.-G. Kim, and G. Nunez, "Nod-like receptors: role in innate immunity and inflammatory disease.," *Annu Rev Pathol*, vol. 4, pp. 365–398, 2009.
- [28] D. D. Leipe, E. V. Koonin, and L. Aravind, "Stand, a class of p-loop ntpases including animal and plant regulators of programmed cell death: multiple, complex domain architectures, unusual phyletic patterns, and evolution by horizontal gene transfer.," *J Mol Biol*, vol. 343, pp. 1–28, Oct 2004.
- [29] E. V. Koonin and L. Aravind, "The nacht family - a new group of predicted ntpases implicated in apoptosis and mhc transcription activation.," *Trends Biochem Sci*, vol. 25, pp. 223–224, May 2000.
- [30] J. P.-Y. Ting, R. C. Lovering, E. S. Alnemri, J. Bertin, J. M. Boss, B. K. Davis, R. A. Flavell, S. E. Girardin, A. Godzik, J. A. Harton, H. M. Hoffman, J.-P. Hugot, N. Inohara, A. Mackenzie, L. J. Maltais, G. Nunez, Y. Ogura, L. A. Otten, D. Philpott, J. C. Reed, W. Reith, S. Schreiber, V. Steimle, and P. A. Ward, "The nlr gene family: a standard nomenclature.," *Immunity*, vol. 28, pp. 285–287, Mar 2008.
- [31] L. Franchi, N. Warner, K. Viani, and G. Nunez, "Function of nod-like receptors in microbial recognition and host defense.," *Immunol Rev*, vol. 227, pp. 106–128, Jan 2009.
- [32] P. Rosenstiel, K. Huse, A. Till, J. Hampe, S. Hellmig, C. Sina, S. Billmann, O. von Kampen, G. H. Waetzig, M. Platzer, D. Seegert, and S. Schreiber, "A short isoform of nod2/card15, nod2-s, is an endogenous inhibitor of nod2/receptor-interacting protein kinase 2-induced signaling pathways.," *Proc Natl Acad Sci U S A*, vol. 103, pp. 3280–3285, Feb 2006.
- [33] K. Schroder and J. Tschopp, "The inflammasomes.," *Cell*, vol. 140, pp. 821–832, Mar 2010.

- [34] T. A. Kufer and P. J. Sansonetti, "Nlr functions beyond pathogen recognition.," *Nat Immunol*, vol. 12, pp. 121–128, Feb 2011.
- [35] S. J. Robertson, S. J. Rubino, K. Geddes, and D. J. Philpott, "Examining host-microbial interactions through the lens of nod: From plants to mammals.," *Semin Immunol*, vol. 24, pp. 9–16, Feb 2012.
- [36] N. Inohara and G. Nunez, "The nod: a signaling module that regulates apoptosis and host defense against pathogens.," *Oncogene*, vol. 20, pp. 6473–6481, Oct 2001.
- [37] B. C. Meyers, A. Kozik, A. Griego, H. Kuang, and R. W. Michelmore, "Genome-wide analysis of nbs-lrr-encoding genes in arabidopsis.," *Plant Cell*, vol. 15, pp. 809–834, Apr 2003.
- [38] J. Li, J. Ding, W. Zhang, Y. Zhang, P. Tang, J.-Q. Chen, D. Tian, and S. Yang, "Unique evolutionary pattern of numbers of gramineous nbs-lrr genes.," *Mol Genet Genomics*, vol. 283, pp. 427–438, May 2010.
- [39] C. Lange, G. Hemmrich, U. C. Klostermeier, J. A. Lopez-Quintero, D. J. Miller, T. Rahn, Y. Weiss, T. C. G. Bosch, and P. Rosenstiel, "Defining the origins of the nod-like receptor system at the base of animal evolution.," *Mol Biol Evol*, vol. 28, pp. 1687–1702, May 2011.
- [40] N. Inohara and G. Nunez, "Nods: intracellular proteins involved in inflammation and apoptosis.," *Nat Rev Immunol*, vol. 3, pp. 371–382, May 2003.
- [41] F. M. Ausubel, "Are innate immune signaling pathways in plants and animals conserved?," *Nat Immunol*, vol. 6, pp. 973–979, Oct 2005.
- [42] T. Maekawa, T. A. Kufer, and P. Schulze-Lefert, "Nlr functions in plant and animal immune systems: so far and yet so close.," *Nat Immunol*, vol. 12, no. 9, pp. 817–826, 2011.
- [43] D. Bulgarelli, C. Biselli, N. C. Collins, G. Consonni, A. M. Stanca, P. Schulze-Lefert, and G. Vale, "The cc-nb-lrr-type rdg2a resistance gene confers immunity to the seed-borne barley leaf stripe pathogen in the absence of hypersensitive cell death.," *PLoS One*, vol. 5, no. 9, 2010.
- [44] N. S. Coll, D. Vercammen, A. Smidler, C. Clover, F. van Breusegem, J. L. Dangl, and P. Epple, "Arabidopsis type i metacaspases control cell death.," *Science*, vol. 330, pp. 1393–1397, Dec 2010.

- [45] E. Elinav, T. Strowig, J. Henao-Mejia, and R. A. Flavell, "Regulation of the antimicrobial response by nlr proteins.," *Immunity*, vol. 34, pp. 665–679, May 2011.
- [46] A. L. Hughes, "Evolutionary relationships of vertebrate nact domain-containing proteins.," *Immunogenetics*, vol. 58, pp. 785–791, Oct 2006.
- [47] S. Kumar and S. B. Hedges, "A molecular timescale for vertebrate evolution.," *Nature*, vol. 392, pp. 917–920, Apr 1998.
- [48] Z. Sha, J. W. Abernathy, S. Wang, P. Li, H. Kucuktas, H. Liu, E. Peatman, and Z. Liu, "Nod-like subfamily of the nucleotide-binding domain and leucine-rich repeat containing family receptors and their expression in channel catfish.," *Dev Comp Immunol*, vol. 33, pp. 991–999, Sep 2009.
- [49] C. Stein, M. Caccamo, G. Laird, and M. Leptin, "Conservation and divergence of gene families encoding components of innate immune response systems in zebrafish.," *Genome Biol*, vol. 8, no. 11, p. R251, 2007.
- [50] B. J. Conti, B. K. Davis, J. H. Zhang, W. O'Connor, K. L. Williams, and J. P. Y. Ting, "Caterpillar 16.2 (clr16.2), a novel nbd/lrr family member that negatively regulates t cell function," *Journal of Biological Chemistry*, vol. 280, pp. 18375–18385, May 2005.
- [51] M. Schneider, A. G. Zimmermann, R. A. Roberts, L. Zhang, K. V. Swanson, H. Wen, B. K. Davis, I. C. Allen, E. K. Holl, Z. Ye, A. H. Rahman, B. J. Conti, T. K. Eitas, B. H. Koller, and J. P.-Y. Ting, "The innate immune sensor nlrc3 attenuates toll-like receptor signaling via modification of the signaling adaptor traf6 and transcription factor nf- κ b.," *Nat Immunol*, vol. 13, pp. 823–831, Sep 2012.
- [52] K. V. Rajendran, J. Zhang, S. Liu, H. Kucuktas, X. Wang, H. Liu, Z. Sha, J. Terhune, E. Peatman, and Z. Liu, "Pathogen recognition receptors in channel catfish: I. identification, phylogeny and expression of nod-like receptors.," *Dev Comp Immunol*, Dec 2011.
- [53] V. Cuvillier-Hot, C. Boidin-Wichlacz, C. Slomianny, M. Salzet, and A. Tasiemski, "Characterization and immune function of two intracellular sensors, hmtlr1 and hmlnr, in the injured cns of an invertebrate.," *Dev Comp Immunol*, vol. 35, pp. 214–226, Feb 2011.
- [54] S. Stobrawa, *Development of a conditional NOD3 Knock-out mouse model*. genoway, 2006.

- [55] J. A. Harton, M. W. Linhoff, J. Zhang, and J. P.-Y. Ting, "Cutting edge: Caterpillar: a large family of mammalian genes containing card, pyrin, nucleotide-binding, and leucine-rich repeat domains.," *J Immunol*, vol. 169, pp. 4088–4093, Oct 2002.
- [56] J. Masumoto, M. Hasegawa, and N. Inohara, "The molecular mechanism of autoinflammatory disease—lessons from the function of nod protein families," *Nihon Rinsho Meneki Gakkai Kaishi*, vol. 30, pp. 68–77, Apr 2007.
- [57] M. Proell, S. J. Riedl, J. H. Fritz, A. M. Rojas, and R. Schwarzenbacher, "The nod-like receptor (nlr) family: a tale of similarities and differences.," *PLoS One*, vol. 3, no. 4, p. e2119, 2008.
- [58] K. Hofmann, P. Bucher, and J. Tschopp, "The card domain: a new apoptotic signalling motif.," *Trends Biochem Sci*, vol. 22, pp. 155–156, May 1997.
- [59] M. Albrecht and F. L. W. Takken, "Update on the domain architectures of nlrs and r proteins.," *Biochem Biophys Res Commun*, vol. 339, pp. 459–462, Jan 2006.
- [60] N. Inohara, T. Koseki, J. Lin, L. del Peso, P. C. Lucas, F. F. Chen, Y. Ogura, and G. Nunez, "An induced proximity model for nf-kappa b activation in the nod1/rikk and rip signaling pathways.," *J Biol Chem*, vol. 275, pp. 27823–27831, Sep 2000.
- [61] J. M. Wilmanski, T. Petnicki-Ocwieja, and K. S. Kobayashi, "Nlr proteins: integral members of innate immunity and mediators of inflammatory diseases.," *J Leukoc Biol*, vol. 83, pp. 13–30, Jan 2008.
- [62] A. Y. Istomin and A. Godzik, "Understanding diversity of human innate immunity receptors: analysis of surface features of leucine-rich repeat domains in nlrs and tlrs.," *BMC Immunol*, vol. 10, p. 48, 2009.
- [63] J. L. Dangl and J. D. Jones, "Plant pathogens and integrated defence responses to infection.," *Nature*, vol. 411, pp. 826–833, Jun 2001.
- [64] N. Inohara, T. Koseki, L. del Peso, Y. Hu, C. Yee, S. Chen, R. Carrio, J. Merino, D. Liu, J. Ni, and G. Nunez, "Nod1, an apaf-1-like activator of caspase-9 and nuclear factor-kappab.," *J Biol Chem*, vol. 274, pp. 14560–14567, May 1999.

- [65] Y. Ogura, N. Inohara, A. Benito, F. F. Chen, S. Yamaoka, and G. Nunez, "Nod2, a nod1/apaf-1 family member that is restricted to monocytes and activates nf-kappab.," *J Biol Chem*, vol. 276, pp. 4812–4818, Feb 2001.
- [66] B. J. Geddes, L. Wang, W. J. Huang, M. Lavellee, G. A. Manji, M. Brown, M. Jurman, J. Cao, J. Morgenstern, S. Merriam, M. A. Glucksmann, P. S. DiStefano, and J. Bertin, "Human card12 is a novel ced4/apaf-1 family member that induces apoptosis.," *Biochem Biophys Res Commun*, vol. 284, pp. 77–82, Jun 2001.
- [67] Z. L. Chu, F. Pio, Z. Xie, K. Welsh, M. Krajewska, S. Krajewski, A. Godzik, and J. C. Reed, "A novel enhancer of the apaf1 apoptosome involved in cytochrome c-dependent caspase activation and apoptosis.," *J Biol Chem*, vol. 276, pp. 9239–9245, Mar 2001.
- [68] A. Ling, F. Soares, D. O. Croitoru, I. Tattoli, L. A. M. Carneiro, M. Boniotto, S. Benko, D. J. Philpott, and S. E. Girardin, "Post-transcriptional inhibition of luciferase reporter assays by the nod-like receptor proteins nlr1 and nlr3.," *J Biol Chem*, vol. 287, pp. 28705–28716, Aug 2012.
- [69] L. Sagan, "On the origin of mitosing cells," *J Theor Biol*, vol. 14, pp. 255–274, Mar 1967.
- [70] D. J. Pagliarini, S. E. Calvo, B. Chang, S. A. Sheth, S. B. Vafai, S.-E. Ong, G. A. Walford, C. Sugiana, A. Boneh, W. K. Chen, D. E. Hill, M. Vidal, J. G. Evans, D. R. Thorburn, S. A. Carr, and V. K. Mootha, "A mitochondrial protein compendium elucidates complex i disease biology.," *Cell*, vol. 134, pp. 112–123, Jul 2008.
- [71] M. W. Pellegrino, A. M. Nargund, and C. M. Haynes, "Signaling the mitochondrial unfolded protein response.," *Biochim Biophys Acta*, vol. 1833, pp. 410–416, Feb 2013.
- [72] A. P. West, G. S. Shadel, and S. Ghosh, "Mitochondria in innate immune responses.," *Nat Rev Immunol*, vol. 11, pp. 389–402, Jun 2011.
- [73] E. Naik and V. M. Dixit, "Mitochondrial reactive oxygen species drive proinflammatory cytokine production.," *J Exp Med*, vol. 208, pp. 417–420, Mar 2011.
- [74] Y. Liu, G. Fiskum, and D. Schubert, "Generation of reactive oxygen species by the mitochondrial electron transport chain.," *J Neurochem*, vol. 80, pp. 780–787, Mar 2002.

- [75] Q. Chen, E. J. Vazquez, S. Moghaddas, C. L. Hoppel, and E. J. Lesnefsky, "Production of reactive oxygen species by mitochondria: central role of complex iii.," *J Biol Chem*, vol. 278, pp. 36027–36031, Sep 2003.
- [76] K. V. Tormos, E. Anso, R. B. Hamanaka, J. Eisenbart, J. Joseph, B. Kalyanaraman, and N. S. Chandel, "Mitochondrial complex iii ros regulate adipocyte differentiation.," *Cell Metab*, vol. 14, pp. 537–544, Oct 2011.
- [77] C. Guichard, E. Pedruzzi, M. Fay, S. Ben Mkaddem, N. Coant, F. Daniel, and E. Ogier-Denis, "[the nox/duox family of ros-generating nadph oxidases].," *Med Sci (Paris)*, vol. 22, pp. 953–959, Nov 2006.
- [78] I. Kim, S. Rodriguez-Enriquez, and J. J. Lemasters, "Selective degradation of mitochondria by mitophagy.," *Arch Biochem Biophys*, vol. 462, pp. 245–253, Jun 2007.
- [79] P. R. Odgren, G. Toukatly, P. L. Bangs, R. Gilmore, and E. G. Fey, "Molecular characterization of mitofilin (hmp), a mitochondria-associated protein with predicted coiled coil and intermembrane space targeting domains.," *J Cell Sci*, vol. 109 (Pt 9), pp. 2253–2264, Sep 1996.
- [80] G. B. John, Y. Shang, L. Li, C. Renken, C. A. Mannella, J. M. L. Selker, L. Rangell, M. J. Bennett, and J. Zha, "The mitochondrial inner membrane protein mitofilin controls cristae morphology.," *Mol Biol Cell*, vol. 16, pp. 1543–1554, Mar 2005.
- [81] C. Koerner, M. Barrera, J. Dukanovic, K. Eydt, M. Harner, R. Rabl, F. Vogel, D. Rapaport, W. Neupert, and A. S. Reichert, "The c-terminal domain of fcj1 is required for formation of crista junctions and interacts with the tob/sam complex in mitochondria.," *Mol Biol Cell*, vol. 23, pp. 2143–2155, Jun 2012.
- [82] R. M. Zerbes, M. Bohnert, D. A. Stroud, K. von der Malsburg, A. Kram, S. Oeljeklaus, B. Warscheid, T. Becker, N. Wiedemann, M. Veenhuis, I. J. van der Klei, N. Pfanner, and M. van der Laan, "Role of minos in mitochondrial membrane architecture: cristae morphology and outer membrane interactions differentially depend on mitofilin domains.," *J Mol Biol*, vol. 422, pp. 183–191, Sep 2012.
- [83] R. M. Zerbes, I. J. van der Klei, M. Veenhuis, N. Pfanner, M. van der Laan, and M. Bohnert, "Mitofilin complexes: conserved organizers of mitochondrial membrane architecture.," *Biol Chem*, vol. 393, pp. 1247–1261, Nov 2012.

- [84] T. A. Weber, S. Koob, H. Heide, I. Wittig, B. Head, A. van der Blik, U. Brandt, M. Mittelbronn, and A. S. Reichert, "Apool is a cardiolipin-binding constituent of the mitofilin/minos protein complex determining cristae morphology in mammalian mitochondria.," *PLoS One*, vol. 8, no. 5, p. e63683, 2013.
- [85] C. A. Mannella, "Structure and dynamics of the mitochondrial inner membrane cristae.," *Biochim Biophys Acta*, vol. 1763, no. 5-6, pp. 542-548, 2006.
- [86] M. Zick, R. Rabl, and A. S. Reichert, "Cristae formation-linking ultrastructure and function of mitochondria.," *Biochim Biophys Acta*, vol. 1793, pp. 5-19, Jan 2009.
- [87] C. A. Wurm and S. Jakobs, "Differential protein distributions define two sub-compartments of the mitochondrial inner membrane in yeast.," *FEBS Lett*, vol. 580, pp. 5628-5634, Oct 2006.
- [88] F. Vogel, C. Bornhoevd, W. Neupert, and A. S. Reichert, "Dynamic subcompartmentalization of the mitochondrial inner membrane.," *J Cell Biol*, vol. 175, pp. 237-247, Oct 2006.
- [89] M. Bohnert, L.-S. Wenz, R. M. Zerbes, S. E. Horvath, D. A. Stroud, K. von der Malsburg, J. M. Mueller, S. Oeljeklaus, I. Perschil, B. Warscheid, A. Chacinska, M. Veenhuis, I. J. van der Klei, G. Daum, N. Wiedemann, T. Becker, N. Pfanner, and M. van der Laan, "Role of mitochondrial inner membrane organizing system in protein biogenesis of the mitochondrial outer membrane.," *Mol Biol Cell*, vol. 23, pp. 3948-3956, Oct 2012.
- [90] N. Wiedemann, A. E. Frazier, and N. Pfanner, "The protein import machinery of mitochondria.," *J Biol Chem*, vol. 279, pp. 14473-14476, Apr 2004.
- [91] K. von der Malsburg, J. M. Mueller, M. Bohnert, S. Oeljeklaus, P. Kwiatkowska, T. Becker, A. Loniewska-Lwowska, S. Wiese, S. Rao, D. Milenkovic, D. P. Hutu, R. M. Zerbes, A. Schulze-Specking, H. E. Meyer, J.-C. Martinou, S. Rospert, P. Rehling, C. Meisinger, M. Veenhuis, B. Warscheid, I. J. van der Klei, N. Pfanner, A. Chacinska, and M. van der Laan, "Dual role of mitofilin in mitochondrial membrane organization and protein biogenesis.," *Dev Cell*, vol. 21, pp. 694-707, Oct 2011.
- [92] M. Harner, W. Neupert, and M. Deponete, "Lateral release of proteins from the tom complex into the outer membrane of mitochondria.," *EMBO J*, vol. 30, no. 16, pp. 3232-3241, 2011.

- [93] S. I. L. Workshop, "Revised nomenclature for antigen-nonspecific t cell proliferation and helper factors.," *J Immunol*, vol. 123, pp. 2928–2929, Dec 1979.
- [94] C. Brocker, D. Thompson, A. Matsumoto, D. W. Nebert, and V. Vasiliou, "Evolutionary divergence and functions of the human interleukin (il) gene family.," *Hum Genomics*, vol. 5, pp. 30–55, Oct 2010.
- [95] G. Scapigliati, F. Buonocore, and M. Mazzini, "Biological activity of cytokines: an evolutionary perspective.," *Curr Pharm Des*, vol. 12, no. 24, pp. 3071–3081, 2006.
- [96] K. Paukku and O. Silvennoinen, "Stats as critical mediators of signal transduction and transcription: lessons learned from stat5.," *Cytokine Growth Factor Rev*, vol. 15, pp. 435–455, Dec 2004.
- [97] J. Darnell, Jr, "Stats and gene regulation.," *Science*, vol. 277, pp. 1630–1635, Sep 1997.
- [98] P. J. Murray, "Stat3-mediated anti-inflammatory signalling.," *Biochem Soc Trans*, vol. 34, pp. 1028–1031, Dec 2006.
- [99] J. P. Priestle, H. P. Schaer, and M. G. Gruetter, "Crystallographic refinement of interleukin 1 beta at 2.0 a resolution.," *Proc Natl Acad Sci U S A*, vol. 86, pp. 9667–9671, Dec 1989.
- [100] S. P. Commins, L. Borish, and J. W. Steinke, "Immunologic messenger molecules: cytokines, interferons, and chemokines.," *J Allergy Clin Immunol*, vol. 125, pp. S53–S72, Feb 2010.
- [101] N. Higa, C. Toma, T. Nohara, N. Nakasone, G. Takaesu, and T. Suzuki, "Lose the battle to win the war: bacterial strategies for evading host inflammasome activation.," *Trends Microbiol*, vol. 21, pp. 342–349, Jul 2013.
- [102] H. E. Barksby, S. R. Lea, P. M. Preshaw, and J. J. Taylor, "The expanding family of interleukin-1 cytokines and their role in destructive inflammatory disorders.," *Clin Exp Immunol*, vol. 149, pp. 217–225, Aug 2007.
- [103] K. A. Smith, L. B. Lachman, J. J. Oppenheim, and M. F. Favata, "The functional relationship of the interleukins.," *J Exp Med*, vol. 151, pp. 1551–1556, Jun 1980.
- [104] N. L. Alves, F. A. Arosa, and R. A. W. van Lier, "Common gamma chain cytokines: dissidence in the details.," *Immunol Lett*, vol. 108, pp. 113–120, Feb 2007.

- [105] S. Bessoles, F. Fouret, S. Dudal, G. S. Besra, F. Sanchez, and V. Lafont, "Il-2 triggers specific signaling pathways in human nkt cells leading to the production of pro- and anti-inflammatory cytokines.," *J Leukoc Biol*, vol. 84, pp. 224–233, Jul 2008.
- [106] C. Conforti-Andreoni, O. Beretta, G. Licandro, H. L. Qian, M. Urbano, F. Vitulli, P. Ricciardi-Castagnoli, and A. Mortellaro, "Synergism of nod2 and nlrp3 activators promotes a unique transcriptional profile in murine dendritic cells.," *J Leukoc Biol*, vol. 88, pp. 1207–1216, Dec 2010.
- [107] J. Scheller, A. Chalaris, D. Schmidt-Arras, and S. Rose-John, "The pro- and anti-inflammatory properties of the cytokine interleukin-6.," *Biochim Biophys Acta*, vol. 1813, pp. 878–888, May 2011.
- [108] S. Akira, T. Taga, and T. Kishimoto, "Interleukin-6 in biology and medicine.," *Adv Immunol*, vol. 54, pp. 1–78, 1993.
- [109] J. Van Snick, J. C. Renaud, R. J. Simpson, C. Uyttenhove, and A. Vink, "Mouse il-6. a hybridoma growth factor with multiple effects on normal b and t cells.," *Ann N Y Acad Sci*, vol. 557, pp. 206–13, discussion 213–4, 1989.
- [110] D. F. Fiorentino, M. W. Bond, and T. R. Mosmann, "Two types of mouse t helper cell. iv. th2 clones secrete a factor that inhibits cytokine production by th1 clones.," *J Exp Med*, vol. 170, pp. 2081–2095, Dec 1989.
- [111] R. de Waal Malefyt, H. Yssel, M. G. Roncarolo, H. Spits, and J. E. de Vries, "Interleukin-10.," *Curr Opin Immunol*, vol. 4, pp. 314–320, Jun 1992.
- [112] A. Zdanov, C. Schalk-Hihi, A. Gustchina, M. Tsang, J. Weatherbee, and A. Wlodawer, "Crystal structure of interleukin-10 reveals the functional dimer with an unexpected topological similarity to interferon gamma.," *Structure*, vol. 3, pp. 591–601, Jun 1995.
- [113] A. A. Cuneo and M. V. Autieri, "Expression and function of anti-inflammatory interleukins: the other side of the vascular response to injury.," *Curr Vasc Pharmacol*, vol. 7, pp. 267–276, Jul 2009.
- [114] Y. Inoue, T. Otsuka, H. Niuro, S. Nagano, Y. Arinobu, E. Ogami, M. Akahoshi, K. Miyake, I. Ninomiya, S. Shimizu, H. Nakashima, and M. Harada, "Novel regulatory mechanisms

- of cd40-induced prostanoid synthesis by il-4 and il-10 in human monocytes.," *J Immunol*, vol. 172, pp. 2147–2154, Feb 2004.
- [115] C. Ward, J. Murray, A. Clugston, I. Dransfield, C. Haslett, and A. G. Rossi, "Interleukin-10 inhibits lipopolysaccharide-induced survival and extracellular signal-regulated kinase activation in human neutrophils.," *Eur J Immunol*, vol. 35, pp. 2728–2737, Sep 2005.
- [116] A. B. Lentsch, T. P. Shanley, V. Sarma, and P. A. Ward, "In vivo suppression of nf-kappa b and preservation of i kappa b alpha by interleukin-10 and interleukin-13.," *J Clin Invest*, vol. 100, pp. 2443–2448, Nov 1997.
- [117] M. Qing, A. Nimmesgern, P. C. Heinrich, K. Schumacher, J. F. Vazquez-Jimenez, J. Hess, G. von Bernuth, and M.-C. Seghaye, "Intrahepatic synthesis of tumor necrosis factor-alpha related to cardiac surgery is inhibited by interleukin-10 via the janus kinase (jak)/signal transducers and activator of transcription (stat) pathway.," *Crit Care Med*, vol. 31, pp. 2769–2775, Dec 2003.
- [118] M. Saraiva and A. O'Garra, "The regulation of il-10 production by immune cells.," *Nat Rev Immunol*, vol. 10, pp. 170–181, Mar 2010.
- [119] L. Chen, L. Lei, Z. Zhou, J. He, S. Xu, C. Lu, J. Chen, Z. Yang, G. Wu, I.-T. Yeh, G. Zhong, and Y. Wu, "Contribution of interleukin-12 p35 (il-12p35) and il-12p40 to protective immunity and pathology in mice infected with chlamydia muridarum.," *Infect Immun*, vol. 81, pp. 2962–2971, Aug 2013.
- [120] F. Koch, U. Stanzl, P. Jennewein, K. Janke, C. Heuffer, E. Kaempgen, N. Romani, and G. Schuler, "High level il-12 production by murine dendritic cells: upregulation via mhc class ii and cd40 molecules and downregulation by il-4 and il-10.," *J Exp Med*, vol. 184, pp. 741–746, Aug 1996.
- [121] J. C. Guery, F. Ria, F. Galbiati, and L. Adorini, "Normal b cells fail to secrete interleukin-12.," *Eur J Immunol*, vol. 27, pp. 1632–1639, Jul 1997.
- [122] W. E. Thierfelder, J. M. van Deursen, K. Yamamoto, R. A. Tripp, S. R. Sarawar, R. T. Carson, M. Y. Sangster, D. A. Vignali, P. C. Doherty, G. C. Grosveld, and J. N. Ihle, "Requirement for stat4 in interleukin-12-mediated responses of natural killer and t cells.," *Nature*, vol. 382, pp. 171–174, Jul 1996.

- [123] W. E. Fogler, K. Volker, M. Watanabe, J. M. Wigginton, P. Roessler, M. J. Brunda, J. R. Ortaldo, and R. H. Wiltrott, "Recruitment of hepatic nk cells by il-12 is dependent on ifn-gamma and vcam-1 and is rapidly down-regulated by a mechanism involving t cells and expression of fas.," *J Immunol*, vol. 161, pp. 6014–6021, Dec 1998.
- [124] M. J. Brunda, L. Luistro, L. Rumennik, R. B. Wright, J. M. Wigginton, R. H. Wiltrott, J. A. Hendrzak, and A. V. Palleroni, "Interleukin-12: murine models of a potent antitumor agent.," *Ann N Y Acad Sci*, vol. 795, pp. 266–274, Oct 1996.
- [125] K. Anwer, F. J. Kelly, C. Chu, J. G. Fewell, D. Lewis, and R. D. Alvarez, "Phase i trial of a formulated il-12 plasmid in combination with carboplatin and docetaxel chemotherapy in the treatment of platinum-sensitive recurrent ovarian cancer.," *Gynecol Oncol*, Jul 2013.
- [126] E. A. Carswell, L. J. Old, R. L. Kassel, S. Green, N. Fiore, and B. Williamson, "An endotoxin-induced serum factor that causes necrosis of tumors," *Proceedings of the National Academy of Sciences*, vol. 72, no. 9, pp. 3666–3670, 1975.
- [127] P. Tang, Hung M-C, and J. Klostergaard, "Human pro-tumor necrosis factor is a homotrimer.," *Biochemistry*, vol. 35, pp. 8216–8225, Jun 1996.
- [128] T. Horiuchi, H. Mitoma, S.-i. Harashima, H. Tsukamoto, and T. Shimoda, "Transmembrane tnf-alpha: structure, function and interaction with anti-tnf agents.," *Rheumatology (Oxford)*, vol. 49, pp. 1215–1228, Jul 2010.
- [129] R. M. Locksley, N. Killeen, and M. J. Lenardo, "The tnf and tnf receptor superfamilies: integrating mammalian biology.," *Cell*, vol. 104, pp. 487–501, Feb 2001.
- [130] A. Aderem and R. J. Ulevitch, "Toll-like receptors in the induction of the innate immune response.," *Nature*, vol. 406, pp. 782–787, Aug 2000.
- [131] H. H. Park, Y.-C. Lo, S.-C. Lin, L. Wang, J. K. Yang, and H. Wu, "The death domain superfamily in intracellular signaling of apoptosis and inflammation.," *Annu Rev Immunol*, vol. 25, pp. 561–586, 2007.
- [132] J. Rajasingh, E. Bord, C. Luedemann, J. Asai, H. Hamada, T. Thorne, G. Qin, D. Goukasian, Y. Zhu, D. W. Losordo, and R. Kishore, "Il-10-induced tnf-alpha mrna destabilization is mediated via il-10 suppression of p38 map kinase activation and inhibition of hur expression.," *FASEB J*, vol. 20, pp. 2112–2114, Oct 2006.

- [133] T. F. Deuel, P. S. Keim, M. Farmer, and R. L. Henrikson, "Amino acid sequence of human platelet factor 4.," *Proc Natl Acad Sci U S A*, vol. 74, pp. 2256–2258, Jun 1977.
- [134] M. Locati, R. Bonecchi, and M. M. Corsi, "Chemokines and their receptors: roles in specific clinical conditions and measurement in the clinical laboratory.," *Am J Clin Pathol*, vol. 123 Suppl, pp. S82–S95, Jun 2005.
- [135] M. Mellado, J. M. Rodriguez-Frade, S. Manes, and C. Martinez-A, "Chemokine signaling and functional responses: the role of receptor dimerization and tk pathway activation.," *Annu Rev Immunol*, vol. 19, pp. 397–421, 2001.
- [136] Y. Kobayashi, "Neutrophil infiltration and chemokines.," *Crit Rev Immunol*, vol. 26, no. 4, pp. 307–316, 2006.
- [137] J. Hol, L. Wilhelmsen, and G. Haraldsen, "The murine il-8 homologues kc, mip-2, and lix are found in endothelial cytoplasmic granules but not in weibel-palade bodies.," *J Leukoc Biol*, vol. 87, pp. 501–508, Mar 2010.
- [138] E. T. Baldwin, I. T. Weber, R. St Charles, J. C. Xuan, E. Appella, M. Yamada, K. Matsushima, B. F. Edwards, G. M. Clore, and A. M. Gronenborn, "Crystal structure of interleukin 8: symbiosis of nmr and crystallography.," *Proc Natl Acad Sci U S A*, vol. 88, pp. 502–506, Jan 1991.
- [139] A. Moeller, U. Lippert, D. Lessmann, G. Kolde, K. Hamann, P. Welker, D. Schadendorf, T. Rosenbach, T. Luger, and B. M. Czarnetzki, "Human mast cells produce il-8.," *J Immunol*, vol. 151, pp. 3261–3266, Sep 1993.
- [140] A. E. Koch, P. J. Polverini, S. L. Kunkel, L. A. Harlow, L. A. DiPietro, V. M. Elner, S. G. Elner, and R. M. Strieter, "Interleukin-8 as a macrophage-derived mediator of angiogenesis.," *Science*, vol. 258, pp. 1798–1801, Dec 1992.
- [141] C. S. M. Oude Nijhuis, E. Vellenga, S. M. G. J. Daenen, W. A. Kamps, and E. S. J. M. De Bont, "Endothelial cells are main producers of interleukin 8 through toll-like receptor 2 and 4 signaling during bacterial infection in leukopenic cancer patients.," *Clin Diagn Lab Immunol*, vol. 10, pp. 558–563, Jul 2003.
- [142] R. M. Strieter, S. L. Kunkel, H. J. Showell, D. G. Remick, S. H. Phan, P. A. Ward, and R. M.

- Marks, "Endothelial cell gene expression of a neutrophil chemotactic factor by tnf-alpha, lps, and il-1 beta.," *Science*, vol. 243, pp. 1467–1469, Mar 1989.
- [143] A. E. Medvedev, K. M. Kopydlowski, and S. N. Vogel, "Inhibition of lipopolysaccharide-induced signal transduction in endotoxin-tolerized mouse macrophages: dysregulation of cytokine, chemokine, and toll-like receptor 2 and 4 gene expression.," *J Immunol*, vol. 164, pp. 5564–5574, Jun 2000.
- [144] A. Imada, K. Ina, M. Shimada, T. Yokoyama, Y. Yokoyama, Y. Nishio, T. Yamaguchi, T. Ando, and K. Kusugami, "Coordinate upregulation of interleukin-8 and growth-related gene product-alpha is present in the colonic mucosa of inflammatory bowel.," *Scand J Gastroenterol*, vol. 36, pp. 854–864, Aug 2001.
- [145] R. Sen and D. Baltimore, "Inducibility of kappa immunoglobulin enhancer-binding protein nf-kappa b by a posttranslational mechanism.," *Cell*, vol. 47, pp. 921–928, Dec 1986.
- [146] A. Oeckinghaus, M. S. Hayden, and S. Ghosh, "Crosstalk in nf-kappab signaling pathways.," *Nat Immunol*, vol. 12, pp. 695–708, Aug 2011.
- [147] M. S. Hayden and S. Ghosh, "Shared principles in nf-kappab signaling.," *Cell*, vol. 132, pp. 344–362, Feb 2008.
- [148] S. T. Smale, "Hierarchies of nf-?b target-gene regulation.," *Nat Immunol*, vol. 12, pp. 689–694, Aug 2011.
- [149] R. Schreck, K. Albermann, and P. A. Baeuerle, "Nuclear factor kappa b: an oxidative stress-responsive transcription factor of eukaryotic cells (a review).," *Free Radic Res Commun*, vol. 17, no. 4, pp. 221–237, 1992.
- [150] T. D. Gilmore, "Introduction to nf-kappab: players, pathways, perspectives.," *Oncogene*, vol. 25, pp. 6680–6684, Oct 2006.
- [151] A. Oeckinghaus, M. S. Hayden, and S. Ghosh, "Crosstalk in nf-?b signaling pathways.," *Nat Immunol*, vol. 12, pp. 695–708, Aug 2011.
- [152] M. Pasparakis, T. Luedde, and M. Schmidt-Supprian, "Dissection of the nf-kappab signalling cascade in transgenic and knockout mice.," *Cell Death Differ*, vol. 13, pp. 861–872, May 2006.

- [153] S. Gerondakis, M. Grossmann, Y. Nakamura, T. Pohl, and R. Grumont, “Genetic approaches in mice to understand rel/nf-kappab and ikappab function: transgenics and knockouts.,” *Oncogene*, vol. 18, pp. 6888–6895, Nov 1999.
- [154] C. S. Gismera and B. S. Aladren, “Inflammatory bowel diseases: a disease (s) of modern times? is incidence still increasing?,” *World J Gastroenterol*, vol. 14, pp. 5491–5498, Sep 2008.
- [155] P. Rosenstiel, C. Sina, A. Franke, and S. Schreiber, “Towards a molecular risk map—recent advances on the etiology of inflammatory bowel disease.,” *Semin Immunol*, vol. 21, pp. 334–345, Dec 2009.
- [156] A. N. Ananthakrishnan, “Environmental triggers for inflammatory bowel disease.,” *Curr Gastroenterol Rep*, vol. 15, p. 302, Jan 2013.
- [157] D. K. Podolsky, “Inflammatory bowel disease.,” *N Engl J Med*, vol. 347, pp. 417–429, Aug 2002.
- [158] B. Sadlack, H. Merz, H. Schorle, A. Schimpl, A. C. Feller, and I. Horak, “Ulcerative colitis-like disease in mice with a disrupted interleukin-2 gene.,” *Cell*, vol. 75, pp. 253–261, Oct 1993.
- [159] R. Kuehn, J. Loehler, D. Rennick, K. Rajewsky, and W. Mueller, “Interleukin-10-deficient mice develop chronic enterocolitis.,” *Cell*, vol. 75, pp. 263–274, Oct 1993.
- [160] I. Okayasu, S. Hatakeyama, M. Yamada, T. Ohkusa, Y. Inagaki, and R. Nakaya, “A novel method in the induction of reliable experimental acute and chronic ulcerative colitis in mice.,” *Gastroenterology*, vol. 98, pp. 694–702, Mar 1990.
- [161] H. Laroui, S. A. Ingersoll, H. C. Liu, M. T. Baker, S. Ayyadurai, M. A. Charania, F. Laroui, Y. Yan, S. V. Sitaraman, and D. Merlin, “Dextran sodium sulfate (dss) induces colitis in mice by forming nano-lipocomplexes with medium-chain-length fatty acids in the colon.,” *PLoS One*, vol. 7, no. 3, p. e32084, 2012.
- [162] F. Miyazawa, O. R. Olijnyk, C. J. Tilley, and T. Tamaoki, “Interactions between dextran sulfate and escherichia coli ribosomes.,” *Biochim Biophys Acta*, vol. 145, pp. 96–104, Aug 1967.

- [163] J. Felling and C. E. Wiley, "The inhibition of pancreatic ribonuclease by anionic polymers.," *Arch Biochem Biophys*, vol. 85, pp. 313–316, Dec 1959.
- [164] L. A. Dieleman, B. U. Ridwan, G. S. Tennyson, K. W. Beagley, R. P. Bucy, and C. O. Elson, "Dextran sulfate sodium-induced colitis occurs in severe combined immunodeficient mice.," *Gastroenterology*, vol. 107, pp. 1643–1652, Dec 1994.
- [165] M. Nanno, Y. Kanari, T. Naito, N. Inoue, T. Hisamatsu, H. Chinen, K. Sugimoto, Y. Shimomura, H. Yamagishi, T. Shiohara, S. Ueha, K. Matsushima, M. Suematsu, A. Mizoguchi, T. Hibi, A. K. Bhan, and H. Ishikawa, "Exacerbating role of gammadelta t cells in chronic colitis of t-cell receptor alpha mutant mice.," *Gastroenterology*, vol. 134, pp. 481–490, Feb 2008.
- [166] M. S. Islam, T. Murata, M. Fujisawa, R. Nagasaka, H. Ushio, A. M. Bari, M. Hori, and H. Ozaki, "Anti-inflammatory effects of phytosteryl ferulates in colitis induced by dextran sulphate sodium in mice.," *Br J Pharmacol*, vol. 154, pp. 812–824, Jun 2008.
- [167] M. Maehler, I. J. Bristol, E. H. Leiter, A. E. Workman, E. H. Birkenmeier, C. O. Elson, and J. P. Sundberg, "Differential susceptibility of inbred mouse strains to dextran sulfate sodium-induced colitis.," *Am J Physiol*, vol. 274, pp. G544–G551, Mar 1998.
- [168] T. Shea-Donohue, K. Thomas, M. J. Cody, A. Zhao, L. J. Detolla, K. M. Kopydlowski, M. Fukata, S. A. Lira, and S. N. Vogel, "Mice deficient in the cxcr2 ligand, cxcl1 (kc/gro-alpha), exhibit increased susceptibility to dextran sodium sulfate (dss)-induced colitis.," *Innate Immun*, vol. 14, pp. 117–124, Apr 2008.
- [169] M. Rousset, "The human colon carcinoma cell lines ht-29 and caco-2: two in vitro models for the study of intestinal differentiation.," *Biochimie*, vol. 68, pp. 1035–1040, Sep 1986.
- [170] F. L. Graham, J. Smiley, W. C. Russell, and R. Nairn, "Characteristics of a human cell line transformed by dna from human adenovirus type 5.," *J Gen Virol*, vol. 36, pp. 59–74, Jul 1977.
- [171] W. F. Scherer, J. T. Syverton, and G. O. Gey, "Studies on the propagation in vitro of poliomyelitis viruses. iv. viral multiplication in a stable strain of human malignant epithelial cells (strain hela) derived from an epidermoid carcinoma of the cervix.," *J Exp Med*, vol. 97, pp. 695–710, May 1953.

- [172] T. G. Fogh, J., *New human tumor cell lines in human tumor cells in vitro. In Human Tumor Cells in Vitro*. Plenum Press, 1975.
- [173] U. Schneider, H. U. Schwenk, and G. Bornkamm, "Characterization of ebv-genome negative "null" and "t" cell lines derived from children with acute lymphoblastic leukemia and leukemic transformed non-hodgkin lymphoma.," *Int J Cancer*, vol. 19, pp. 621–626, May 1977.
- [174] S. Tsuchiya, M. Yamabe, Y. Yamaguchi, Y. Kobayashi, T. Konno, and K. Tada, "Establishment and characterization of a human acute monocytic leukemia cell line (thp-1).," *Int J Cancer*, vol. 26, pp. 171–176, Aug 1980.
- [175] K. Vidal, I. Grosjean, J. P. evillard, C. Gespach, and D. Kaiserlian, "Immortalization of mouse intestinal epithelial cells by the sv40-large t gene. phenotypic and immune characterization of the mode-k cell line.," *J Immunol Methods*, vol. 166, pp. 63–73, Nov 1993.
- [176] W. C. Raschke, S. Baird, P. Ralph, and I. Nakoinz, "Functional macrophage cell lines transformed by abelson leukemia virus.," *Cell*, vol. 15, pp. 261–267, Sep 1978.
- [177] F. Sanger, S. Nicklen, and A. R. Coulson, "Dna sequencing with chain-terminating inhibitors.," *Proc Natl Acad Sci U S A*, vol. 74, pp. 5463–5467, Dec 1977.
- [178] O. H. Lowry, N. J. Rosebrough, A. L. Farr, and R. J. Randall, "Protein measurement with the folin phenol reagent.," *J Biol Chem*, vol. 193, pp. 265–275, Nov 1951.
- [179] U. K. Laemmli, "Cleavage of structural proteins during the assembly of the head of bacteriophage t4.," *Nature*, vol. 227, pp. 680–685, Aug 1970.
- [180] C. P. Hunter, "Genetics: a touch of elegance with rnai.," *Curr Biol*, vol. 9, pp. R440–R442, Jun 1999.
- [181] G. P. Lampson, A. A. Tytell, A. K. Field, M. M. Nemes, and M. R. Hilleman, "Inducers of interferon and host resistance. i. double-stranded rna from extracts of penicillium funiculosum.," *Proc Natl Acad Sci U S A*, vol. 58, pp. 782–789, Aug 1967.
- [182] G. R. Stark, I. M. Kerr, B. R. Williams, R. H. Silverman, and R. D. Schreiber, "How cells respond to interferons.," *Annu Rev Biochem*, vol. 67, pp. 227–264, 1998.

- [183] S. M. Elbashir, J. Harborth, W. Lendeckel, A. Yalcin, K. Weber, and T. Tuschl, "Duplexes of 21-nucleotide rnas mediate rna interference in cultured mammalian cells.," *Nature*, vol. 411, pp. 494–498, May 2001.
- [184] S. H. Kwon, L. Florens, S. K. Swanson, M. P. Washburn, S. M. Abmayr, and J. L. Workman, "Heterochromatin protein 1 (hp1) connects the fact histone chaperone complex to the phosphorylated ctd of rna polymerase ii.," *Genes Dev*, vol. 24, pp. 2133–2145, Oct 2010.
- [185] J. Weischenfeldt and B. Porse, "Bone marrow-derived macrophages (bmm): Isolation and applications.," *CSH Protoc*, vol. 2008, p. pdb.prot5080, 2008.
- [186] S. Wirtz, C. Neufert, B. Weigmann, and M. F. Neurath, "Chemically induced mouse models of intestinal inflammation.," *Nat Protoc*, vol. 2, no. 3, pp. 541–546, 2007.
- [187] C. Becker, M. C. Fantini, S. Wirtz, A. Nikolaev, R. Kiesslich, H. A. Lehr, P. R. Galle, and M. F. Neurath, "In vivo imaging of colitis and colon cancer development in mice using high resolution chromoendoscopy.," *Gut*, vol. 54, pp. 950–954, Jul 2005.
- [188] S. M. Kim, C. W. Rico, S. C. Lee, and M. Y. Kang, "Modulatory effect of rice bran and phytic acid on glucose metabolism in high fat-fed c57bl/6n mice.," *J Clin Biochem Nutr*, vol. 47, pp. 12–17, Jul 2010.
- [189] D. Pomplun, M. Moehlig, J. Spranger, A. F. H. Pfeiffer, and M. Ristow, "Elevation of blood glucose following anaesthetic treatment in c57bl/6 mice.," *Horm Metab Res*, vol. 36, pp. 67–69, Jan 2004.
- [190] M. G. Claros and P. Vincens, "Computational method to predict mitochondrially imported proteins and their targeting sequences.," *Eur J Biochem*, vol. 241, pp. 779–786, Nov 1996.
- [191] I. Small, N. Peeters, F. Legeai, and C. Lurin, "Predotar: A tool for rapidly screening proteomes for n-terminal targeting sequences.," *Proteomics*, vol. 4, pp. 1581–1590, Jun 2004.
- [192] R. Gilmore, G. Blobel, and P. Walter, "Protein translocation across the endoplasmic reticulum. i. detection in the microsomal membrane of a receptor for the signal recognition particle.," *J Cell Biol*, vol. 95, pp. 463–469, Nov 1982.
- [193] A. Chacinska, C. M. Koehler, D. Milenkovic, T. Lithgow, and N. Pfanner, "Importing mitochondrial proteins: machineries and mechanisms.," *Cell*, vol. 138, pp. 628–644, Aug 2009.

- [194] K. Kokame, H. Kato, and T. Miyata, "Identification of erse-ii, a new cis-acting element responsible for the atf6-dependent mammalian unfolded protein response.," *J Biol Chem*, vol. 276, pp. 9199–9205, Mar 2001.
- [195] H. Yoshida, T. Okada, K. Haze, H. Yanagi, T. Yura, M. Negishi, and K. Mori, "Endoplasmic reticulum stress-induced formation of transcription factor complex ersf including nf-y (cbf) and activating transcription factors 6alpha and 6beta that activates the mammalian unfolded protein response.," *Mol Cell Biol*, vol. 21, pp. 1239–1248, Feb 2001.
- [196] H. Yoshida, K. Haze, H. Yanagi, T. Yura, and K. Mori, "Identification of the cis-acting endoplasmic reticulum stress response element responsible for transcriptional induction of mammalian glucose-regulated proteins. involvement of basic leucine zipper transcription factors.," *J Biol Chem*, vol. 273, pp. 33741–33749, Dec 1998.
- [197] M. Li, P. Baumeister, B. Roy, T. Phan, D. Foti, S. Luo, and A. S. Lee, "Atf6 as a transcription activator of the endoplasmic reticulum stress element: thapsigargin stress-induced changes and synergistic interactions with nf-y and yy1.," *Mol Cell Biol*, vol. 20, pp. 5096–5106, Jul 2000.
- [198] M. Wang, S. Wey, Y. Zhang, R. Ye, and A. S. Lee, "Role of the unfolded protein response regulator grp78/bip in development, cancer, and neurological disorders.," *Antioxid Redox Signal*, vol. 11, pp. 2307–2316, Sep 2009.
- [199] H. Wu and J. R. Arron, "Traf6, a molecular bridge spanning adaptive immunity, innate immunity and osteoimmunology.," *Bioessays*, vol. 25, pp. 1096–1105, Nov 2003.
- [200] C. C. Davies, T. W. Mak, L. S. Young, and A. G. Eliopoulos, "Traf6 is required for traf2-dependent cd40 signal transduction in nonhemopoietic cells.," *Mol Cell Biol*, vol. 25, pp. 9806–9819, Nov 2005.
- [201] Y. H. O. F. Y. T. C. Y. A. S. K. T. Y. A. K. T. Yoshida R, Takaesu G, "Traf6 and mekk1 play a pivotal role in the rig-i-like helicase antiviral pathway.," *J Biol Chem.*, vol. 283, 2008.
- [202] F. K. Swirski, M. Nahrendorf, M. Etzrodt, M. Wildgruber, V. Cortez-Retamozo, P. Panizzi, J.-L. Figueiredo, R. H. Kohler, A. Chudnovskiy, P. Waterman, E. Aikawa, T. R. Mempel, P. Libby, R. Weissleder, and M. J. Pittet, "Identification of splenic reservoir monocytes and their deployment to inflammatory sites.," *Science*, vol. 325, pp. 612–616, Jul 2009.

- [203] M. Laudien, R. Haesler, J. Wohlers, J. Boeck, S. Lipinski, L. Bremer, R. Podschun, P. Ambrosch, P. Lamprecht, P. Rosenstiel, and A. Till, "Molecular signatures of a disturbed nasal barrier function in the primary tissue of wegener's granulomatosis.," *Mucosal Immunol*, vol. 4, pp. 564–573, Sep 2011.
- [204] R. J. Falk, W. L. Gross, L. Guillevin, G. Hoffman, D. R. W. Jayne, J. C. Jennette, C. G. M. Kallenberg, R. Luqmani, A. D. Mahr, E. L. Matteson, P. A. Merkel, U. Specks, and R. Watts, "Granulomatosis with polyangiitis (wegerer's): an alternative name for wegener's granulomatosis.," *Ann Rheum Dis*, vol. 70, p. 704, Apr 2011.
- [205] B. Siegmund, H. A. Lehr, G. Fantuzzi, and C. A. Dinarello, "Il-1 beta -converting enzyme (caspase-1) in intestinal inflammation.," *Proc Natl Acad Sci U S A*, vol. 98, pp. 13249–13254, Nov 2001.
- [206] E. Rath, E. Berger, A. Messlik, T. Nunes, B. Liu, S. C. Kim, N. Hoogenraad, M. Sans, R. B. Sartor, and D. Haller, "Induction of dsrna-activated protein kinase links mitochondrial unfolded protein response to the pathogenesis of intestinal inflammation.," *Gut*, vol. 61, pp. 1269–1278, Sep 2012.
- [207] Y. Yin, Y. Yan, X. Jiang, J. Mai, N. C. Chen, H. Wang, and X.-F. Yang, "Inflammasomes are differentially expressed in cardiovascular and other tissues.," *Int J Immunopathol Pharmacol*, vol. 22, no. 2, pp. 311–322, 2009.
- [208] H. L. Rosenzweig, S. R. Planck, and J. T. Rosenbaum, "Nlrs in immune privileged sites.," *Curr Opin Pharmacol*, vol. 11, pp. 423–428, Aug 2011.
- [209] L. Franchi, J.-H. Park, M. H. Shaw, N. Marina-Garcia, G. Chen, Y.-G. Kim, and G. Nunez, "Intracellular nod-like receptors in innate immunity, infection and disease.," *Cell Microbiol*, vol. 10, pp. 1–8, Jan 2008.
- [210] D. Arnoult, F. Soares, I. Tattoli, C. Castanier, D. J. Philpott, and S. E. Girardin, "An n-terminal addressing sequence targets nlrx1 to the mitochondrial matrix.," *J Cell Sci*, vol. 122, pp. 3161–3168, Sep 2009.
- [211] R. B. Seth, L. Sun, C.-K. Ea, and Z. J. Chen, "Identification and characterization of mavs, a mitochondrial antiviral signaling protein that activates nf-kappab and irf 3.," *Cell*, vol. 122, pp. 669–682, Sep 2005.

- [212] Y. Lei, C. B. Moore, R. M. Liesman, B. P. O'Connor, D. T. Bergstralh, Z. J. Chen, R. J. Pickles, and J. P.-Y. Ting, "Mavs-mediated apoptosis and its inhibition by viral proteins.," *PLoS One*, vol. 4, no. 5, p. e5466, 2009.
- [213] C. B. Moore, D. T. Bergstralh, J. A. Duncan, Y. Lei, T. E. Morrison, A. G. Zimmermann, M. A. Accavitti-Loper, V. J. Madden, L. Sun, Z. Ye, J. D. Lich, M. T. Heise, Z. Chen, and J. P.-Y. Ting, "Nlr1 is a regulator of mitochondrial antiviral immunity.," *Nature*, vol. 451, pp. 573–577, Jan 2008.
- [214] S. Benko, D. J. Philpott, and S. E. Girardin, "The microbial and danger signals that activate nod-like receptors.," *Cytokine*, vol. 43, pp. 368–373, Sep 2008.
- [215] J. Tschopp and K. Schroder, "Nlr3 inflammasome activation: The convergence of multiple signalling pathways on ros production?," *Nat Rev Immunol*, vol. 10, pp. 210–215, Mar 2010.
- [216] R. Zhou, A. S. Yazdi, P. Menu, and J. Tschopp, "A role for mitochondria in nlr3 inflammasome activation.," *Nature*, vol. 469, pp. 221–225, Jan 2011.
- [217] M. Yoneyama, M. Kikuchi, T. Natsukawa, N. Shinobu, T. Imaizumi, M. Miyagishi, K. Taira, S. Akira, and T. Fujita, "The rna helicase rig-i has an essential function in double-stranded rna-induced innate antiviral responses.," *Nat Immunol*, vol. 5, pp. 730–737, Jul 2004.
- [218] M. Yoneyama and T. Fujita, "Structural mechanism of rna recognition by the rig-i-like receptors.," *Immunity*, vol. 29, pp. 178–181, Aug 2008.
- [219] O. Takeuchi and S. Akira, "Pattern recognition receptors and inflammation.," *Cell*, vol. 140, pp. 805–820, Mar 2010.
- [220] A. P. West, I. E. Brodsky, C. Rahner, D. K. Woo, H. Erdjument-Bromage, P. Tempst, M. C. Walsh, Y. Choi, G. S. Shadel, and S. Ghosh, "Tlr signalling augments macrophage bactericidal activity through mitochondrial ros.," *Nature*, vol. 472, pp. 476–480, Apr 2011.
- [221] S. B. Singh, A. S. Davis, G. A. Taylor, and V. Deretic, "Human irgm induces autophagy to eliminate intracellular mycobacteria.," *Science*, vol. 313, pp. 1438–1441, Sep 2006.
- [222] S. B. Singh, W. Ornatowski, I. Vergne, J. Naylor, M. Delgado, E. Roberts, M. Ponpuak, S. Master, M. Pilli, E. White, M. Komatsu, and V. Deretic, "Human irgm regulates autophagy and cell-autonomous immunity functions through mitochondria.," *Nat Cell Biol*, vol. 12, pp. 1154–1165, Dec 2010.

- [223] D. Arnoult, F. Soares, I. Tattoli, and S. E. Girardin, "Mitochondria in innate immunity.," *EMBO Rep*, vol. 12, pp. 901–910, Sep 2011.
- [224] C. Ott, K. Ross, S. Straub, B. Thiede, M. Goetz, C. Goosmann, M. Krischke, M. J. Mueller, G. Krohne, T. Rudel, and V. Kozjak-Pavlovic, "Sam50 functions in mitochondrial intermembrane space bridging and biogenesis of respiratory complexes.," *Mol Cell Biol*, vol. 32, pp. 1173–1188, Mar 2012.
- [225] M. Darshi, V. L. Mendiola, M. R. Mackey, A. N. Murphy, A. Koller, G. A. Perkins, M. H. Ellisman, and S. S. Taylor, "Chchd3, an inner mitochondrial membrane protein, is essential for maintaining crista integrity and mitochondrial function.," *J Biol Chem*, vol. 286, pp. 2918–2932, Jan 2011.
- [226] J. Xie, M. F. Marusich, P. Souda, J. Whitelegge, and R. A. Capaldi, "The mitochondrial inner membrane protein mitofilin exists as a complex with sam50, metaxins 1 and 2, coiled-coil-helix coiled-coil-helix domain-containing protein 3 and 6 and dnajc11.," *FEBS Lett*, vol. 581, pp. 3545–3549, Jul 2007.
- [227] W. A. Baseler, E. R. Dabkowski, C. L. Williamson, T. L. Croston, D. Thapa, M. J. Powell, T. T. Razunguzwa, and J. M. Hollander, "Proteomic alterations of distinct mitochondrial subpopulations in the type 1 diabetic heart: contribution of protein import dysfunction.," *Am J Physiol Regul Integr Comp Physiol*, vol. 300, pp. R186–R200, Feb 2011.
- [228] A. Omori, S. Ichinose, S. Kitajima, K. W. Shimotohno, Y. L. Murashima, K. Shimotohno, and A. Seto-Ohshima, "Gerbils of a seizure-sensitive strain have a mitochondrial inner membrane protein with different isoelectric points from those of a seizure-resistant strain.," *Electrophoresis*, vol. 23, pp. 4167–4174, Dec 2002.
- [229] C. M. Haynes and D. Ron, "The mitochondrial upr - protecting organelle protein homeostasis.," *J Cell Sci*, vol. 123, pp. 3849–3855, Nov 2010.
- [230] T. Tatsuta and T. Langer, "Quality control of mitochondria: protection against neurodegeneration and ageing.," *EMBO J*, vol. 27, pp. 306–314, Jan 2008.
- [231] T. Yoneda, C. Benedetti, F. Urano, S. G. Clark, H. P. Harding, and D. Ron, "Compartment-specific perturbation of protein handling activates genes encoding mitochondrial chaperones.," *J Cell Sci*, vol. 117, pp. 4055–4066, Aug 2004.

- [232] A. M. Nargund, M. W. Pellegrino, C. J. Fiorese, B. M. Baker, and C. M. Haynes, "Mitochondrial import efficiency of atfs-1 regulates mitochondrial upr activation.," *Science*, vol. 337, pp. 587–590, Aug 2012.
- [233] K. Yamamoto, H. Yoshida, K. Kokame, R. J. Kaufman, and K. Mori, "Differential contributions of atf6 and xbp1 to the activation of endoplasmic reticulum stress-responsive cis-acting elements erse, upre and erse-ii.," *J Biochem*, vol. 136, pp. 343–350, Sep 2004.
- [234] C. Han, M.-K. Nam, H.-J. Park, Y.-M. Seong, S. Kang, and H. Rhim, "Tunicamycin-induced er stress upregulates the expression of mitochondrial htra2 and promotes apoptosis through the cytosolic release of htra2.," *J Microbiol Biotechnol*, vol. 18, pp. 1197–1202, Jun 2008.
- [235] Y. Inokuchi, Y. Nakajima, M. Shimazawa, T. Kurita, M. Kubo, A. Saito, H. Sajiki, T. Kudo, M. Aihara, K. Imaizumi, M. Araie, and H. Hara, "Effect of an inducer of bip, a molecular chaperone, on endoplasmic reticulum (er) stress-induced retinal cell death.," *Invest Ophthalmol Vis Sci*, vol. 50, pp. 334–344, Jan 2009.
- [236] L. He, S. O. Kim, O. Kwon, S. J. Jeong, M. S. Kim, H. G. Lee, H. Osada, M. Jung, J. S. Ahn, and B. Y. Kim, "Atm blocks tunicamycin-induced endoplasmic reticulum stress.," *FEBS Lett*, vol. 583, pp. 903–908, Mar 2009.
- [237] L. Bouchier-Hayes and S. J. Martin, "Card games in apoptosis and immunity.," *EMBO Rep*, vol. 3, pp. 616–621, Jul 2002.
- [238] H.-A. Eum, R. Vallabhaneni, Y. Wang, P. A. Loughran, D. B. Stolz, and T. R. Billiar, "Characterization of disc formation and tnfr1 translocation to mitochondria in tnf- α -treated hepatocytes.," *Am J Pathol*, vol. 179, pp. 1221–1229, Sep 2011.
- [239] S. Lacour, O. Micheau, A. Hammann, V. Drouineaud, J. Tschopp, E. Solary, and M.-T. Dimanche-Boitrel, "Chemotherapy enhances tnf-related apoptosis-inducing ligand disc assembly in ht29 human colon cancer cells.," *Oncogene*, vol. 22, pp. 1807–1816, Mar 2003.
- [240] S. Saito, T. Murata, T. Kanda, H. Isomura, Y. Narita, A. Sugimoto, D. Kawashima, and T. Tsurumi, "Epstein-barr virus deubiquitinase downregulates traf6-mediated nf-kappab signaling during productive replication.," *J Virol*, vol. 87, pp. 4060–4070, Apr 2013.

- [241] K. D. Taganov, M. P. Boldin, K.-J. Chang, and D. Baltimore, “Nf-kappab-dependent induction of microrna mir-146, an inhibitor targeted to signaling proteins of innate immune responses.,” *Proc Natl Acad Sci U S A*, vol. 103, pp. 12481–12486, Aug 2006.
- [242] G. Ferwerda, B. J. Kullberg, D. J. de Jong, S. E. Girardin, D. M. L. Langenberg, R. van Crevel, T. H. M. Ottenhoff, J. W. M. Van der Meer, and M. G. Netea, “Mycobacterium paratuberculosis is recognized by toll-like receptors and nod2.,” *J Leukoc Biol*, vol. 82, pp. 1011–1018, Oct 2007.
- [243] F. Martinon and J. Tschopp, “Nlrs join tlrs as innate sensors of pathogens.,” *Trends Immunol*, vol. 26, pp. 447–454, Aug 2005.
- [244] M. G. Netea, G. Ferwerda, D. J. de Jong, T. Jansen, L. Jacobs, M. Kramer, T. H. J. Naber, J. P. H. Drenth, S. E. Girardin, B. J. Kullberg, G. J. Adema, and J. W. M. Van der Meer, “Nucleotide-binding oligomerization domain-2 modulates specific tlr pathways for the induction of cytokine release.,” *J Immunol*, vol. 174, pp. 6518–6523, May 2005.
- [245] E. Kopp, R. Medzhitov, J. Carothers, C. Xiao, I. Douglas, C. A. Janeway, and S. Ghosh, “Ecsit is an evolutionarily conserved intermediate in the toll/il-1 signal transduction pathway.,” *Genes Dev*, vol. 13, pp. 2059–2071, Aug 1999.
- [246] P. J. Cejas, M. C. Walsh, E. L. Pearce, D. Han, G. M. Harms, D. Artis, L. A. Turka, and Y. Choi, “Traf6 inhibits th17 differentiation and tgf-beta-mediated suppression of il-2.,” *Blood*, vol. 115, pp. 4750–4757, Jun 2010.
- [247] Y. Chen, P. Thai, Y.-H. Zhao, Y.-S. Ho, M. M. DeSouza, and R. Wu, “Stimulation of airway mucin gene expression by interleukin (il)-17 through il-6 paracrine/autocrine loop.,” *J Biol Chem*, vol. 278, pp. 17036–17043, May 2003.
- [248] T. Kinugasa, T. Sakaguchi, X. Gu, and H. C. Reinecker, “Claudins regulate the intestinal barrier in response to immune mediators.,” *Gastroenterology*, vol. 118, pp. 1001–1011, Jun 2000.
- [249] J. Shen, Y. Qiao, Z. Ran, and T. Wang, “Different activation of traf4 and traf6 in inflammatory bowel disease.,” *Mediators Inflamm*, vol. 2013, p. 647936, 2013.
- [250] C. Wang, X. Yu, Q. Cao, Y. Wang, G. Zheng, T. K. Tan, H. Zhao, Y. Zhao, Y. Wang,

- and D. C. Harris, "Characterization of murine macrophages from bone marrow, spleen and peritoneum.," *BMC Immunol*, vol. 14, p. 6, 2013.
- [251] B. Derfalvi, P. Igaz, K. A. Fulop, C. Szalai, and A. Falus, "Interleukin-6-induced production of type ii acute phase proteins and expression of junb gene are downregulated by human recombinant growth hormone in vitro.," *Cell Biol Int*, vol. 24, no. 2, pp. 109–114, 2000.
- [252] P. C. Heinrich, J. V. Castell, and T. Andus, "Interleukin-6 and the acute phase response.," *Biochem J*, vol. 265, pp. 621–636, Feb 1990.
- [253] M. Ligumsky, P. L. Simon, F. Karmeli, and D. Rachmilewitz, "Role of interleukin 1 in inflammatory bowel disease–enhanced production during active disease.," *Gut*, vol. 31, pp. 686–689, Jun 1990.
- [254] L. A. Dieleman, C. O. Elson, G. S. Tennyson, and K. W. Beagley, "Kinetics of cytokine expression during healing of acute colitis in mice.," *Am J Physiol*, vol. 271, pp. G130–G136, Jul 1996.
- [255] M. Z. Mazlam and H. J. Hodgson, "Interrelations between interleukin-6, interleukin-1 beta, plasma c-reactive protein values, and in vitro c-reactive protein generation in patients with inflammatory bowel disease.," *Gut*, vol. 35, pp. 77–83, Jan 1994.
- [256] J. Hiscott, J. Marois, J. Garoufalis, M. D'Addario, A. Roulston, I. Kwan, N. Pepin, J. Lacoste, H. Nguyen, and G. Bensi, "Characterization of a functional nf-kappa b site in the human interleukin 1 beta promoter: evidence for a positive autoregulatory loop.," *Mol Cell Biol*, vol. 13, pp. 6231–6240, Oct 1993.
- [257] T. T. MacDonald, A. Vossenkaemper, M. Fantini, and G. Monteleone, "Reprogramming the immune system in ibd.," *Dig Dis*, vol. 30, no. 4, pp. 392–395, 2012.
- [258] D. F. Fiorentino, A. Zlotnik, T. R. Mosmann, M. Howard, and A. O'Garra, "Il-10 inhibits cytokine production by activated macrophages.," *J Immunol*, vol. 147, pp. 3815–3822, Dec 1991.
- [259] C. Asseman, S. Mauze, M. W. Leach, R. L. Coffman, and F. Powrie, "An essential role for interleukin 10 in the function of regulatory t cells that inhibit intestinal inflammation.," *J Exp Med*, vol. 190, pp. 995–1004, Oct 1999.

- [260] H. Braat, M. P. Peppelenbosch, and D. W. Hommes, “Interleukin-10-based therapy for inflammatory bowel disease.,” *Expert Opin Biol Ther*, vol. 3, pp. 725–731, Aug 2003.
- [261] H. Braat, P. Rottiers, D. W. Hommes, N. Huyghebaert, E. Remaut, J.-P. Remon, S. J. H. van Deventer, S. Neiryck, M. P. Peppelenbosch, and L. Steidler, “A phase i trial with transgenic bacteria expressing interleukin-10 in crohn’s disease.,” *Clin Gastroenterol Hepatol*, vol. 4, pp. 754–759, Jun 2006.
- [262] R. N. Fedorak, A. Gangl, C. O. Elson, P. Rutgeerts, S. Schreiber, G. Wild, S. B. Hanauer, A. Kilian, M. Cohard, A. LeBeaut, and B. Feagan, “Recombinant human interleukin 10 in the treatment of patients with mild to moderately active crohn’s disease. the interleukin 10 inflammatory bowel disease cooperative study group.,” *Gastroenterology*, vol. 119, pp. 1473–1482, Dec 2000.
- [263] G. J. Marlow, D. van Gent, and L. R. Ferguson, “Why interleukin-10 supplementation does not work in crohn’s disease patients.,” *World J Gastroenterol*, vol. 19, pp. 3931–3941, Jul 2013.
- [264] J. K. Ariffin and M. J. Sweet, “Differences in the repertoire, regulation and function of toll-like receptors and inflammasome-forming nod-like receptors between human and mouse.,” *Curr Opin Microbiol*, Mar 2013.
- [265] S. Melgar, A. Karlsson, and E. Michaelsson, “Acute colitis induced by dextran sulfate sodium progresses to chronicity in c57bl/6 but not in balb/c mice: correlation between symptoms and inflammation.,” *Am J Physiol Gastrointest Liver Physiol*, vol. 288, pp. G1328–G1338, Jun 2005.
- [266] S. Schreiber, S. Nikolaus, and J. Hampe, “Activation of nuclear factor kappa b inflammatory bowel disease.,” *Gut*, vol. 42, pp. 477–484, Apr 1998.
- [267] A. Nenci, C. Becker, A. Wullaert, R. Gareus, G. van Loo, S. Danese, M. Huth, A. Nikolaev, C. Neufert, B. Madison, D. Gumucio, M. F. Neurath, and M. Pasparakis, “Epithelial nemo links innate immunity to chronic intestinal inflammation.,” *Nature*, vol. 446, pp. 557–561, Mar 2007.
- [268] F. Driessler, K. Venstrom, R. Sabat, K. Asadullah, and A. J. Schottelius, “Molecular mechanisms of interleukin-10-mediated inhibition of nf-kappab activity: a role for p50.,” *Clin Exp Immunol*, vol. 135, pp. 64–73, Jan 2004.

- [269] P. Wang, P. Wu, M. I. Siegel, R. W. Egan, and M. M. Billah, "Interleukin (il)-10 inhibits nuclear factor kappa b (nf kappa b) activation in human monocytes. il-10 and il-4 suppress cytokine synthesis by different mechanisms.," *J Biol Chem*, vol. 270, pp. 9558–9563, Apr 1995.
- [270] P. Dharmani, P. Leung, and K. Chadee, "Tumor necrosis factor- α and muc2 mucin play major roles in disease onset and progression in dextran sodium sulphate-induced colitis.," *PLoS One*, vol. 6, no. 9, p. e25058, 2011.
- [271] R. Carey, I. Jurickova, E. Ballard, E. Bonkowski, X. Han, H. Xu, and L. A. Denson, "Activation of an il-6:stat3-dependent transcriptome in pediatric-onset inflammatory bowel disease.," *Inflamm Bowel Dis*, vol. 14, pp. 446–457, Apr 2008.
- [272] G. Leung, A. Wang, M. Fernando, V. C. Phan, and D. M. McKay, "Bone-marrow derived alternatively activated macrophages reduce colitis without promoting fibrosis: participation of il-10.," *Am J Physiol Gastrointest Liver Physiol*, Mar 2013.
- [273] Q. Zhao, J. Wang, I. V. Levichkin, S. Stasinopoulos, M. T. Ryan, and N. J. Hoogenraad, "A mitochondrial specific stress response in mammalian cells.," *EMBO J*, vol. 21, pp. 4411–4419, Sep 2002.
- [274] E. Rath and D. Haller, "Unfolded protein responses in the intestinal epithelium: sensors for the microbial and metabolic environment.," *J Clin Gastroenterol*, vol. 46 Suppl, pp. S3–S5, Oct 2012.
- [275] X. Chen, J. J. Oppenheim, and O. M. Z. Howard, "Balb/c mice have more cd4+cd25+ t regulatory cells and show greater susceptibility to suppression of their cd4+cd25- responder t cells than c57bl/6 mice.," *J Leukoc Biol*, vol. 78, pp. 114–121, Jul 2005.
- [276] V. De Vooght, J. A. J. Vanoirbeek, K. Luyts, S. Haenen, B. Nemery, and P. H. M. Hoet, "Choice of mouse strain influences the outcome in a mouse model of chemical-induced asthma.," *PLoS One*, vol. 5, no. 9, p. e12581, 2010.
- [277] M. L. Gueler, J. D. Gorham, C. S. Hsieh, A. J. Mackey, R. G. Steen, W. F. Dietrich, and K. M. Murphy, "Genetic susceptibility to leishmania: Il-12 responsiveness in th1 cell development.," *Science*, vol. 271, pp. 984–987, Feb 1996.

- [278] P. C. Amrein, E. C. Attar, T. Takvorian, E. P. Hochberg, K. K. Ballen, K. M. Leahy, D. C. Fisher, A. S. Lacasce, E. D. Jacobsen, P. Armand, R. P. Hasserjian, L. Werner, D. Neuberg, and J. R. Brown, "Phase ii study of dasatinib in relapsed or refractory chronic lymphocytic leukemia.," *Clin Cancer Res*, vol. 17, pp. 2977–2986, May 2011.
- [279] P. Viatour, M. Bentires-Alj, A. Chariot, V. Deregowski, L. de Leval, M.-P. Merville, and V. Bours, "Nf- kappa b2/p100 induces bcl-2 expression.," *Leukemia*, vol. 17, pp. 1349–1356, Jul 2003.
- [280] P. Rosenstiel, S. Derer, A. Till, R. Haesler, H. Eberstein, B. Bewig, S. Nikolaus, A. Nebel, and S. Schreiber, "Systematic expression profiling of innate immune genes defines a complex pattern of immunosenescence in peripheral and intestinal leukocytes.," *Genes Immun*, vol. 9, pp. 103–114, Mar 2008.
- [281] M. Hong, S.-i. Yoon, and I. A. Wilson, "Structure and functional characterization of the rna-binding element of the nlr1 innate immune modulator.," *Immunity*, vol. 36, pp. 337–347, Mar 2012.
- [282] J. Mo, J. P. Boyle, C. B. Howard, T. P. Monie, B. K. Davis, and J. A. Duncan, "Pathogen sensing by nucleotide-binding oligomerization domain-containing protein 2 (nod2) is mediated by direct binding to muramyl dipeptide and atp.," *J Biol Chem*, vol. 287, pp. 23057–23067, Jun 2012.
- [283] E.-S. Lee, C.-H. Yoon, Y.-S. Kim, and Y.-S. Bae, "The double-strand rna-dependent protein kinase pkr plays a significant role in a sustained er stress-induced apoptosis.," *FEBS Lett*, vol. 581, pp. 4325–4332, Sep 2007.
- [284] M. Kamizato, K. Nishida, K. Masuda, K. Takeo, Y. Yamamoto, T. Kawai, S. Teshima-Kondo, T. Tanahashi, and K. Rokutan, "Interleukin 10 inhibits interferon gamma- and tumor necrosis factor alpha-stimulated activation of nadph oxidase 1 in human colonic epithelial cells and the mouse colon.," *J Gastroenterol*, vol. 44, no. 12, pp. 1172–1184, 2009.
- [285] S. Liarte, E. Chaves-Pozo, E. Abellan, J. Meseguer, V. Mulero, A. V. M. Canario, and A. Garcia-Ayala, "Estrogen-responsive genes in macrophages of the bony fish gilthead seabream: a transcriptomic approach.," *Dev Comp Immunol*, vol. 35, pp. 840–849, Aug 2011.

- [286] L. Papa and D. Germain, "Estrogen receptor mediates a distinct mitochondrial unfolded protein response.," *J Cell Sci*, vol. 124, pp. 1396–1402, May 2011.
- [287] C. M. Klinge, "Estrogenic control of mitochondrial function and biogenesis," *Journal of Cellular Biochemistry*, vol. 105, no. 6, pp. 1342–1351, 2008.
- [288] C. M. Krawczyk, T. Holowka, J. Sun, J. Blagih, E. Amiel, R. J. DeBerardinis, J. R. Cross, E. Jung, C. B. Thompson, R. G. Jones, and E. J. Pearce, "Toll-like receptor-induced changes in glycolytic metabolism regulate dendritic cell activation.," *Blood*, vol. 115, pp. 4742–4749, Jun 2010.
- [289] A. Garedew, S. O. Henderson, and S. Moncada, "Activated macrophages utilize glycolytic atp to maintain mitochondrial membrane potential and prevent apoptotic cell death.," *Cell Death Differ*, vol. 17, pp. 1540–1550, Oct 2010.
- [290] A. Garedew, S. O. Henderson, and S. Moncada, "Retraction: Activated macrophages utilize glycolytic atp to maintain mitochondrial membrane potential and prevent apoptotic cell death.," *Cell Death Differ*, Aug 2012.
- [291] D. R. Clayburgh, L. Shen, and J. R. Turner, "A porous defense: the leaky epithelial barrier in intestinal disease.," *Lab Invest*, vol. 84, pp. 282–291, Mar 2004.
- [292] S. Kitajima, S. Takuma, and M. Morimoto, "Histological analysis of murine colitis induced by dextran sulfate sodium of different molecular weights.," *Exp Anim*, vol. 49, pp. 9–15, Jan 2000.
- [293] Y. Xu, N. H. Hunt, and S. Bao, "The correlation between proinflammatory cytokines, madcam-1 and cellular infiltration in the inflamed colon from tnf-alpha gene knockout mice.," *Immunol Cell Biol*, vol. 85, no. 8, pp. 633–639, 2007.
- [294] Y. Yan, V. Kolachala, G. Dalmaso, H. Nguyen, H. Laroui, S. V. Sitaraman, and D. Merlin, "Temporal and spatial analysis of clinical and molecular parameters in dextran sodium sulfate induced colitis.," *PLoS One*, vol. 4, no. 6, p. e6073, 2009.
- [295] M. Perse and A. Cerar, "Dextran sodium sulphate colitis mouse model: traps and tricks.," *J Biomed Biotechnol*, vol. 2012, p. 718617, 2012.
- [296] F. Baer, W. Bochmann, A. Widok, K. von Medem, R. Pagel, M. Hirose, X. Yu, K. Kalies, P. Koenig, R. Boehm, T. Herdegen, A. T. Reinicke, J. Buening, H. Lehnert, K. Fellermann,

- S. Ibrahim, and C. Sina, "Mitochondrial gene polymorphisms that protect mice from colitis.," *Gastroenterology*, Jul 2013.
- [297] C. Mauro, S. C. Leow, E. Anso, S. Rocha, A. K. Thotakura, L. Tornatore, M. Moretti, E. De Smaele, A. A. Beg, V. Tergaonkar, N. S. Chandel, and G. Franzoso, "Nf- κ b controls energy homeostasis and metabolic adaptation by upregulating mitochondrial respiration.," *Nat Cell Biol*, vol. 13, pp. 1272–1279, Oct 2011.
- [298] E. Mileti, G. Matteoli, I. D. Iliev, and M. Rescigno, "Comparison of the immunomodulatory properties of three probiotic strains of lactobacilli using complex culture systems: prediction for in vivo efficacy.," *PLoS One*, vol. 4, no. 9, p. e7056, 2009.
- [299] R. El Asmar, P. Panigrahi, P. Bamford, I. Berti, T. Not, G. V. Coppa, C. Catassi, A. Fasano, and R. El Asmar, "Host-dependent zonulin secretion causes the impairment of the small intestine barrier function after bacterial exposure.," *Gastroenterology*, vol. 123, pp. 1607–1615, Nov 2002.
- [300] T. D. Klingberg, M. H. Pedersen, A. Cencic, and B. B. Budde, "Application of measurements of transepithelial electrical resistance of intestinal epithelial cell monolayers to evaluate probiotic activity.," *Appl Environ Microbiol*, vol. 71, pp. 7528–7530, Nov 2005.
- [301] J. Y. Kim and K. Ozato, "The sequestosome 1/p62 attenuates cytokine gene expression in activated macrophages by inhibiting ifn regulatory factor 8 and tnf receptor-associated factor 6/nf-kappab activity.," *J Immunol*, vol. 182, pp. 2131–2140, Feb 2009.
- [302] E. Ang, N. J. Pavlos, S. L. Rea, M. Qi, T. Chai, J. P. Walsh, T. Ratajczak, M. H. Zheng, and J. Xu, "Proteasome inhibitors impair rankl-induced nf-kappab activity in osteoclast-like cells via disruption of p62, traf6, cyld, and ikappabalpha signaling cascades.," *J Cell Physiol*, vol. 220, pp. 450–459, Aug 2009.
- [303] M. T. Diaz-Meco and J. Moscat, "The atypical pkcs in inflammation: Nf- κ b and beyond.," *Immunol Rev*, vol. 246, pp. 154–167, Mar 2012.
- [304] S. R. Calcagno, S. Li, M. W. Shahid, M. B. Wallace, M. Leitges, A. P. Fields, and N. R. Murray, "Protein kinase c iota in the intestinal epithelium protects against dextran sodium sulfate-induced colitis.," *Inflamm Bowel Dis*, vol. 17, pp. 1685–1697, Aug 2011.

Danksagung

Mein erster Dank gilt Prof. Dr. Philip Rosenstiel für die Bereitstellung des Themas und die freundliche Aufnahme am IKMB.

Herrn Prof. Dr. Thomas Roeder danke ich für die Übernahme des Co-Referats.

Bei meiner Betreuerin Dr. Simone Lipinski bedanke ich mich für die Möglichkeit frei zu forschen und mein Thema von unterschiedlichen Seiten zu beleuchten.

Dr. Susanne Billmann-Born war eine wertvolle Hilfe bei der Mikroskopie. Ausserdem danke ich ihr für das Lektorat und den Y2H screen.

Für kollegiale Hilfe und fachliche Unterstützung bedanke ich mich bei den Mitarbeitern des IKMBs, besonders im Hinblick auf die Mausexperimente.

Prof. Dr. A. Tholey und D. Linke gebührt mein Dank für die MS/MS Analysen.

Dr. M. Brosch und C. Fritsch haben mich bei der Aufreinigung der Mitochondrien via Ultrazentrifugation unterstützt.

Wertvolle praktische Unterstützung bei der Mausezucht und Haltung erhielt ich durch die Mitarbeiter der Tierställe.

Mein persönlicher Dank gilt meiner Familie und meinen Freunden, deren Unterstützung unverzichtbar war und ist.

Linda- für das was war, ist und sein wird!

Diese Arbeit wurde finanziell gefördert durch die Bruhn Stiftung und das LL-Lab-Stipendium.

Lars Bremer

geb.: 18. Juni 1983 in Datteln

deutsch

Hochschulausbildung

- seit 04.2010 **Promotion am Institut für Klinische Molekularbiologie, Kiel**
Thema: Functional characterization of the NOD-like receptor NLRC3
- 08.2009-03.2010 **Diplom am Leibniz-Institut für Meereswissenschaften, Kiel**
Thema: Vergleichende biogeochemische und genetische Analysen zur mikrobiellen Silikatverwitterung in marinen Sedimenten
- 10.2007-07.2009 **Christian-Albrechts-Universität zu Kiel**
Studiengang: Biochemie/Molekularbiologie (Diplom)
- 10.2005-09.2007 **Friedrich-Schiller-Universität zu Jena**
Studiengang: Biochemie/Molekularbiologie (Diplom)

Auszeichnungen

- 2010 Förderpreis der Bruhn-Stiftung

Publikationen

- 2012 **Bremer L**, Lipinski S, Schreiber S, Rosenstiel P. The role of the NOD-like receptor NLRC3 in the innate immune system (Immunology, Abstract)
- 2011 Laudien M, Haesler R, Wohlers J, Böck J, Lipinski S, **Bremer L**, Podschun R, Ambrosch P, Lamprecht P, Rosenstiel P, Till A. Molecular signatures of a disturbed nasal barrier function in the primary tissue of Wegener's granulomatosis. (Mucosal Immunology)
- 2011 Lipinski S, **Bremer L**, Lammers T, Thieme F, Schreiber S, Rosenstiel P. Coagulation and inflammation. Molecular insights and diagnostic implications (Haemostaseologie)
- 2010 **Bremer L**. Vergleichende biogeochemische und genetische Analysen zur mikrobiellen Silikatverwitterung in marinen Sedimenten (Thesis)

Poster

- 2012 Functional characterization of the NOD-like receptor NLRC3,
35. Norddeutsche Immunologentagung, Borstel/Deutschland
- 2012 The role of the NOD-like receptor NLRC3 in the innate immune system,
European Congress of Immunology, Glasgow/UK

Eidesstattliche Erklärung

Hiermit erkläre ich an Eides statt die vorliegende Dissertation mit dem Titel:

Functional Characterization of NLRC3

selbstständig nach den Regeln der guten wissenschaftlichen Praxis der Deutschen Forschungsgemeinschaft, unter der wissenschaftlichen Anleitung meines Betreuers und unter der ausschließlichen Verwendung der angegebenen Literatur und Hilfsmittel erstellt zu haben. Stellen, die wörtlich oder sinngemäß aus veröffentlichten oder noch nicht veröffentlichten Quellen entnommen sind, sind als solche kenntlich gemacht. Die Arbeit wurde bisher in gleicher oder ähnlicher Form keiner anderen Fakultät im Rahmen einer Prüfung vorgelegt. Ein Teil der Ergebnisse (Kap. 4.7.1) wurde bereits in einer ausgegliederten wissenschaftlichen Publikation unter meiner Mitarbeit veröffentlicht [203].

Ich erkläre, kein anderes Promotionsverfahren ohne Erfolg beendet zu haben und dass keine Aberkennung eines bereits erworbenen Doktorgrades vorliegt.

Kiel, den 02. März 2014

Lars Bremer